PHOSPHORYLATION PATTERNS, AGGREGATION PROPENSITIES, AND MORPHOLOGICAL STUDIES OF THE VARIOUS TAU PROTEIN ISOFORMS

by

ERVING TORGBOR LARYEA

A dissertation submitted in partial fulfillment of the
requirements for the degree of

DOCTOR OF PHILOSOPHY

2022

Oakland University
Rochester, Michigan

Doctoral Advisory Committee:

Colin G. Wu, Ph.D., Chair
Sanela Martic-Milne, Ph.D., Co-chair.
Adam Avery, Ph.D.
Gerard Madlambayan, Ph.D.

To my mother and father

ACKNOWLEDGMENTS

To God be all the glory and the praise for making graduate school a possibility. I am most grateful.

First and foremost, I would like to express my profound gratitude to Dr. Colin G. Wu and Dr. Sanela Martic – Milne for mentoring and co-mentoring me during my entire stay in Oakland University.

I would also want to say a special thank you to my committee members, Dr. Adam Avery and Dr. Gerard Madlambayan for taking time of their busy schedules to help me put together this dissertation.

I am also very grateful to the entire Laryea family especially my parents, Mr., and Mrs. Joseph Laryea for their support and prayers. Special thanks to Rev. Philip Quaye for all his love and care.

Finally, special thanks go to all my laboratory mates who in one way or the other contributed to my growth and experiments throughout my Ph.D. program

Erving Torgbor Laryea

PREFACE

It is estimated that over 45 million people worldwide live with diverse forms of dementias, and this is expected to increase to 130 million by 2050. Alzheimer's disease (AD) has been established as the commonest cause of dementia and it is also the sixth leading cause of death in the elderly in the United States. Tau is a microtubule-associated protein, and it is mainly found in the central nervous system. Tau protein is primarily involved in the development and maintenance of the neurons in the brain. However, under pathological conditions, Tau protein abnormally assembles into insoluble aggregates in neuronal membranes causing synaptic dysfunction and neuronal cell death. Pathological Tau first aggregates as oligomers, then into paired helical filaments (PHFs), and finally as neurofibrillary tangles (NFTs), after it has been post- translationally modified (PTM). There are several PTMs including phosphorylation, glycosylation, acetylation, ubiquitination, conformational changes, nitration, and truncation (proteolytic cleavage). Of all these forms of post-translational modifications (PTMs), hyperphosphorylation has been identified as the major cause of Tau fibrillation and increased cell cytotoxicity.

My interest in Alzheimer's research stemmed from my passion to develop effective therapeutic options to treat AD in the near future. This I hope to achieve by having a greater understanding of how posttranslational modification, herein hyperphosphorylation, identified as the commonest cause of Tau fibrillization, leads to all the debilitating effects AD has been identified to comes with.

ABSTRACT

PHOSPHORYLATION PATTERNS, AGGREGATION PROPENSITIES, AND MORPHOLOGICAL STUDIES OF THE VARIOUS TAU PROTEIN ISOFORMS

by

ERVING TORGBOR LARYEA

Advisers: Colin G. Wu, Ph.D. and Sanela Martic-Milne, Ph.D.

Tau protein is a microtubule-binding protein as well as a biomarker of neurodegeneration. Its core function is to stabilize microtubules for proper neuronal communication. When hyperphosphorylated, it detaches itself from microtubules and self-assembles into cytotoxic structures. However, little is known about how phosphorylation, the commonest posttranslational modification process found in eukaryotic cells regulate Tau protein structure, conformation, and function. Herein, the role of specific kinases or kinase combinations from the three main classes of proteins kinases that phosphorylate Tau: Proline-directing protein kinase (Glycogen synthase kinase (GSK-3β)) and non-proline directing protein kinase (Microtubule associated regulating kinase (MARK4)) and Tyrosine kinase (Fyn) were systematically evaluated *in vitro*. After the expression and purification of all the six Tau isoforms from *E. Coli* cells, Tau 441, also known as full length Tau, which comprises of all the domains found in the other isoforms was extensively investigated. Phosphorylation of Tau 441 by GSK-3β, MARK4 and Fyn was detected by immunostaining using phosphospecific antibodies. With Tau protein been identified to co-localize with sulfated aminoglycans such as

heparin and heparin sulfates, single and multi-kinase phosphorylated aggregation studies of Tau 441 were conducted in the presence or absence of heparin. Functional assays including proteostat assays, turbidity assays and SDS-PAGE were used to evaluate the aggregation properties of Tau 441 after phosphorylation.

The phosphosites on all the single and multi-kinase phosphorylated Tau 441 samples were characterized by Tandem mass spectrometry. Tau 441 protein structure and conformational changes after phosphorylation was also determined by Hydrogen Deuterium Exchange mass spectrometry (HDX-MS). The flexibility and accessibility to the first and second hexapeptide repeats (H1 and H2), a repeat motif found in the MTBR of Tau protein identified to increase the aggregation tendencies of Tau protein were used to describe the single kinase or multi-kinase combinations evaluated ability to promote Tau fibrillization.

TABLE OF CONTENTS

TABLE OF CONTENTS—Continued

TABLE OF CONTENTS—Continued

TABLE OF CONTENTS—Continued

LIST OF TABLES

LIST OF FIGURES

LIST OF FIGURES—Continued

LIST OF FIGURES—Continued

LIST OF ABBREVIATIONS

AD	Alzheimer's disease
PTM	Posttranslational modification
TRESI MS - HDX	Time resolved electro-ionization mass spectrometry-Hydrogen deuterium exchange
LC/MS/MS	Liquid Chromatography/Mass spectrometry/Mass Spectrometry
DTT	Dithiothreitol
NFTs	Neurofibrillary tangles
TFA	Trifluoroacetic acid
CID	Collision induced dissociation
ETD	Electron transfer dissociation
FDR	False discovery rate
NTD	N-terminal domain
CTD	C-terminal domain
PRD	Proline rich domain
SDS-PAGE	Sodium dodecyl sulphate-polyacrylamide gel electrophoresis
MAP	Microtubule associated protein
CNS	Central nervous system
MBD	Microtubule binding domain
UV	Ultraviolet
TEM	Transmission electron microscopy
PHFs	Pair helical filaments

HMW	High molecular weight
kDa	Kilodalton
MW	Molecular weight
WB	Western blot
FS	Fluorescence spectroscopy
FI	Fluorescence intensity
ALS	Amyotrophic lateral sclerosis
HD	Huntington’s disease
SMD	Spinal muscular dystrophy
PD	Parkinson’s disease

CHAPTER ONE

INTRODUCTION

1.0 Neurodegeneration

Neurodegeneration is defined as the progressive loss of neuronal structure or function in the human body[1]. The loss of neuronal structure and function is caused or aggravated by neurodegenerative processes[2][3].

Because neurons are the building blocks of the nervous system[4], neuronal injuries or deaths cause a gradual decline or shutdown in the processes the neurons are involved in. The progressive nature of these degenerations or neuronal cell death makes treatment of these neurological disorders extremely challenging. Currently, there is no known cure for neurodegenerative diseases[5]. However, Alzheimer's treatment targeting amyloid-β appears to be very promising. Numerous researchers have reported neurodegeneration at various sites in the neuron, including the axons, cell bodies, and the dendrites[6][7]. Most neurodegenerative diseases, including Alzheimer's disease (AD), Spinal muscular dystrophy (SMD), Lewy body disease (LDD), Amyotrophic lateral sclerosis (ALS), Parkinson's disease (PD), and Huntington's disease (HD), worsen as the neurodegenerative process worsens.

Although AD and PD are the commonest neurodegenerative diseases[8][9], the most researched are AD, PD, HD, and ALS[10]. While every neurodegenerative disorder is characterized by the progressive loss of neuronal structure and function, yet, they all have distinct pathophysiological and clinical hallmarks, which are critical for their identification and diagnoses. A greater understanding of the differences and similarities

between these conditions at both the molecular and systemic levels will lead to discovering better therapeutic options to improve the lives of persons living with the diseases.

1.1 Alzheimer's disease

AD is a neurodegenerative disease characterized by the loss of neuronal and synaptic activity[11]. The loss of neuronal and synaptic activity results from the gross atrophy observed in the cerebral cortex, subcortical regions, as well as degeneration in the temporal lobe, parietal lobe, and parts of the frontal cortex and cingulate gyrus in AD brains[12][13]. AD causes a gradual decline in memory and learning skills[14]. Age, family history, genetics, down syndrome, head injuries, past head trauma, and mild cognitive impairment predisposes an individual to AD[15][16][17].

Emil Kraepelin first identified AD symptoms; however, the neuropathological characteristics were first observed by Alois Alzheimer (both German psychiatrists). AD brains, at the molecular level, are characterized by two lesions, namely: the extraneuronal amyloid plaques and intraneuronal neurofibrillary tangles (NFTs)[18][19][20].

The amyloid plaques are made up of small peptides, called beta-amyloid (A-beta or Aβ); usually, 30 – 51 amino acids long[21]. Aβ peptides are fragments of a precursor protein called amyloid precursor protein (APP) located on chromosome 21 and are made up of 19 exons[22][23][24]. APP usually runs between 110 to 140 kDa on an SDS – PAGE. APP is made up of a heterogeneous group of ubiquitously expressed polypeptides. The heterogeneity is due to alternative splicing and ligation of the 19 exons and the post-translational modifications the protein undergoes. APP is sequentially cleaved by beta-secretase and gamma-secretase into Aβ40/Aβ42[25].

These fragments can cluster outside the neuron as β-amyloid fibrils, amyloid plaques, or senile plaques [26]. Even though Aβ deposits extra neuronally, the amyloid plaques also penetrate neuronal membranes because they are transmembrane proteins [27]. Increased levels of both Aβ40 and Aβ42 have been implicated in either familial or sporadic AD forms, with Aβ42 being the most prone to amyloidosis because of its hydrophobic core [28].

Even though Aβ can exist both in monomeric and oligomeric forms, recent studies have pointed to oligomeric Aβ as the most toxic to nerve cells[29][30]. Also, because oligomeric Aβ is flexible and soluble, it aggregates easily; hence, it is responsible for the prion-like infection seen in AD. Even though the processes that lead to the accumulation of oligomeric Aβ in the central nervous system are not well understood, there is enough evidence showing the mechanism via which misfolded Aβ can induce the misfolding of the other proteins, particularly Tau[31].

Neurodegenerative disorders with misfolded Tau implicated are called tauopathies. The morphological changes observed in the Tau structure via its aggregation into NFTs in AD patients' are observed in neurons located in regions of the brain responsible for motor and cognitive function[32][33]. The density of the aggregated fibrils and filaments from Tau protein has been shown to correlates with the observed decline in intellectual power associated with patients living AD and other tauopathies[34]. The detailed mechanism describing the formation of NFTs is yet to be deciphered, and the peripheral role of NFTs in AD is still being investigated.

1.2 AD facts

AD is the sixth leading cause of death in the United States of America, with it being the cause of one out of every three senior death[35]. AD has also been identified to kill more than both breast cancer and prostate cancers put together[36]. Every 70 seconds, someone in America develops AD; by 2050, this time is expected to decrease every 33 seconds[37]. Over the coming decades, the "baby-boom" population is projected to add 10 million people to these numbers[37]. Thus, in 2050, the incidence of AD is expected to come up to nearly a million people per year, with a total estimated prevalence of 11 to 16 million people[37]. Significant cost implications related to AD and other dementias include an estimated $148 billion annually in direct (Medicare/Medicaid) and indirect (e.g., decreased business productivity, foregone earnings for patients and their family members) costs[37]. In addition, more than 11 million family members and other unpaid caregivers provided an estimated 15.3 billion hours of care to people with Alzheimer's or other dementias in 2020[38].

1.3 Tau protein

Tau protein, a microtubule-associated protein (MAP), is predominantly expressed in the neurons of the central nervous system. It is primarily involved in maintaining the cytoskeletal network's proper function, that is, microtubule stabilization and its assembly[39]. Tau protein was first discovered in 1975 in Marc Kirschner’s laboratory at Princeton University [40]. Tau is intrinsically distorted and in its native state does not cluster, but when it is hyperphosphorylated in neurodegenerative diseases, it aggregates as NFTs in neuronal bodies[41].

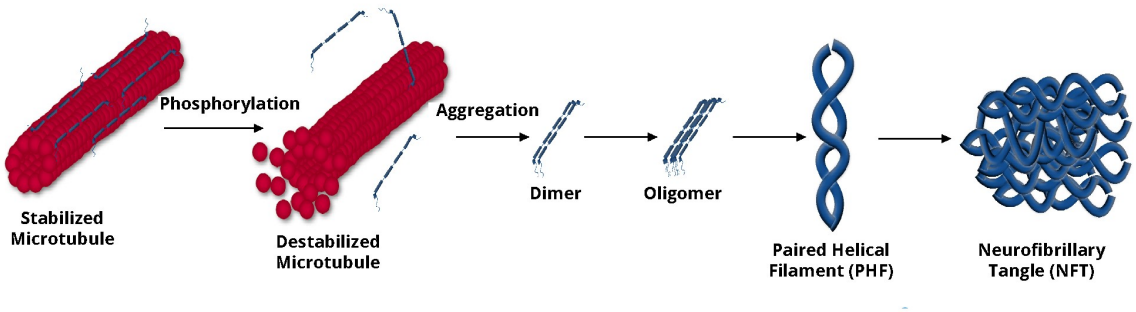

Figure 1.1: Formation of neurofibrillary tangles from Tau epitopes: Microtubules are stabilized by phosphorylated Tau epitopes. Hyperphosphorylation of Tau by kinases destabilizes the microtubules making Tau dissociate from the microtubules as monomeric Tau. Monomeric Tau aggregates into oligomeric Tau and then aggregates into neurofibrillary tangles. Image adopted from StressMarq Bioscience Inc, (Jan 28, 2008).

Phosphorylated Tau epitopes stabilize the microtubules[42][43]. When Tau is hyperphosphorylated, it destabilizes the microtubules, and this causes monomeric Tau to assemble as oligomers and then into PHFs. PHFs further clusters as NFTs[44][45]. Hyperphosphorylation of Tau, one of the main causes of tauopathies, triggers Tau's dissociation from microtubules and promotes its aggregation[46].

Extensive research has been done on Aβ and its role in the familial onset of AD has been established. However, a growing body of evidence points to Tau protein and its role in the pathogenesis of AD. The aggregation of Tau fibrils within neuronal bodies ultimately bursts the cell membrane[47]. Several mutated forms of Tau have been identified, and how they impact neurodegenerative diseases have been studied. Thus, this confirms the role of mutated Tau as the causative agent for synaptic failure and cell dysfunction[48], [49].

However, it remains largely unknown how the differentially phosphorylated states of Tau aggregates and disrupts memory loss and motor function. In addition, how the aggregates contribute to cell toxicity is also not well understood. A greater understanding of how the various Tau epitopes aggregate and contribute to cell toxicity will lead to developing effective therapies for AD.

1.3.1 Tau Isoforms

The MAPT gene that encodes for the Tau protein is located on chromosome 17q21[50]. Via alternative splicing, the 16 exons of the MAPT gene are alternatively ligated to form the six isoforms of Tau[51][52]. These Tau isoforms exhibit reduced mobility on sodium dodecyl sulfate-polyacrylamide gel electrophoresis (SDS-PAGE), such that their apparent molecular weights do not correspond to their actual molecular weights. Their primary function is to stabilize the microtubules via polymerization[53].

The six isoforms range from 352 to 441 (36.8 to 45.9 kDa) amino acids long[54]. Although Tau expression is developmentally regulated, all the six Tau isoforms are expressed in the CNS of the adult human brain. But in the fetal brain, only the shortest Tau isoform (Tau 352) is expressed[54]. The variation in the amino acid sequence is because of the involvement of the three to four microtubule-binding carboxy-terminal repeats encoded by exon 9, 10, 11, and 12[55], and the presence of at least two amino acid inserts 29 amino acids long also encoded for by exon 2 and 3. The inclusion or exclusion of exon 2 or 3 or both gives rise to the Tau isoforms with 0, 1, or 2 N – terminal inserts, while the inclusion and exclusion of exon 10 generate the 3R and 4R microtubule-binding repeats[56].

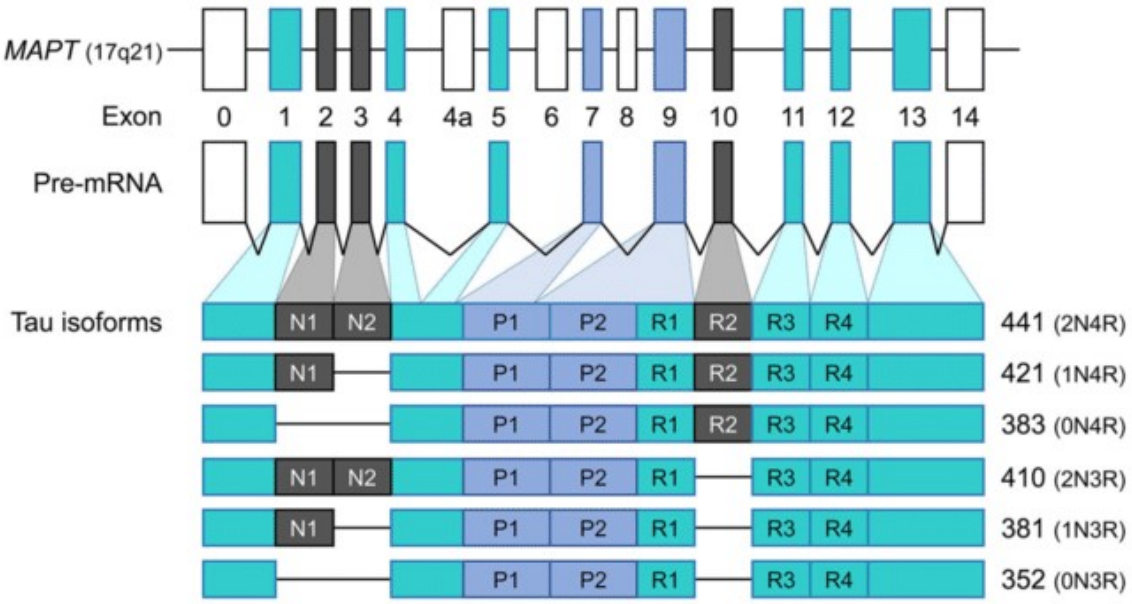

Figure 1.2: Splicing of MAPT gene: The MAPT gene comprises 16 exons and is located on chromosome 17q21. The 16 exons are alternatively spliced and ligated into the 6 Tau isoforms. The longest isoform is Tau 441 (441 amino acids), and the shortest is Tau 352 (352 amino acids). The various isoforms are differentially expressed in the human body, with Tau 352 being predominantly found in fetal brains while the other isoforms are mainly found in adult brains. Image adopted from cellular biology of Tau diversity and pathogenic conformers (Sang-Gyun *et al,* 2020)[57]

All the six Tau isoforms mentioned above contain the amino-terminal projection domains and the acidic insertions or repeats are represented with the letter N[55]. They also have proline-rich regions [58] and a microtubule-binding domain (MBD) made up of either three (3R), or four (4R) repeats. Each repeat is made up of between 31 to 32 amino acid residues. The MBDs that binds onto microtubules are found in the C-terminal region of the protein. The MBD and the proline-rich regions are both positively charged. The N-terminal domain and a short portion of the C-terminus are acidic[55].

1.3.2 Microtubules

Microtubules are made up of polymers of the globular proteins α- and β-tubulins[59][60]. Each subunit has an approximate molecular mass of 50 kDa. These two subunits form the αβ-tubulin heterodimer, which has been identified as the structural and functional unit of the microtubule[61]. The α and β subunits in the heterodimer are folded independent of each other, and each subunit is GTP bound. Whereas the α-subunit cannot be accessed for biochemical reactions because the GTP attached to it cannot be exchanged with GDP, the GTP bound to the β- subunit can be hydrolyzed twice. Firstly, during the formation of the αβ-tubulin heterodimer and secondly, during the incorporation of the heterodimer into the microtubule[60].

The αβ-tubulin heterodimer incorporated into microtubules follows a complex mechanism, and several chaperone proteins, including CCT and prefoldin, are involved in this process[60]. Besides these tubulin chaperone proteins, there are also tubulin folding cofactors[62] that are also molecular chaperones that are specifically required in the αβ-tubulin dimerization process and the acquisition of the αβ-tubulin quaternary structure[63]. Stabilization of the microtubule cytoskeleton maintains neuronal functions, and this is achieved via the intercalation of microtubules with microtubule-binding proteins, of which Tau is one of them.

Tau is mainly expressed in the neurons, and it stabilizes axonal microtubules by decreasing its inherent instability. The six Tau isoforms differentially regulate microtubular instability. The three or four microtubule-binding regions on Tau bind the heterodimers at the microtubule lattices. These microtubule-binding repeats are made up of prolines and essential amino acid residues that counteract the acidic amino acid

residues found on the surface of the microtubules allowing for selective binding. Tau then binds the structural and functional subunit of the microtubules in different Tau-αβ tubulin heterodimer conformations, hence improving the stability of the microtubule. Paclitaxel, discodermolide, and epothilones, plus other microtubule-stabilizing compounds[64][65], compete with Tau for the same binding sites on the β-tubulin subunit on the microtubule. To understand how Tau protein polymerizes or detaches itself from microtubules, these compounds are used as controls in microtubule polymerization assays.

1.3.3 Post-translational modifications

Biomolecules including proteins undergo chemical changes, which in turn activate or deactivate them. These changes are known as post-translational modifications. Proteins are post-translationally modified after translation via changes in their structure and active sites. These modifications are typically catalyzed by enzymes[66]. These enzymes recognize and target specific amino acid sequences in particular proteins[66]. These chemical changes are crucial in regulating the ability of these modified proteins to target distinct subcellular compartments. Their interaction with ligands or other proteins, protein folding, and their functional state, such as catalytic properties if they were enzymes or their signaling functions if they were signaling molecules, are all greatly modified[67].

Post-translational modification results in the cleavage of specific sites on precursor proteins, formation of disulfide bonds, or covalent addition and/or removal of low-molecular-weight groups[68]. The chemical modifications proteins undergo are as follows; acetylation, amidation, biotinylation, glutathionylation, glycation (nonenzymatic

conjugation with carbohydrates), glycosylation (enzymatic conjugation with carbohydrates), hydroxylation, methylation, mono-ADP-ribosylation, myristoylation, cysteinylation, deamidation, farnesylation, formylation, geranylgeranylation, oxidation, palmitoylation, phosphorylation, poly (ADP-ribosyl) ation, stearoylation, or sulfation[69]. Of all these post-translational modifications proteins undergo, phosphorylation and glycosylation are the major post-translational modification players that determine protein activity and function.

1.3.4.1 Phosphorylation

Phosphorylation which is the attachment of the phosphoryl group to biomolecules is the most predominant post-translational modification in eukaryotic cells. Phosphorylation occurs on serine, threonine, and tyrosine residues via the formation of phosphodiester bonds[69][70], on histidine, lysine, and arginine via the formation of phosphoramidate bonds[72][73], and aspartic acid and glutamic acid via the formation of mixed anhydride linkages.

Only serine, threonine, and tyrosine phosphorylations will be discussed since they occur in eukaryotic cells, and they are relevant to Alzheimer's disease pathogenesis. The addition of phosphoryl groups to hydroxyl groups on serine, threonine, or tyrosine amino acids is achieved via an esterification reaction [74]. Serine phosphorylation is the commonest form of phosphorylation, followed by that of threonine[75]. Although tyrosine phosphorylation is comparatively rare, is critical for many protein signaling pathways[76] Tyrosine phosphorylated proteins have been widely studied using protein antibody interactions since they are relatively easy to purify[77].

1.3.4.2 Tau Phosphorylation

Phosphorylation of Tau stabilizes microtubules (MTs) for proper neuronal communication [78][79]. When Tau gets hyperphosphorylated in AD, monomeric Tau accumulates as oligomeric Tau, then to PHFs, and lastly as NFTs[80]. With the identification of hyperphosphorylated Tau as the fundamental component of NFTs, Tau phosphorylation is considered the rate-determining step of Tau fibrillization[81]. Hyperphosphorylated Tau detaches itself from MTs, resulting in the collapse of the microtubular cytoskeleton[82].

In tauopathies, Tau becomes hyperphosphorylated at multiple serine and threonine residues, with Tau phosphorylation occurring mainly in the proline-rich domain (PRDs) (~22 sites out of 93 amino acids in the PRD can be phosphorylated)[83]. Tau in AD-derived PHFs can be phosphorylated at ~45 residues. Tau can be phosphorylated by several protein kinases, including glycogen synthase kinase 3β (GSK-3β), protein kinase A (PKA), cyclin-dependent kinase 5 (cdk5), microtubule-associated regulatory kinase (MARK), and stress-activated kinase / C-Jun N-terminal kinase (SAPK/JNK)[84].

Phosphorylation of the KXGS motifs[85][86] in the microtubule-binding domain precedes Tau amyloidogenesis and promotes Tau dissociation from the MTs[87]. The four sites mostly phosphorylated in this region are S258, S262, S289, and S356[88]. Phosphorylation at these residues significantly affects MT-Tau binding abilities, with S262 been the first site to be phosphorylated in AD[89].

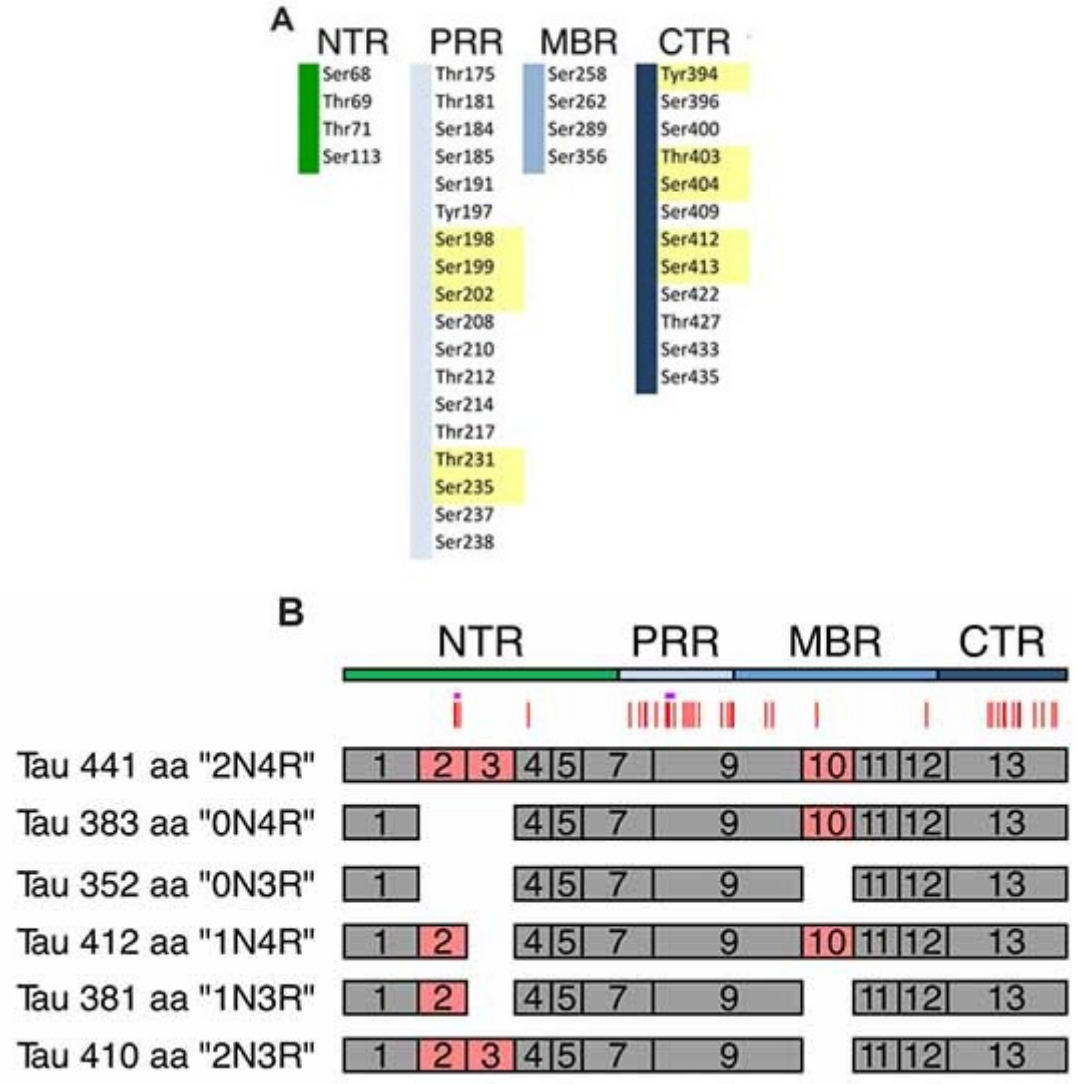

Figure 1.3: Schematic showing all the phosphorylation sites in the various domains on all the isoforms of Tau: (A) Figure 4A shows the distribution of Tau all the phosphorylation sites in the various domains as determined by Hanger et al. in 2007 using mass spectroscopy. The different Tau domains are also colour coded for easy identification; green (N-Terminal domain), gray (Proline-rich domain), light blue (Microtubule binding domain), and dark blue (Terminal domain). All the major phosphorylation sites that promote Tau aggregation or detachment from microtubules are shown in yellow.

(B) Figure 4B also shows all six spliced isoforms of Tau in the CNS. The alternatively spliced exons that lead to the formation of all the six isoforms are identified as red boxes. Vertical red lines at the top of Figure 4B represent the phosphorylation sites in all the isoforms and spots the phosphosites listed in Figure 4A are located in Figure 4B. Image adopted from Morishima-Kawashima *et al,* (1995)[90].

The phosphorylation of other sites has been strongly linked to the pathogenesis of AD[91]. It is still unclear whether elevated phosphorylation levels are required to induce Tau aggregation *in vivo* and the extent to which phosphorylated Tau epitopes are neurotoxic.

1.4 Tau aggregation

Aggregation triggers conformational changes in Tau[92], and this is the primary cause of neurodegeneration in neurodegenerative diseases. *In vitro* studies have shown that hyperphosphorylated Tau co-aggregates with native Tau, deactivating the functional molecules' in native Tau[93]. The overall aggregation of Tau into NFTs causes loss of cognitive and motor functions.

Although the Tau aggregation process is not well understood, several studies have tried to understand it by investigating the cause of aggregation from the perspective of the different domains on the protein. With native Tau being very soluble, the movement of the C-Terminal domain away from the MTBRs, causes it to associate with the N-Terminal region, making Tau adopt an amyloid-prone conformation[94], promoting aggregation.

1.4.1 Mechanisms of protein aggregation

The mechanisms for Tau aggregation are still being studied and not adequately understood. Rather, broad protein aggregation mechanisms that have been proposed, and Tau protein is believed to also follow these propositions. It also important to note that a combination of two or more of the mechanisms to be discussed leads to the formation of the Tau protein aggregates observed. Five protein aggregation mechanisms are discussed below.

The first is the reverse association of monomeric proteins mechanism. This mechanism is based on the intrinsic ability of the native monomeric protein to self-associate and dissociate reversibly[95]. However, over time, these reversible associations form small or large oligomeric structures that are irreversible[96].

With some native monomeric proteins not having an inherent ability to associate and dissociate reversibly, a second mechanism was proposed. Here, when a protein assumes an altered conformation, they show a high tendency to associate. And via this process they aggregate into highly ordered oligomers[97]. This mechanism is usually followed when stress is applied to the protein sample in a form of heat or temperature change.

The third, which is the primary nucleation mechanism is the most widely used to explain the formation of fibrils and filaments as seen in Tau proteins[98]. Before a protein aggregates following this mechanism to be discussed, the critical nucleus, which is the building block for the oligomerization process has to be formed. No visible aggregates are observed, until after the critical nucleus forms. This time is called the lag phase. It is after this phase that visible oligomerization and amyloid fibril formation is observed.

The fourth which is the secondary nucleation mechanism is preceded by the primary nucleation mechanism[99]. Fibrils of smaller sizes, formed via primary nucleation act as nucleus for further oligomerization[100]. Morphological structures and surface area of the fibrils act as kinetic traps for the further oligomerization[101].

The last which is the 3D domain swapping is another striking mechanism for amyloid fibril formation. In this mechanism, identical proteins replace their domain with

an identical domain of another subunit. The swapped domain may be an alpha helix, β-sheet, or an entire tertiary globular domain. The result is usually an intertwined dimer or a highly ordered oligomer[102]. Ribonuclease A adopt this mechanism to form amyloid like fibrils[103].

1.4.2 Methodologies for aggregation detection

Due to the nature of protein interactions, protein aggregation may occur at various points throughout the lifetime of a protein. Tau protein aggregation properties have been studied with numerous techniques, including electron microscopy, SDS-PAGE, dynamic light scattering, sedimentation, Circular dichroism, Fluorescence spectroscopy, (FT-) infrared spectroscopy, Raman spectroscopy, Nuclear magnetic resonance spectroscopy, and birefringence following the binding of dyes such as Congo red, thioflavin T (ThT1), or thioflavin S (ThS), among others. The techniques mentioned above are currently used for protein aggregation and describe the presently employed analytical techniques and emerging technologies for aggregate detection, characterization, and quantification. Each analytical approach has its specific advantages but also has its limitations. The limits of detection and the possibility of creating artifacts through sample preparation by inducing or destroying aggregates need to be considered with each method used.

1.4.2.1 Fluorescence spectroscopy

Fluorescence spectroscopy is a rapid, non-destructive technique that allows for protein aggregation detection [104][105]. Here, the fluorescence intensity recorded equals the level of protein aggregation. The fluorescence intensity of the aggregated protein is measured by either exciting the electrons of the dye added to the protein

samples or by measuring the fluorescent intensity of intrinsic fluorescent amino acids such as tryptophan. The fluorescence signals measured is based on the dye's sensitivity to solvent polarity, viscosity and temperature.

The most frequently used extrinsic dyes for protein aggregate characterization are 1-anilinonaphthalene-8-sulfonate (ANS) and 4,4′ -bis-1- anilinonaphthalene-8-sulfonate (Bis-ANS), Nile Red and SYPRO Orange. Bis-ANS and ANS hardly fluoresce in aqueous environments but strongly fluoresce when interacting with hydrophobic sites. Hydrophobic interactions and electrostatic interactions have both been discussed as the mechanism by which of ANS binds to proteins. For Bis-ANS, hydrophobic interactions are seen as the most dominant[106]. However, the major limitation of using of using Bis - ANS is experienced due to its larger size, which causes fluorescence to be inhibited as a result of steric hindrance.

Another class of dyes called molecular rotors, used extensively for protein aggregates characterization show significantly increased fluorescence intensities due to the decrease in the torsional relaxation of the molecules they are made of. These molecular rotors rotate freely in solution, however changes to the micro-environment constrict the dye's movement, causing them to fluorescence. One such example is Thioflavin T (ThT). A novel protein aggregation dye, ProteoStat manufactured by Enzo Life Sciences Inc., which I used in this dissertation for my studies is also a molecular rotor. The ProteoStat dye, in the absence of protein aggregates, spins in solution and does not fluorescence. But, in the presence of protein aggregates, the dye slides into the exposed cavities of the aggregated protein, constraining the rotation of the dye, causing it

to fluorescence[107]. It is currently the only commercial dye marketed for protein aggregate detection for visible to sub-visible aggregates.

1.4.2.2 Transmission electron microscopy

Transmission electron microscopy has a wide range of application in the physical, chemical, and biological sciences. In this analytical technique, a beam of electrons is transmitted through a specimen to form an image. The specimen is usually an ultrathin section less than 100 nm thick or a suspension on a grid. An image is formed from the interaction of the electrons with the sample as the beam is transmitted through the specimen. The image is then magnified and focused onto an imaging device, such as a fluorescent screen, a layer of photographic film, or a sensor such as a charged coupled-device.

Transmission electron microscopes are capable of imaging at a significantly higher resolutions, owing to the smaller de Broglie wavelength of electrons. This enables the instrument to capture fine detail of aggregated proteins such as Tau fibrils and filaments. At lower magnifications, TEM image contrast is due to differential absorption of electrons by the material due to differences in composition or thickness of the grid. At higher magnifications, complex wave interactions modulate the intensity of the image, requiring expert analysis of observed images. Alternate modes of use allow for the TEM to observe modulations in chemical identity, crystal orientation, electronic structure, and sample-induced electron phase shift, as well as regular absorption-based imaging. The TEM images below were adopted from the Rankin *et al*, (2008) paper “Pre-assembled tau

filaments phosphorylated by GSK-3β form large tangle-like structures" to emphasis lower and higher resolution TEM images[108].

.

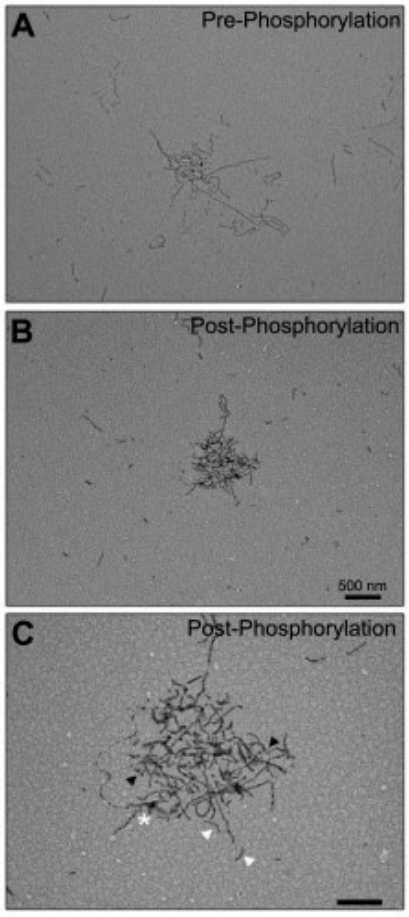

Figure 1.4: TEM micrographs showing tangle-like filaments after GSK-3β phosphorylation: Micrographs of image A and B were taken at 20,000 ×. The scale bar of 500 nm on image B is applicable to Image A. Panel C is the same field of Panel B but was imaged at 50,000 × at a scale of 250 nm. Tangle characteristics, such as non-touching filaments (△), branching filaments (*) and tendril-like fibers between longer filaments (▲) are identified on the micrograph.

The TEM images A and B above shows images were taken at a lower resolution and image C taken at a higher resolution. This goes to affirm how owing to the smaller de Broglie wavelength of electrons, finer details of fibrils and filaments are captured.

1.5 Dissertation research

Tau protein aggregation is one of the key features common to Tauopathies, a group of neurodegenerative diseases including Alzheimer's disease (AD). Although Tau is always found aggregated and hyperphosphorylated in these pathologies, the precise role of the one or two 29-member amino acid N-terminal repeat and phosphorylation in the Tau aggregation process still remains to be established.

Although Amadoro *et al*. (2004)[109] established the physiological role of the N-terminal imperfect repeats in the N-terminal domain, his research did not focus on how these repeats can affect Tau protein aggregation. After confirming the ability of the expressed and purified Tau isoforms to form fibrils and filaments (Chapter 2), the ability the various isoforms to co-exist based on their N-terminal repeats and the role of the N-terminal repeats in Tau aggregation promoting neuronal cell death was investigated in Chapter 3.

With Tau fibrillization being at the center of loss of neuronal communication in AD, there is the need to investigate which kinases or kinase combinations cause Tau to misfold, leading to the improper neuronal communication. Multi-site phosphorylation occurs in NFT-Tau, and this is as a result of the catalytic activities of the different kinases, although the functional significance of this phenomenon is not completely understood. Three main kinases classes phosphorylate Tau; namely the serine and threonine proline-directed protein kinases, serine and threonine non-proline directed

protein kinases, and protein tyrosine kinases. GSK-3β, MARK4 and Fyn, the three protein kinases used in this dissertation were each selected from these three classes. With over 85 putative sites on Tau that can be phosphorylated, individual phosphorylation at specific serine/threonine/tyrosine residues elicits a biological effect that corresponds to a unique physiological role [110][111]. GSK-3β was extensively studied in this dissertation since recent evidence has confirmed its role in signaling is essential for the coordination of progenitor cell proliferation and differentiation during brain development[112]. Of the 36 sites on Tau that GSK-3β has been identified to phosphorylate [113], and the main phosphorylation sites identified are Ser199, Thr231, Ser396, and Ser413[114]. These sites have been shown to play a key role in facilitating the function of multiple signaling molecules activity (including DISC1, Par3/6, and Wnts) that are key in regulating neuronal development[115]. This makes GSK-3β a key kinase to study extensively and understand its role in tauopathies, in my case AD. MARK4, a non-proline directed serine-threonine kinase that phosphorylates MAP proteins including Tau was also studied extensively studied in this dissertation. MARK4 plays a significant role in the microtubule dynamics, cell polarity, cell cycle, neuronal differentiation, and programmed cell death[116]. MARK4 phosphorylates amino acids in the microtubule-binding region of Tau and regulates the transition between stable and dynamic microtubules[117]. My research into MARK4 was prompted by the observation of the phosphorylated KXGS motifs in Tau protein and their strong effect on microtubule affinity. Fyn exerts several distinct functions such as axon-glial signal transduction, oligodendrocyte maturation and myelination, and it is implicated in neuroinflammatory

processes. Based on these established findings, research into Fyn to understand it's role in neurodegenerative diseases, particularly Alzheimer disease is critical[118].

Gamblin *et al.* (2007) phosphorylated Tau with GSK-3β, a serine and threonine proline-directed protein kinase[119]. Although the phosphorylation of Tau with GSK-3β did not yield much aggregation, they observed the formation of tangle-like filament characteristics of AD[119]. With Goedert *et al.* (1996) having discovered the co-localization of heparin or heparan sulfate to Tau preventing Tau from binding to microtubules inducing microtubule disassembly[120], Gamblin *et al.* (2008) further tested the role arachidonic acid, also a protein aggregation inducer like heparin played in neurofibrillary pathology[108]. Phosphorylation of Tau by GSK-3β either prior to or following polymerization of Tau with heparin promoted polymer/polymer interactions that result in stable clusters of Tau filaments[108]. Based on these findings others also tested out other kinases. In Chapter 4, I investigated the single and combinatorial phosphorylation properties of all three kinases (GSK-3β, MARK4 and Fyn) with or without heparin.

Although Tau protein is flexible, NFT-Tau is highly insoluble. During the course of NFT formation, hyperphosphorylation causes Tau protein progressively assumes a rigid conformation. Elucidating the structural factors that drive Tau pathology is crucial to understanding the shift in conformational bias induced by hyperphosphorylation. Wilson *et al.* (2015), however, studied GSK-3β phosphorylated Tau using Time-Resolved ElectroSpray Ionization Mass Spectrometry - Hydrogen/Deuterium Exchange (TRESI-MS HDX) to gain insight into the structure and conformation of differentially phosphorylated Tau proteins[121]. HDX-MS, unlike other protein structure and

conformational studies techniques, provides a detailed picture of the residual structure of Tau and the shifts in conformational bias induced by hyperphosphorylation[122]. By comparing the native and hyperphosphorylated ensembles of Tau, specific conformational preferences that can easily enhance Tau protein aggregation can be identified. GSK-3β hyperphosphorylation resulted in the release of the Tau's global fold, causing the development of new intramolecular interactions in the MTBD. This significantly increased the exposure of the second hexapeptide (H2) repeat; however, the first hexapeptide (H1) repeat, which has also been implicated in amyloidogenesis, remained largely sequestered[121]. To identify the role other kinases, play in the structural and conformational changes observed in Tau pathology, I dedicated Chapter 5 to study GSK-3β, MARK4 and Fyn single and sequentially phosphorylated Tau proteins using HDX-MS.

CHAPTER TWO

EXPRESSION AND PURIFICATION OF ALL SIX ISOFORMS OF TAU

2.0 Introduction

Recombinant Tau has been shown to closely mimic the essential properties of naturally occurring human Tau protein[123]. Hence, recombinant human Tau is used extensively to study the molecular, biochemical, and cellular aspects of Tau-related diseases known as Tauopathies. Recombinant Tau also makes high yield pure Tau, a critical substrate for all the *in vitro* tauopathy studies done, ranging from (i) Tau-Tau interactions leading to its aggregation into straight filaments (SFs) and paired helical filaments (PHFs) that are similar to those isolated from brains of patients with Tauopathies[124] (ii) Tau – microtubules (MTs) interactions to understand how Tau polymerizes MTs, and also to[125] (iii) the interaction of misfolded Tau proteins with normal Tau proteins causing the cellular spread of their prion-like character[126][127]. Expression and purification of Tau, like most proteins that self-assemble, are usually complicated by high protein aggregation and truncation tendencies, making it very challenging and expensive to purify and store.

Therefore, in this chapter, I sought to identify parameters that would ensure optimal expression and purification steps for the six Tau isoforms (352 – 441). The following expression conditions were investigated: the choice of *E. Coli* host strain to use, the induction temperature, duration of induction, IPTG concentration to use and the storage buffer that would help to maintain the integrity of the protein before and after the cleavage of the his-tag from the C-terminal domain (CTD). After the optimization stage,

the newly established protocols were employed to do large-scale protein expression and purification for all the Tau isoforms.

Expression and purity check for all the Tau isoforms after the purification process was assessed by SDS – PAGE and Western blots. Image analysis software's were also employed to assess the Tau isoforms sample purity.

2.1 Materials

All the buffers and reagents were prepared with reagent-grade chemicals and double distilled water that was further purified with a Smart2Pure 6 UV/UF system (ThermoFisher, Waltham, MA, USA). All the solutions after preparation, were filtered with a 0.22- μM PES filter. The stock solution of A1 buffer was prepared to have final concentrations of 20 mM NaPi pH 7.5, 300 mM NaCl, 30 mM Imidazole, and 1 mM DTT, 5% (v/v) glycerol. The stock solution of A2 buffer was prepared to have final concentrations of 20 mM NaPi pH 7.5, 30 mM NaCl, 30 mM Imidazole, and 1 mM DTT, 5% glycerol and the stock solution of B1 buffer used to detach the protein of choice from the nickel beads was also prepared to have final concentrations of 20 mM NaPi pH 7.5, 300 mM NaCl, 2M Imidazole, 1 mM DTT, 5% (v/v) glycerol. The codon-optimized constructs used to express the recombinant human Tau (amino acid residues 352 to 441) in *E. coli* was synthesized by VectorBuilder Inc. (Chicago, IL, USA). NiCo21(DE3), Acella and Rosetta 2 competent cells the DNA plasmids were transformed into was purchased from New England Biolabs (Ipswich, MA, USA). Odyssey blocking buffer was purchased form Li-Cor Biosciences (Nebraska, USA). Laemmli sample buffer was purchased from Bio-Rad Laboratories (Hercules, CA, USA).

2.2 Methods

2.2.1 Transformation of Tau plasmid DNA into NiCo21 (DE3), Acella and Rosetta 2 competent cells

Recombinant Tau plasmid DNA extracted from the six Tau isoforms were transformed into competent cells. 1.5 µL (~85 ng/mL) of isolated Tau (381 - 441) plasmid DNA was added to 50 µL of NiCo21 (*DE3*) cells (New England Biolabs, Ipswich, MA, USA), and that of Tau 352 was added to Acella and Rosetta 2 competent cells (New England Biolabs, Ipswich, MA, USA). The competent cells and plasmid DNA mixtures were incubated on ice for 30 min. The cells were heat-shocked at 42 °C for 1 min and incubated on ice for 3 mins. 400 µL of super optimal (SOC) medium (ThermoFisher Scientific, USA) was added, and the mixtures were incubated at 37 °C for 1 h. 100 µL of the NiCo21 (*DE3*) and Acella competent cells with the plasmid DNA mixtures were plated on Lysogeny broth (LB) agar supplemented with Carbacillin (50 µg/mL) while the Rosetta 2 competent cells with Tau plasmid DNA mixture was plated on Lysogeny broth (LB) agar supplemented with both Carbacillin (50 µg/mL) and Chloramphenicol (34 µg/mL). The plates were incubated overnight at 37 °C. The codon-optimized constructs used to express recombinant Tau (amino acid residues 352 to 441) in *E. Coli* cells were synthesized by Vector Builder Inc. (Chicago, IL, USA).

2.2.2 Expression of the Tau constructs (352 - 441)

Medium to large single colonies from NiCo21 and Acella plates were inoculated into 10 mL LB broth supplemented with 10 µL of Carbacillin (50 µg/mL). In contrast, the Rosetta 2 colonies were inoculated into 10mL LB broth supplemented with 10 µL each of

Chloramphenicol (34 μg/mL) and Carbenicillin (50 μg/mL). The cultures were grown overnight at 37 °C. After 24 hours, 1 mL of the overnight cultures were inoculated into 50 mL LB broth supplemented with 10 μL of Carbenicillin and grown at 37 °C with 250 rpm agitation. The cultures were grown until an OD_{675} = 0.4–0.6 was reached. The addition of 50 μL isopropyl β-d-thiogalactoside (IPTG 1mM) to the cultures induced the expression of Tau. The culture was allowed to grow overnight. A 10 mL sample was aliquoted from the cultures pre IPTG and labeled negative IPTG samples. Both pre IPTG and post IPTG cultures were centrifuged at ~6,000×*g* for 5 min. The soluble (supernatant) fraction was pipetted into an Eppendorf tube for sodium dodecyl sulfate-polyacrylamide gel electrophoresis (SDS PAGE). The resultant pellet was resuspended in 150 μL Tris HCl (10 mM) and sonicated (10% power, 5 s), and centrifuged (~6,000×*g* for 5 min). Tau expression in the soluble and insoluble fractions of pre-IPTG and post IPTG cultures were analyzed by SDS-PAGE and Western blotting (WB).

2.2.3 SDS-PAGE and Western Blot

To access Tau protein expression in the various Tau constructs, SDS-PAGE and WB were run. The Tau protein samples (352 - 441) from the soluble and insoluble fractions were loaded and separated on standard 10% SDS-PAGE gel. The samples were analyzed against a protein ladder from New England BioLabs (Molecular weight range = 15 – 250 kDa) for 45 mins at 180 V in a BioRad Mini-PROTEAN Tetra system (BioRad Laboratories, California, USA). The gels were stained with a Coomassie-based stain (Cambridge, UK) overnight at room temperature (RT). The gels were imaged with a ChemiDoc Touch imaging system (BioRad Laboratories, California, USA). To identify

Tau-positive bands, WB was performed prior to antibody detection as described below. For the WB, after the Tau protein samples were separated on 10 % polyacrylamide gel, the gels were equilibrated in Towbin buffer (25mM Tris base, 190mM Glycine, 20% (v/v) methanol) for 60 minutes. The proteins were then transferred from the gel to Immobilon®- FL PVDF membrane from Millipore Sigma. After the transfer, the remaining protein-binding sites of the membrane were blocked with Odyssey® Blocking Buffer (Li-Cor Biosciences) for 60 mins at RT. After blocking the protein sites with the blocking buffer, the blots were incubated overnight with rabbit monoclonal anti-his-tag antibody (1:1000 dilution) at 4 °C. After the overnight incubation, the unbound antibody was washed off three times for 15 mins with 1x TBS containing 0.05 % Tween 20 before the blots were further incubated with a secondary antibody IRDye® 800 Conjugated Affinity Purified Goat anti-rabbit IgG (1:5000 dilution) for 45 minutes at RT. The blots were washed three 3 x 15 mins with 1x TBS containing 0.05 % Tween 20 and 3 x 15 mins with 1x TBS. The blots were visualized with Li-Cor's Odyssey Infrared Imaging System, and Li-Cor's Image Studio 2.0 software to capture images and for densitometric analysis.

2.2.4 Large-scale expression of Tau constructs (352 - 441)

Large scale cultures for Tau expression were produced by inoculating 4L of terrific broth (TB) with the overnight cultures using the expression parameters described above. The overnight cell growth was done at 16°C. The cells from the C-terminal His-tag Tau constructs 352 – 441 were harvested by centrifugation at 4000 rpm for 90 mins at 4°C. The cell pellets were resuspended in a lysis binding buffer {(20 mM NaPi pH 7.5,

300 mM NaCl, 30 mM Imidazole, 1 mM DTT, 5 % glycerol +1 % NP40} and 1mM PMSF. The suspended pellets were sonicated on ice at 45% amplitude using a Fisher 505 dismembrator (Fisher Scientific, Hampton, NH, USA). After sonicating for 30 min (15 s on, 45 s off), the cell lysates were heated for 90 mins at 75^0C. The cell lysates were clarified by centrifugation (18,000 rpm at 4 °C) for 90 mins. The supernatants were then filtered through a 0.45 μm PES membrane. The C-terminal His-tag Tau protein of the various isoforms were isolated from their crude extracts using affinity chromatography.

2.2.5 Protein purification using affinity Chromatography

A Ni-NTA column (GE Healthcare, Chicago, IL, USA) was used for the affinity chromatography step of the large-scale purification process. The filtered supernatant was mixed with Nickel beads for 15 minutes and then run through the column. The filtrate was collected as flow through (FT). Several washes were done, and the fractions collected for SDS-PAGE and WB. The first of three washes using 75 mL of A1 buffer was collected and labelled Wash 1 (W1). The first of three washes using 75 mL of A2 buffer was collected and labelled Wash 2 (W2). The final wash was done using 25 mL of the B1 buffer was collected and labeled Elute (El). This final wash detaches the C-Terminus Tau 441 from the Nickel beads. The His_6- tag was cleaved by incubating the elute containing the protein of choice (Tau 352 - 441) with TEV protease at room temperature for 72 h in the ratio of 1 mole of TEV protease to 10,000 moles of Tau while dialyzing into storage buffer (20 mM NaPi pH 7.5, 300 mM NaCl, 2 M Imidazole, 1 mM DTT, 5% glycerol). The protein in the Vivaspin 20 dialysis bag contained the dialyzed Tau protein in storage buffer. The Vivaspin 20 dialysis bag was selected based on the molecular weight of the protein been cleaved (5 kDa cut off). After cleavage, a second

affinity purification was done to separate the cleaved His_6 - tag Tau and the TEV protease.

At each step of the purification process, aliquots were taken for SDS-PAGE and WB analysis. Protein concentration and purity were estimated using the Bicinchoninic acid assay (BCA) (G-Biosciences, Missouri, USA) and SDS-PAGE, respectively.

2.3 Results and discussion

In order to avoid the purchase of Tau protein for my experiments from commercial sources, I expressed and purified all the six Tau isoforms using E. *Coli* cells. Buffers of different imidazole concentrations were used at the different stages of the purification process. Five different samples were saved at each step of the affinity purification process. They were labelled supernatant (SNT), flow through (FT), wash1 (W1), wash 2 (W2) and elution (EL). These samples collected were separated on a 10% SDS – PAGE alongside a protein ladder. This was done to access the purity of all the six Tau isoforms expressed. All the gels run confirmed the successful expression and purification of the six isoforms of Tau (352 - 441). Although the molecular weights of the isoforms range from 36.8 – 45.9 kDa, they run a little higher on the gels.

Recombinant Tau 441, the longest isoform of Tau expressed using *E. Coli* cells was purified by affinity chromatography. An SDS-PAGE was later run to confirm the sample purity. Figure 2.1 shows an elution (EL) lane with a single, clean, intense band indicating t Tau 441 expression and the cleanliness of the gel shows the absence of contaminants after the purification stage.

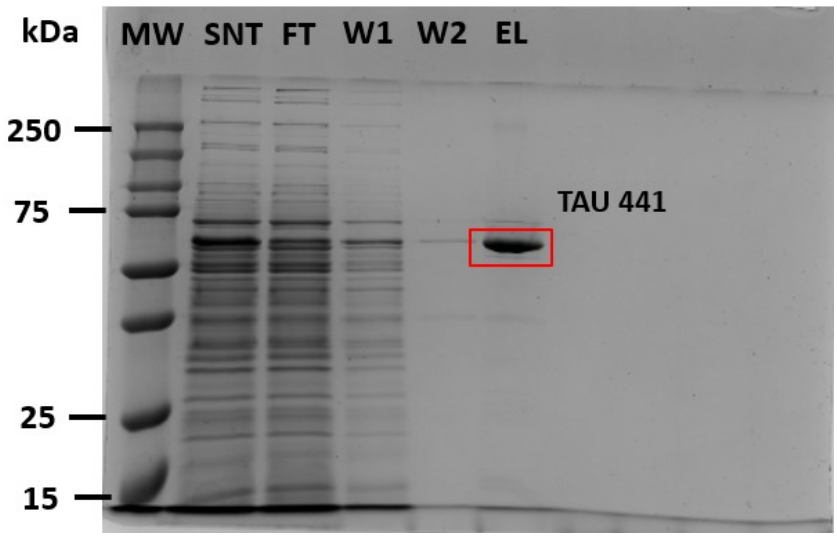

Figure 2.1: SDS-PAGE showing expressed and purified Tau 441: The gel is an SDS - PAGE analysis showing expressed and purified Tau 441 from E. Coli cells via affinity chromatography. The first lane contains molecular weight marker. Lanes 2 through to 6 contains the supernatant (SNT), flow through (FT), wash 1 (W1), wash 2 (W2) and elution (EL). After several washes with A1 buffer and A2 buffer, the elution buffer (B1) high in imidazole concentration was used to detach Tau 410 from the nickel beads.

. After scanning the gel with the ChemiDoc Touch imaging system, the purity level of Tau 441 was quantified using the Image Lab 6.0 from BioRad (an image analysis software). Purified recombinant Tau 441 had a purity level above >90%.

Tau 412, the 1N4R isoform expressed by NiCo21 cells was also purified by affinity chromatography. Figure 6 indicates an elution (EL) lane showing a single, strong, clean band of Tau 412. The image analysis software, Image Lab 6.0 from BioRad also showed the purity level of Tau 412 to be above >80%, comparable to the purity level from rPeptide (Watkinsville, GA, USA).

.The purity level >80% obtained for Tau 412 was also comparable to the purity level obtained after purifying Tau 441.

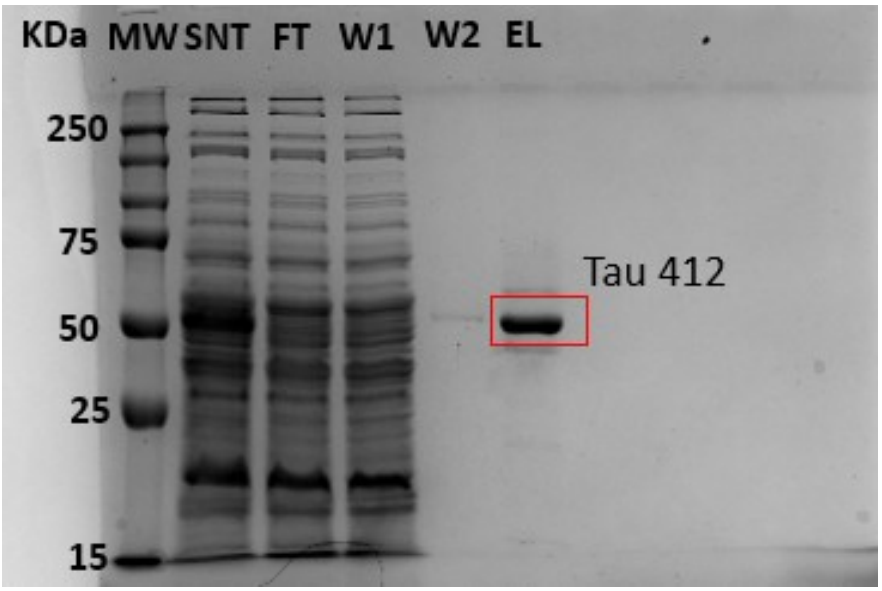

Figure 2.2: SDS-PAGE showing expressed and purified Tau 412: The gel is an SDS - PAGE analysis showing expressed and purified Tau 412 from E. Coli cells via affinity chromatography. The first lane contains molecular weight marker. Lanes 2 through to 6 contains the supernatant (SNT), flow through (FT), wash 1 (W1), wash 2 (W2) and elution (EL). After several washes with A1 buffer and A2 buffer, the elution buffer (B1) high in imidazole concentration was used to detach Tau 412 from the nickel beads.

Tau 410, the 2N3R isoform was expressed in NiCo21 cells. After the expression, Tau 410 was also purified by affinity chromatography. A high imidazole salt buffer was employed at the end of the purification process to elute his-tag Tau 410 from the nickel beads. Figure 7 shows an SDS-PAGE with an elution (EL) lane indicating a single, intense, clean band of Tau 410, indicating the expression and purity of Tau 410. The purity level of Tau 412 was also assessed to be above >80%. This was comparable to the purity level of full-length Tau, Tau 441 and Tau 412 as showed in the SDS-PAGE above.

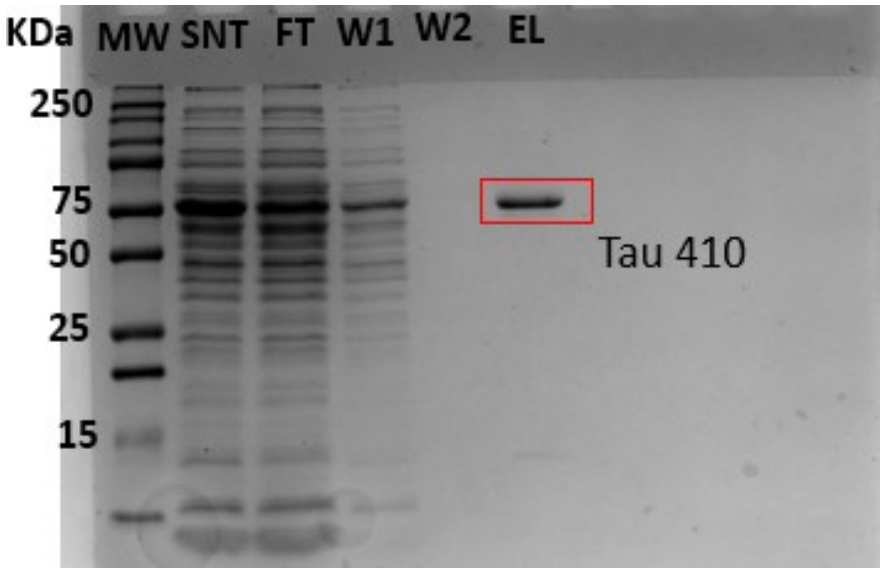

Figure 2.3: SDS-PAGE showing expressed and purified Tau 410: The gel is an SDS - PAGE analysis showing expressed and purified Tau 410 from E. Coli cells via affinity chromatography. The first lane contains molecular weight marker. Lanes 2 through to 6 contains the supernatant (SNT), flow through (FT), wash 1 (W1), wash 2 (W2) and elution (EL). After several washes with A1 buffer and A2 buffer, the elution buffer (B1) high in imidazole concentration was used to detach Tau 410 from the nickel beads.

After the elution of Tau 383 from nickel beads used for the purification process, an SDS-PAGE was employed to assess the expression and purity of the 0N4R isoform expressed by NiCo21 cells. Figure 8 shows an elution (EL) lane also with a single, intense, clean band showing expressed and purified Tau 383. The purity level of Tau 383 was assessed to be above >80%, which is comparable to the earlier expressed and purified isoforms.

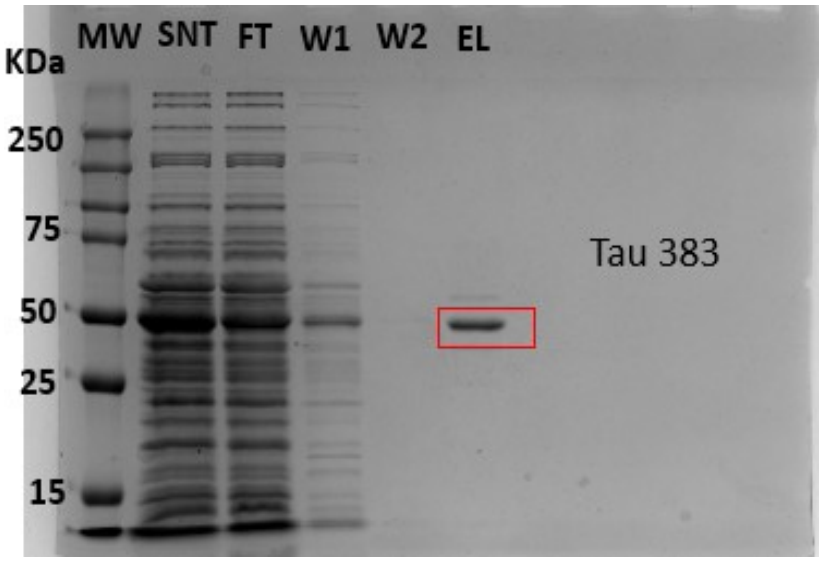

Figure 2.4: SDS-PAGE showing expressed and purified Tau 383: The gel is an SDS - PAGE analysis showing expressed and purified Tau 383 from E. Coli cells via affinity chromatography. The first lane contains molecular weight marker. Lanes 2 through to 6 contains the supernatant (SNT), flow through (FT), wash 1 (W1), wash 2 (W2) and elution (EL). After several washes with A1 buffer and A2 buffer, the elution buffer (B1) high in imidazole concentration was used to detach Tau 383 from the nickel beads.

The SDS-PAGE in Figure 9 shows expressed and purified Tau 381 from *E. Coli* cells. The elution (EL) lane shows a single, intense, clean band showing expressed and purified Tau 381. The purity level of Tau 381 was assessed to be above >80%. Protein purification uses a multistep process aiming to isolate a protein of interest from a diverse mixture utilizing unique physico-chemical characteristics including mass, net charge, isoelectric point, solubility etc . Although Tau 381 is a 3R, the buffers that were used for the washes and extraction of the final protein sample from the nickel beads were the same buffers used for Tau 441 and Tau 412 which are 4R isoforms.

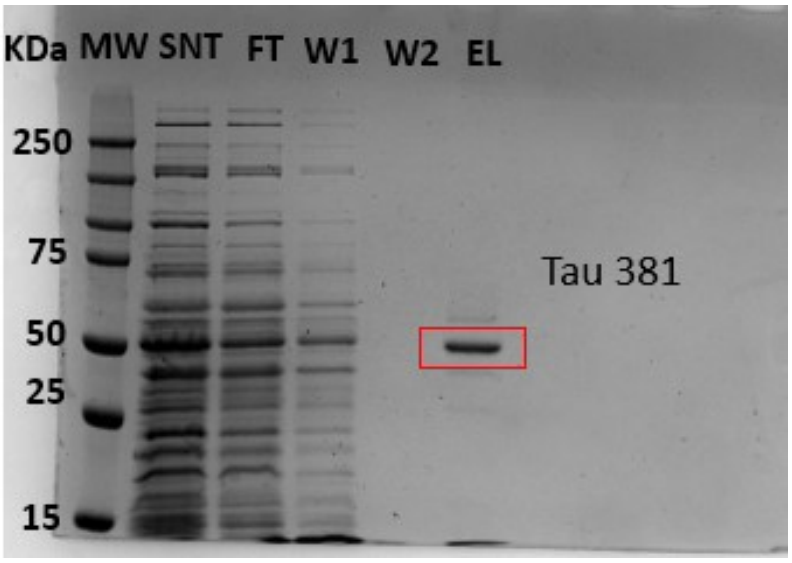

Figure 2.5: SDS-PAGE showing expressed and purified Tau 381: The gel is an SDS - PAGE analysis showing expressed and purified Tau 381 from E. Coli cells via affinity chromatography. The first lane contains molecular weight marker. Lanes 2 through to 6 contains the supernatant (SNT), flow through (FT), wash 1 (W1), wash 2 (W2) and elution (EL). After several washes with A1 buffer and A2 buffer, the elution buffer (B1) high in imidazole concentration was used to detach Tau 381 from the nickel beads.

Tau 352, the shortest Tau isoform was expressed in both Acella and Rosetta 2 cell lines due to the low yield observed in the NiCo21 cell lines used. The 0N3R isoform expressed in Acella and Rosetta 2 was also purified by affinity chromatography. Figure 10 shows elution (EL) lanes of single, intense, clean band of Tau 352 from both Acella and Rosetta 2 cell lines. The purity level of Tau 352 was assessed by the image analysis software, Image Lab 6.0 from BioRad showed Tau 352 bands purity levels to be above >80%.

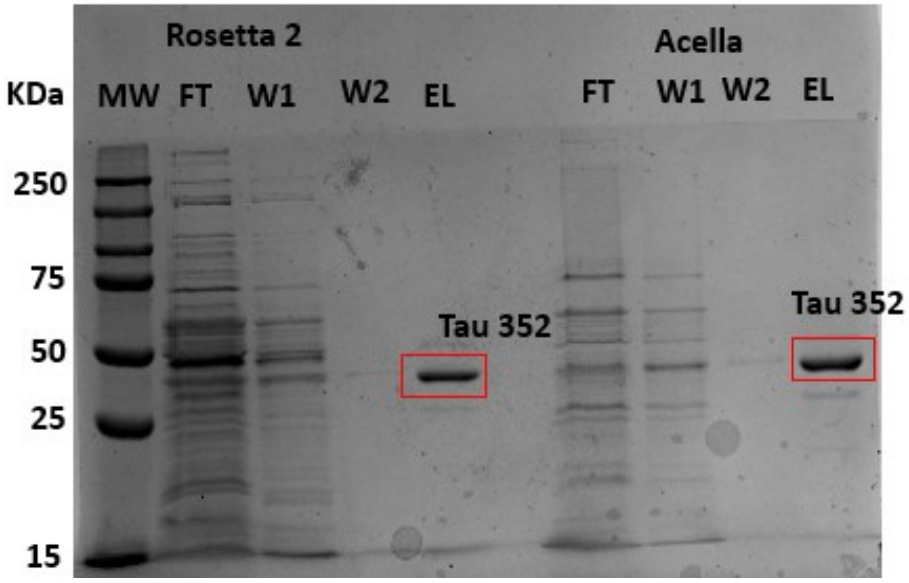

Figure 2.6: SDS-PAGE showing expressed and purified Tau 352: The gel is an SDS – PAGE showing expressed and purified Tau 352 from Acella and Rosetta 2 cell lines via affinity chromatography. The first lane is the protein ladder with known molecular weight marker. Lanes 2 through to 5 contains the flow through (FT), wash 1 (W1), wash 2 (W2) and elution (EL) from the Rosetta 2 cell lines while lanes 7 through to 10 contains the flow through (FT), wash 1 (W1), wash 2 (W2) and elution (EL) from the Acella cell lines. After several washes with A1 buffer and A2 buffer, the elution buffer (B1) high in imidazole concentration was used to detach Tau 352 from the nickel beads. The SDS-PAGE shows a single clean band in the elution lanes which is Tau 352.

All the purified isoforms were subjected to an SDS-PAGE and a Western blot. The SDS-PAGE below is a summary gel showing all the Tau isoforms. The elutions from all the expressed and purified Tau isoforms were loaded and separated on a 10% gel. The protein bands from lanes 2 through to 7 are loaded from the highest number of amino acids (Tau 441, lane 2) to the least number of amino acids (Tau 352, lane 7).

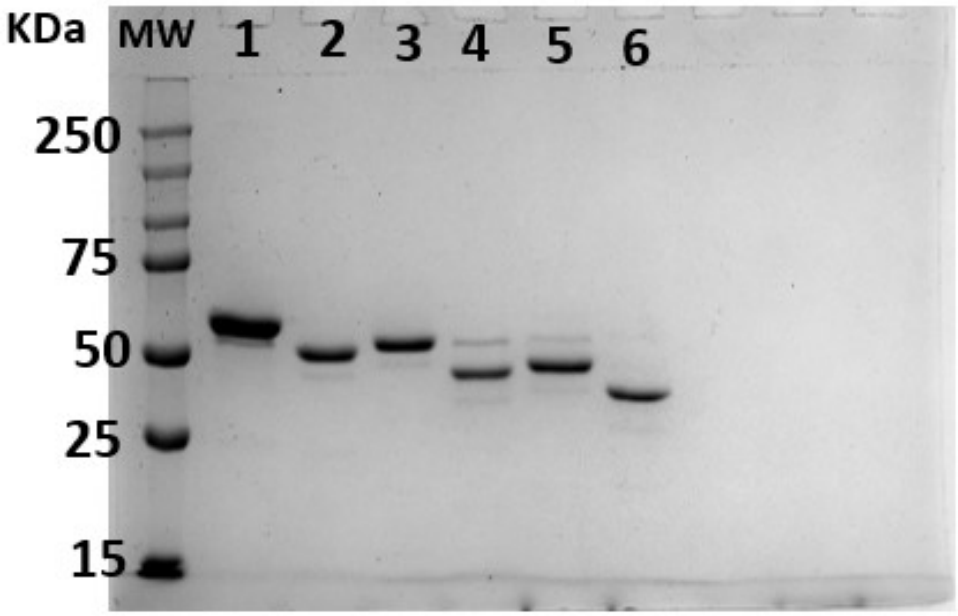

1 = Tau 441 , 2 = Tau 412, 3 = Tau 410, 4 = Tau 383 , 5 = Tau 381, 6 = Tau 352

Figure 2.7: Summary SDS-PAGE of all Tau isoforms: Aliquots of the Tau samples (elutions) collected from the affinity purification process were used for the summary western blot. From left to right: lane 1 is the protein ladder with known molecular weights. Lanes 2 through to lane 7 has the various Tau isoforms loaded from the isoform with the highest number of amino acids (Tau 441) to the Tau isoform with the least number of acids (Tau 352).

WBs were also done to assess the identity of the expressed and purified Tau isoform with an anti – His-tag antibody. Six different blots were run, using Tau samples from the isoform with the highest number of amino acids (Tau 441) through to the isoform with the least number of amino acids (Tau 352).

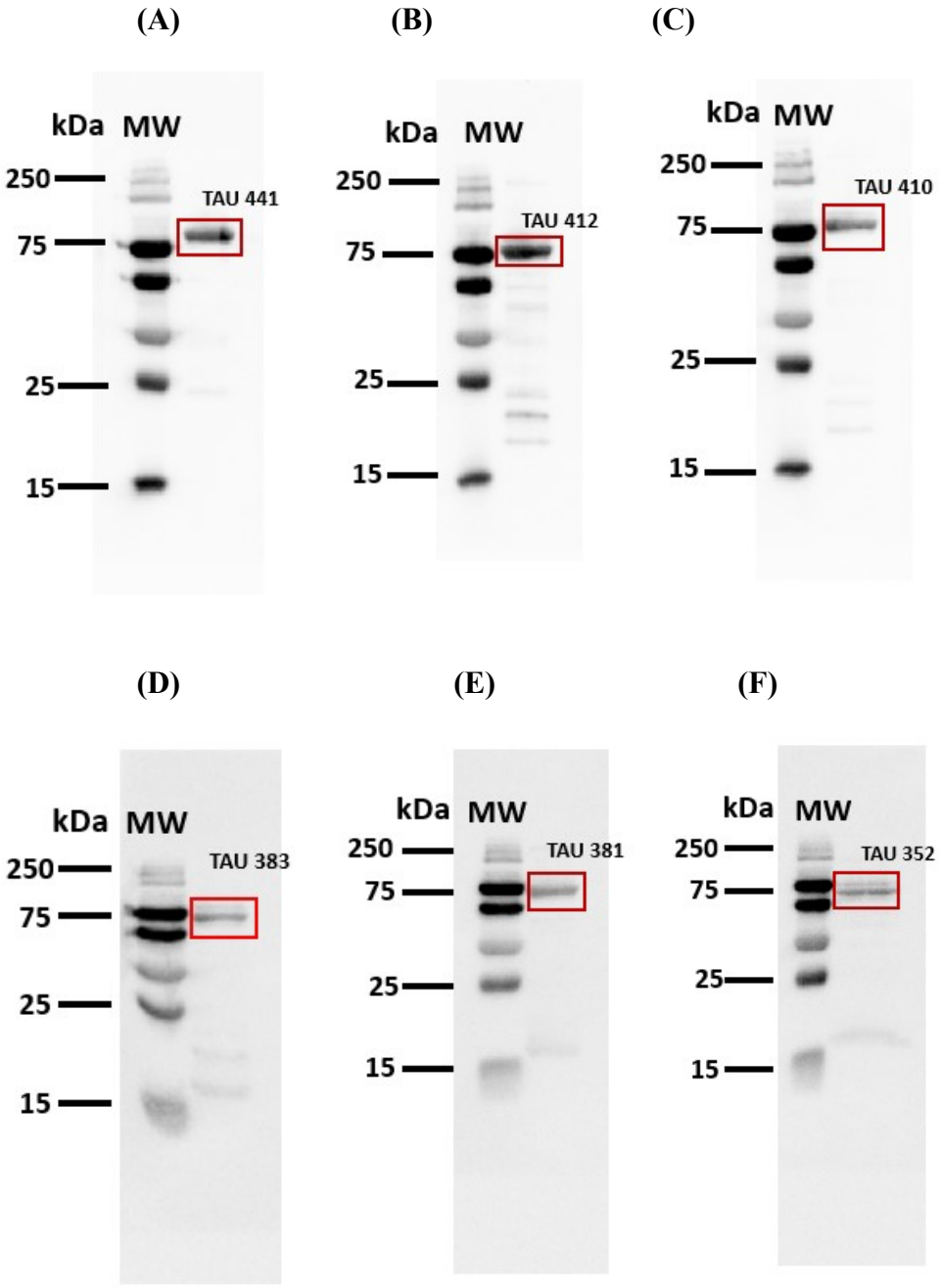

Figure 2.8: Western blots of all the Tau isoforms: Aliquots of the various elutions collected were used for the running of the western blot. From the alphabets A to F above, the first lanes show a protein standard to right: lane 1 is the protein ladder with known molecular weights, lanes 2 through to lane 7 has the various Tau isoforms loaded from the isoform with the highest number of amino acids (Tau 441) to the Tau isoform with the least number of acids (Tau 352). An anti his-tag antibody was used as the primary antibody to detect all the Tau isoforms.

2.4 Conclusions

In this chapter, the expression and purification of all the Tau isoforms via the optimization of the expression and purification process was assessed.

All the Tau isoforms were successfully expressed and purified via the use of affinity chromatography. After the expression of the Tau isoforms, affinity chromatography was employed to separate the protein of interest from their crude extracts. The purity of the Tau samples (elutions) collected at the end of the purification process was accessed on an SDS – PAGE. The gels from the SDS – PAGEs showed that all the Tau isoforms were expressed, and the single, clear, clean bands seen on the gels also showed that the various isoforms were clean. Via the use of an anti-his-tag antibody, WBs was also used to confirm the purified samples were the various Tau isoforms. The image analysis software, Image Lab 6.0 from BioRad was used to evaluate the purity levels of the Tau isoforms. The purity levels for all the isoforms were >80% comparable to commercially Tau from rPeptide (Watkinsville, GA, USA).

CHAPTER THREE

AGGREGATION OF NON – PHOSPHORYLATED ISOFORMS OF TAU

3.0 Introduction

Tau is a MAP protein, and it primarily stabilizes the microtubules. Although Tau is mostly found in the central nervous system, recent advances made to fully understanding the role it plays has led to its discovery outside the CNS. Tau has been identified to have diverse roles in molecular pathways including cell signaling, regulation of genomic stability, binding to and regulating mitochondria proteins, maintaining the cytoskeleton and improvement of synaptic plasticity. Although Tau is naturally a highly soluble unfolded protein, it aggregates into fibrils and filaments under pathological conditions. Tau protein on aggregation deposits inside neuronal bodies destabilizing microtubules and eventually disrupts neuronal communication. The six Tau isoforms differ by the presence of either zero, one, or two N-terminal acidic inserts or three or four C-terminal microtubule-binding repeats[128]. And each isoform is developmentally generated based on the functionality of the neurons it is been expressed in. Tau containing pair helical filaments or neurofibrillary tangles are the closest link with cell loss and intellectual decline. Several technological advancements have been made to understand Tau pathology and this includes the use of MRI of the brain and histopathological analyses.

But to better understand the aggregation properties and morphological changes Tau protein undergoes, the Tau fibrillization process must be usually replicated by adding polyanionic co-factors such as heparin, poly-Glutamine, nucleic acids, etc. and anionic

surfactants such as fatty acids, alkyl sulfate detergents, etc. to recombinant Tau. The fibrils and filaments formed resemble those observed in A.D. brains and other tauopathies[129][130][131][132]. Hence recombinant Tau protein has proven to be a valuable tool to study the biochemistry and effects of Tau aggregation.

In the healthy adult brain, the 3R and 4R isoforms exist at an equal ratio. However, it has been observed that the ratio between the 3R and 4R isoforms are distorted in different tauopathies. The preferential deposition of specific isoforms occurs in different tauopathies because they all influence microtubule dynamics differently. While Tau tangles formed in Pick's disease (PiD) mainly consist of 3R-Tau isoforms, the 4R-Tau isoforms are also mostly aggregated in progressive supranuclear palsy (PSP) and corticobasal degeneration [133][134]. While the cause of these disease-specific Tau isoforms (3R/4R) aggregation differences is unknown, these variations observed may be related to either the degeneration of specific cell populations or aberrant cell trafficking of the individual Tau isoforms.

Microtubule, a major component of the cytoskeleton is formed when tubulin binds to Tau. Tubulin binding to Tau is regulated by the function of the neuron. In AD, all six Tau isoforms (both 3R- and 4R-isoforms) are abnormally aggregated into paired helical filaments.

It still largely remains unknown how each of these Tau isoforms, when aggregated via hyperphosphorylation, affects memory loss and motor function. It is also unknown how the N-terminal imperfect repeats impact aggregation.

This chapter, besides assessing the individual aggregation properties of the six isoforms, the aggregation dynamics of the different isoforms of Tau, with three or four

microtubule-binding repeats but a different number of N-terminal acidic inserts, were evaluated using protein aggregation techniques and transmission electron microscopy method to assess the role of these N-terminal repeats in aggregation. The ability of the six isoforms to co-exist based on their N-terminal imperfect repeats will also be evaluated.

Here, heparin was employed as the anionic polymer to induce aggregation. The different Tau isoforms were aggregated in the presence of heparin. The aggregation properties of all the Tau isoforms were monitored as a function of time using fluorescence spectroscopy. The morphological changes of all the aggregated isoforms were also evaluated with transmission electron microscopy.

3.1 Materials

All the Tau isoforms (1mg/mL, amino acids 352 - 441) used for the aggregation studies were expressed and purified from the Wu laboratory as described in chapter 2. Heparin sodium salt from porcine (53.54 μM) used to induce aggregation was purchased from Sigma-Aldrich (St. Louis, MO, U.S.A.). The 1 % Uranyl acetate (Amresco, Solon, OH, U.S.A.) and 2 % glutaraldehyde (Sigma-Aldrich, St. Louis, MO, U.S.A) were prepared with double-distilled water. Formvar carbon film on 200 mesh nickel grids were purchased from Electron Microscopy Science (Hatfield, PA, USA).

3.2 Methods

3.2.1 Fluorescence spectroscopy

All the expressed and purified recombinant Tau isoforms (Tau 441 - 352) with their His-tag cleaved were aggregated *in vitro* using heparin in a Tau to heparin ratio 4:1. 50μL of all the Tau isoforms (352 – 441) at 1 mg/mL were incubated with 5μL (53.54 μM) of heparin. All the samples were incubated at 37^0C for 14 days, during which a

time-dependent aggregation study was conducted. The extent of aggregation was evaluated on days 3, 5, 7, and 14. This was to assess which day had the most fibrils and filaments formed. 10µL aliquot of the Tau – heparin samples were obtained on the days mentioned above, and 1µL of Proteostat fluorescence dye was added. The aggregated Tau samples (Tau 352 – 441) were incubated in the Proteostat dye at room temperature for 15 minutes. 3µL of the samples were spotted on the H1 Synergy TAKE – 3 BioTek plate reader (BioTek Instruments Inc., VT, U.S.A.). The fluorescence measurements were then taken (Emission 550nM, Excitation 600nM, 25^0C). Experiments were done in triplicates.

3.2.2 Transmission electron microscopy (T.E.M)

Transmission electron microscopy (T.E.M.) was carried out on the F.E.I. Morgagni M268D transmission electron microscope (Eye Research Institute, Oakland University). The aggregated Tau – heparin samples were incubated for 14 days at 37 ºC were used for the T.E.Ms. 10 µL of each sample (aggregated Tau isoforms in the presence of heparin) were deposited on Formvar-carbon coated 200 mesh nickel grids (Electron Microscopy Science, Hatfield, PA, USA) and allowed to absorb for 2 hours in ambient light. The grids were washed three times with 1mL DI water and blotted dry. 2% glutaraldehyde solution (Sigma-Aldrich, St. Louis, MO, U.S.A.) was loaded onto the grid for 5 minutes. This was to stabilize the fibrils and filaments. The grids were rewashed with 1mL DI water, blotted dry, and loaded with 1% Uranyl Acetate (Amresco, Solon, OH, U.S.A.) solution also for 5 minutes. This was to stain the fibrils and filaments for ease of imaging by electron microscopy. The grids were finally washed three times with 1mL DI water, blotted dry, and imaged at 22000x, 56000x, and 140000x magnification to

obtain an overall evaluation of the samples. The grids for each sample were made in duplicates.

3.3 Results and discussion

3.3.1 Aggregation of each Tau isoform (352 - 441)

With the exceptions of full-length Tau or C-terminal Tau mutants forming aggregates at submicromolar concentrations, Tau, like any other amyloidogenic or prion-like protein, does not typically spontaneously aggregate when incubated at physiological pH, temperature, ionic strength, and concentration (1–10 μM)[135]. Typically, full-length Tau protein and their C-terminal mutants are prone to spontaneous aggregation above 200 μM, and this could be attributed to the high concentrations being required to overcome charge repulsion within the peptide or protein. Hence to easily overcome charge repulsion, kinetic and thermodynamic barriers to observe fibrillization in Tau *in vitro* for fibrils and filament studies, polyanionic co-factors are employed. Although the mechanisms through which Tau protein aggregates remain elusive, Kuret *et al.* in 2005 identified a five-step pathway amyloidogenic proteins, including Tau protein, follows to form clusters in the presence of anionic inducers[136][137].

The five-step pathway they proposed are

(1) covalent modifications, such as disulfide bond formation, or from noncovalent intramolecular interactions stemming from partially folded species of Tau are trapped into assembly-competent intermediate.

(2) this assembly-competent intermediate is formed when the kinetic and thermodynamic fibrillization barriers are overcome.

(3) the assembly-competent intermediates clusters into nuclei.

(4) Elongation of competent assembly conformations of Tau.

(5) Lastly, equilibrium is attained between filamentous and all non-filamentous tau species, together with unfolded and partially folded species.

It is assumed that all the Tau isoforms in order to aggregate in the presence of heparin must follow this stepwise pathway. The addition of heparin to the recombinantly expressed and purified Tau isoforms resulted in all the isoforms clustering and forming fibrils and filaments. Esteves-Villanueva *et al.* (2015), a past member of the Martic laboratory-confirmed aggregation in Tau using heparin as an inducer. He further confirmed the formation of fibrils and filaments using transmission electron microscopy[138]. The Martic laboratory also has, on several occasions, confirmed protein aggregation by fluorescence spectroscopy and fibril/filament formation using transmission electron microscopy. The aggregation propensities of the six isoforms were completed within 0 – 14 days. All the Tau isoforms showed an increase in aggregation over time in the presence of heparin, with the highest aggregation been observed usually on the 14^{th} day for all six Tau subtypes. Proteostat aggregation studies, which is arguably the simplest and most widely used technique to monitor Tau aggregation into fibrils and filaments, was used. The Proteostat dye in the presence of the aggregated Tau isoforms gave a characteristic sigmoidal increase in fluorescence intensities that showed the difference between their monomeric and fibril or filamentous states.

Transmission electron microscopy (T.E.M.) is a static imaging technique that complements approaches such as Proteostat aggregation assay, thioflavin-dye fluorescence, and laser-light-scattering spectroscopies by detecting individual Tau fibrils and filaments at nanometer resolution.

To gain insight and to also establish the type of aggregates formed after the recombinant Tau isoforms were induced with heparin, this tool was used. The aggregated Tau samples spotted onto the T.E.M. grids after 14 days all confirmed the formation of fibrils and filaments in all six Tau isoforms. Demonstrating the increase in F.I. recorded as a result of Tau fibrillization.

Protein aggregation is a complex phenomenon, and parameters such as the hydrophobicity of the protein alongside the isoelectric points also contribute to protein aggregation[139]. This was established through numerous kinetic studies on the formation of amyloid fibrils. A decrease in solubility, which leads to aggregation of the unfolded protein molecules, is due to the exposure of hydrophobic groups on the protein. Also, since at the isoelectric point, the net charge on the protein is zero, at this pH, the protein is expected to be most insoluble.

Recombinant Tau 441, typically referred to as full-length Tau, was aggregated in the presence of heparin. Tau 441 showed a gradual increase in fluorescence intensity (F.I.), with the highest F.I observed on the 14^{th} day (Figure 3.1A). Although the difference in F.I. between days 5 and 7 was not significant, a drastic increment in FI was observed between day 7 and 14^{th} day (Figure 3.1A). The calculated p-value of 0.0031 for day 7 versus day 14 indicated that the observed increment was statistically significant. Aggregation of Tau 441 resulted in a change in its morphology. The 14^{th} day aggregated Tau 441 T.E.M images showed the intrinsically disordered protein (IDP) forming fibrils and filaments (Figure 3.1B).

Heparin being anionic upon binding Tau repels the anionic amino acids, causing Tau protein distortion, leading to clustering, which promotes the formation of these insoluble precipitates observed with T.E.Ms.

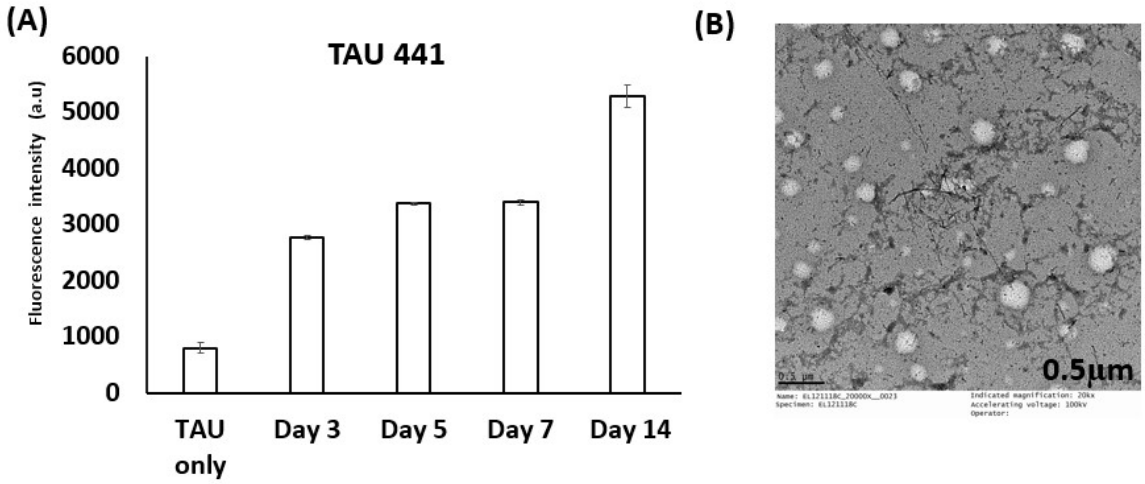

Figure 3.1: Aggregation plot and T.E.M images of Tau 441: Tau 441 was aggregated in the presence of heparin in the Tau to Heparin ratio of 4:1. Aggregation studies were done by measuring the fluorescence intensities of aggregated Tau 441. Tau/Heparin sample was incubated for 14 days, with aliquots been obtained on days 3, 5, 7, and 14 for analysis. Measurements were done in triplicates. Figure 3.1A shows a gradual increase in aggregation of Tau 441 over time, with the highest aggregation of Tau 441 observed on the 14^{th} day. Aggregated Tau 441 samples from Day 14 were used for the morphological studies. Tau 441 showed fibril and filament formation after 14 days of incubation, as observed in Figure 3.1B. {Graph = Mean ± SD, n value = 9, paired t test : Day 7 vs Day 14 (p value = 0.0031)}.

Tau 412 similarly showed a gradual increase in the F.I., with the highest recorded on the 14^{th} day (Figure 3.2A).

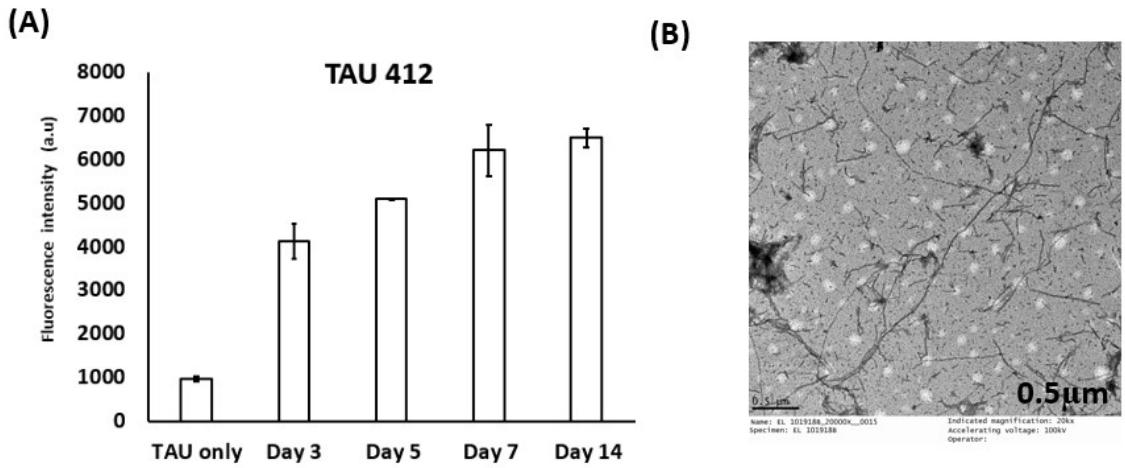

Figure 3.2: Aggregation plot and T.E.M images of Tau 412: Fluorescence aggregation assay was employed to evaluate the aggregation property of Tau 412. An aliquot of Tau 412 was aggregated with heparin in a Tau to Heparin ratio 4:1 at 37 ºC. All the measurements done on each day were done in triplicates. Figure 3.2A shows a gradual increase in aggregation of Tau 412 over time, with aggregation leveling off on the 7th day. The change in Tau 412 morphology was shown by forming very clear and distinct fibrils plus filaments, as shown in Figure 3.2B. {Graph = Mean ± SD, n value = 9, paired t test : Day 7 vs Day 14 (p value = 0.6135)}.

Unlike Tau 441, where a drastic increment in F.I. was observed from day 7 to day 14 (Figure 3.1A), in Tau 412, the aggregation intensities started to level off by day 7 through 14 (Figure 3.2A). The calculated p-value of 0.6135 for day 7 versus day 14 showed the difference in F.I observed on these days was not statistically significant. The 14th day aggregated Tau 412 T.E.M grids also showed the formation of very clear and distinct fibrils and filaments (Figure 3.2B), consistent with the morphological changes observed in Tau 441 (Figure 3.1B). Although Tau 441 has 2 N-terminal repeats and Tau 412 has 1 N-terminal repeat, both isoforms in the presence of heparin, formed of fibrils and filaments.

In Tau 410, the highest F.I. was also observed on the 14th day (Figure 3.3A), just like Tau 441 and Tau 412. Unlike the first two isoforms aggregated, the F.I. of Tau 410 started to level off from day 3 through day 7 (Figure 3.3A) with the highest aggregation observed on the 14th day. With a calculated p-value of 0.0067, the observed increment in F.I on day 14, identified as the highest for the 2N3R isoform (Tau 410) was not due to chance.

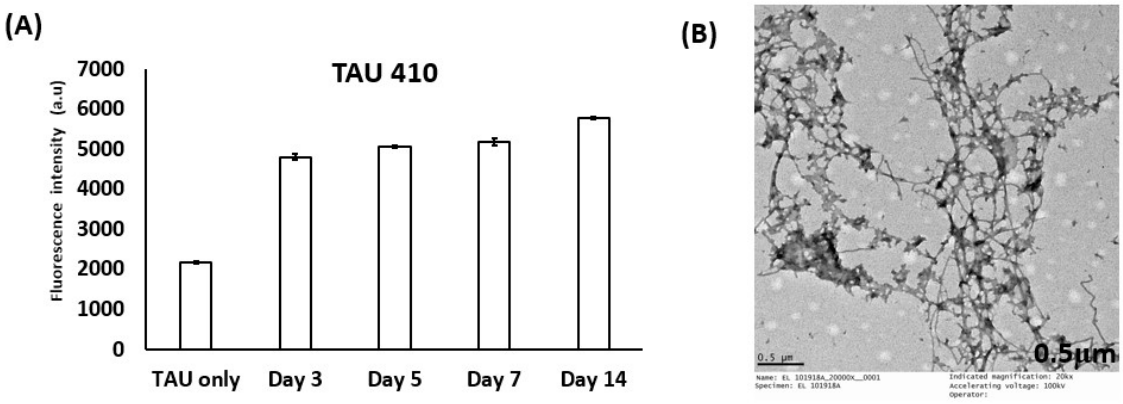

Figure 3.3: Aggregation plot and T.E.M of Tau 410: Tau 410 aggregation propensity was monitored by measuring the fluorescence intensities of aggregated Tau 410 using Proteostat fluorescence dye. Samples were incubated at 37 ºC for 14 days. Figure 3.3A shows a rapid increase in aggregation in Tau 410 even at Day 3. Aggregation in Tau 410 levels off from Day 3 through to Day 7, observed on the 14th day with the highest aggregation. A change in the Tau 410 protein structure was also observed. Transmission electron microscope images of Tau 410 in Figure 3.3B showed the extensive formation of fibrils and filaments. {Graph = Mean ± SD, n value = 9, paired t test : Day 7 vs Day 14 (p value = 0.0067)}.

. Even though Tau 410 has 2 N-terminal repeats and 3 MTBDs, the highest F.I. observed on day 14 was comparable to the F.I. observed in Tau 441, which has 2 N-terminal repeats and 4 MTBDs. This similarity in F.I. observed could be attributed to the same number of N-terminal repeats. The T.E.M images of Tau 410 showed the formation of clear and distinct fibrils and filaments (Figure 3.3B) extensively. The increased F.I. readings that indicate aggregation and the extensive formation of fibrils and filaments observed in Tau's 441, 412, and 410 are expected. These isoforms are predominantly expressed in the adult brain and are therefore implicated in A.D.

Tau 383 showed a gradual increase in aggregation with the highest F.I. also observed on the 14^{th} day (Figure 3.4A). Just as it was observed in Tau 441 and 410, the calculated p-value of 0.0344 for Tau 383 showed the observed increment on day 14 was statistically significant. Aggregation was observed in Tau 383, a 0N4R isoform, just as it was also observed in full-length Tau, or Tau 441, which has 2 N-terminal repeats and 4 MTBDs.

This decrease observed in F.I. on day 14 between Tau 383 and Tau 412 could be as attributed to the absence of the 1 N-terminal inserts in Tau 383. Indicating the role, the N-terminal acidic role may play in promoting Tau aggregation. Going to affirm the need to assess or evaluate the ability or role of the N-terminal repeats play in the Tau aggregation process. TEM samples were also prepared and imaged on the 14^{th} day. Tau 383 TEM images also extensively showed fibrils and filaments' formation (Figure 3.4B) like it was observed in Tau 441 (2N4R), 412 (1N4R), and 410 (2N3R), all with different N-terminal acidic inserts and microtubule binding regions.

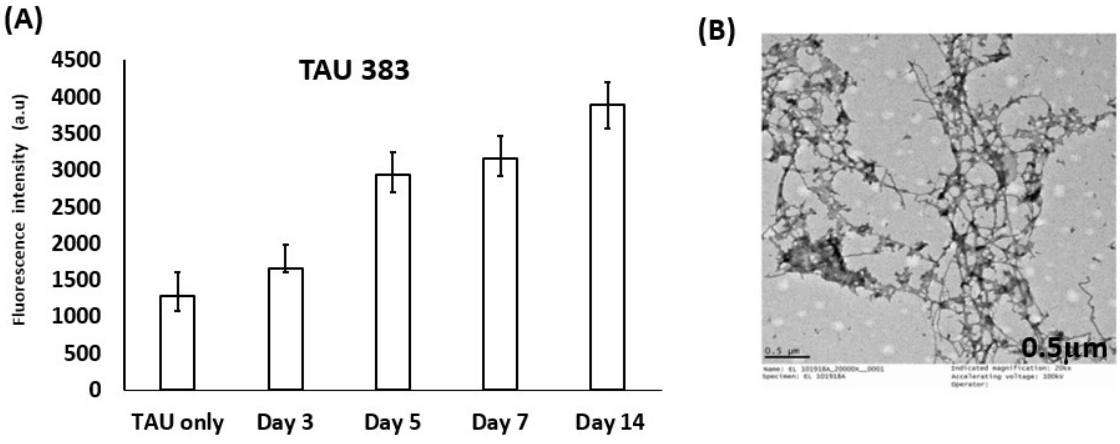

Figure 3.4: Aggregation plot and T.E.M images of Tau 383: A representation of Tau 383 fluorescence intensity plot vs. days and its corresponding T.E.M. images from day 14 after aggregation. Samples for the aggregation studies were incubated for 14 days at 37^0C. Samples were prepared for analysis for reproducibility of results. In Figure 3.4A, aggregation was leveling off in Tau 383 on Day 5 and 7, with the highest aggregation intensity observed on Day 14. In Figure 3.4B, Tau 383 showed the extensive formation of fibrils and filaments. {Graph = Mean ± SD, n value = 9, paired t test : Day 7 vs Day 14 (p-value = 0.0344)}.

Tau 381 was like the other isoforms was also aggregated with heparin, and the F.I. measured with fluorescence spectroscopy, as shown in Figure 3.5A. Herein, the F.I. of Tau 381 also increased gradually, with a p-value of 0.0214 confirming the highest aggregation observed on the 14^{th} day was not due to chance. Like the other isoforms aggregated earlier (Tau 441, 412, 410, and 383), Tau 381, a 1N3R isoform similarly showed the widespread formation of fibrils and filaments (Figure 3.5B) just as expected in AD brains. The observance of fibrils and filaments in all these isoforms also confirms the identification of different isoforms aggregation in different tauopathies.

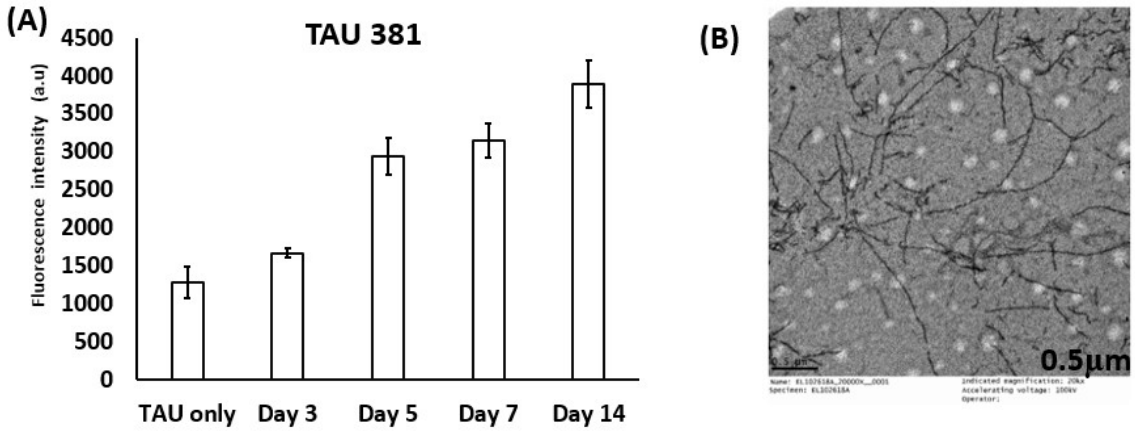

Figure 3.5: Aggregation plot and T.E.M images of Tau 381: Tau 381 was aggregated with Heparin, a polyanionic polysaccharide, and its aggregation property was evaluated on days 3, 5, 7, and 14. All measurements were done in triplicates. Transmission electron microscope grids of aggregated Tau 381 samples were prepared for the day 14 sample and imaged. Figure 3.5A shows a gradual increase in aggregation of Tau 381 over time, with the highest aggregation of Tau 381 observed on the 14th day. Widespread formation of fibrils and filaments was also observed in Tau 381, as shown in Figure 3.5B. {Graph = Mean ± SD, n value = 9, paired t test : Day 7 vs Day 14 (p value = 0.0214)}.

Via alternative splicing, Tau 352, the isoform with the least number of amino acids is formed. With all the isoforms been developmentally expressed, although Tau 352 is commonly observed in neonates, it also aggregated in the presence of heparin. The F.I. started to level off after day 7, with very little difference between F.I. observed on day 7 and day 14 (Figure 3.6A). The p-value of 0.9097 confirmed the difference between the F.I observed for Tau 352 on day 7 versus day 14, like in Tau 412 was not statistically significant. Of all the six isoforms, the least F.I. was recorded in Tau 352, indicating the least aggregation (Figure 3.6A). Although aggregated Tau 352 showed the formation of

fibrils and filament, the least fibril and filament formation was also observed in Tau 352 (Figure 3.6B).

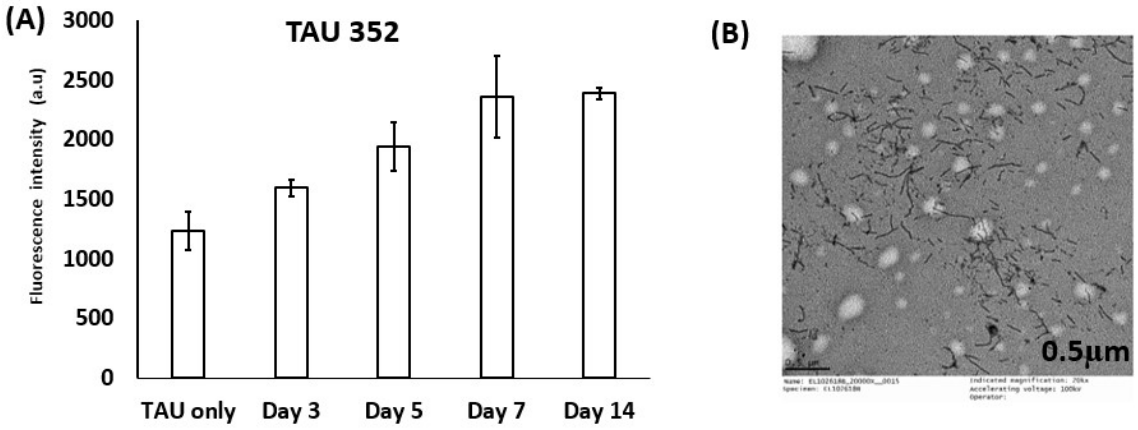

Figure 3.6: Aggregation plot and T.E.M images of Tau 352: Tau 352, the shortest isoform of Tau, were aggregated, and its aggregation property was assessed. The fluorescence intensities observed in Figure 3.6A show a gradual increase in the aggregation of Tau 352 over time, with the highest aggregation of Tau 352 observed on the 14th day. Although aggregation was seen in Tau 352, it showed the least aggregation. More so, even though there was the formation of fibrils and filaments in Figure 3.6B, Tau 352 also showed the least number of fibrils and filaments. {Graph = Mean ± SD, n value = 9, paired t test : Day 7 vs Day 14 (p value = 0.9097)}.

Besides the use of heparin, in other vitro assays, the use of arachidonic acid as an inducer to model aggregation, has been pivotal in gaining an understanding of how Tau aggregates into fibrils and filaments, especially in the longest Tau isoform (2N4R). However, other aggregation inducers have been less successful for modeling aggregation in the shorter 1N4R and 0N4R Tau isoforms *in vitro*. Herein, Tau aggregation into fibrils and filaments in all the isoforms was achieved using heparin.

Besides the use of heparin, the Martic laboratory has also confirmed Tau protein aggregation using other protein aggregation inducers including arachidonic acid. Goedert *et al.*, 1996; Wilson & Binder, 1997 and Combs, 2017 also showed that *in vitro* Tau aggregation was greatly enhanced by the addition of heparin and arachidonic acid as an aggregation inducer. They also observed aggregation of Tau into fibrils and filaments[120][140][141]. Results from these studies are consistent with the findings of the fluorescence study and the T.E.M images from our research.

Since A.D. is characterized by the formation of fibrils and filaments, this proof of principle was critical as this establishes that all the recombinant Tau isoforms expressed and purified all form fibrils and filaments when aggregated

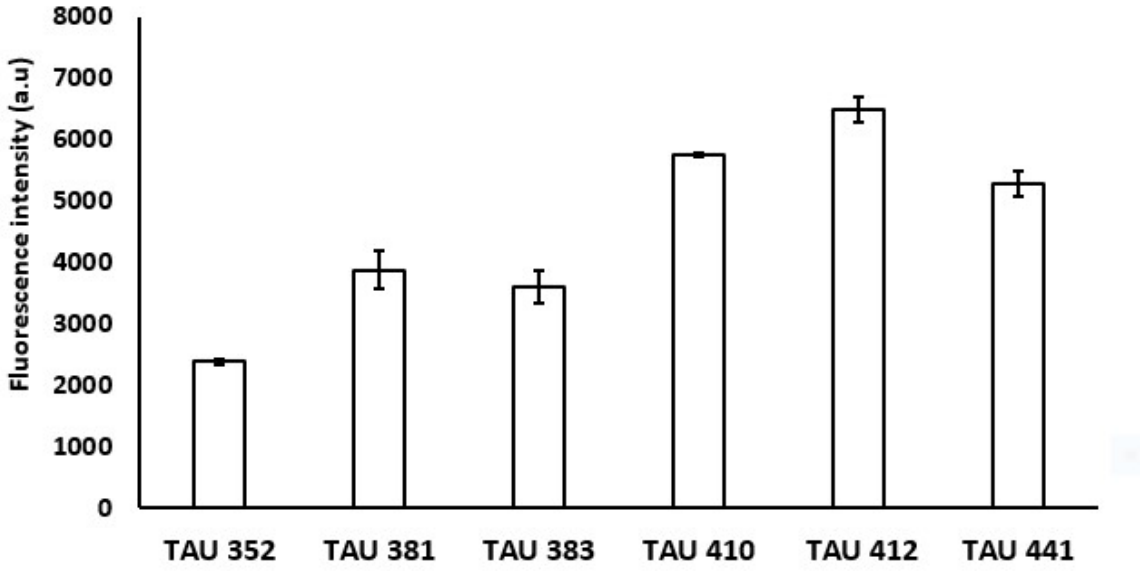

Figure 3.7: Aggregation plot of all the six Tau isoforms: Shows a summary plot of all the Tau isoforms at day 14, with Tau 412 showing the highest aggregation and Tau 352, the shortest isoform showing the least aggregation. (Graph = Mean ± SD, n value = 9)

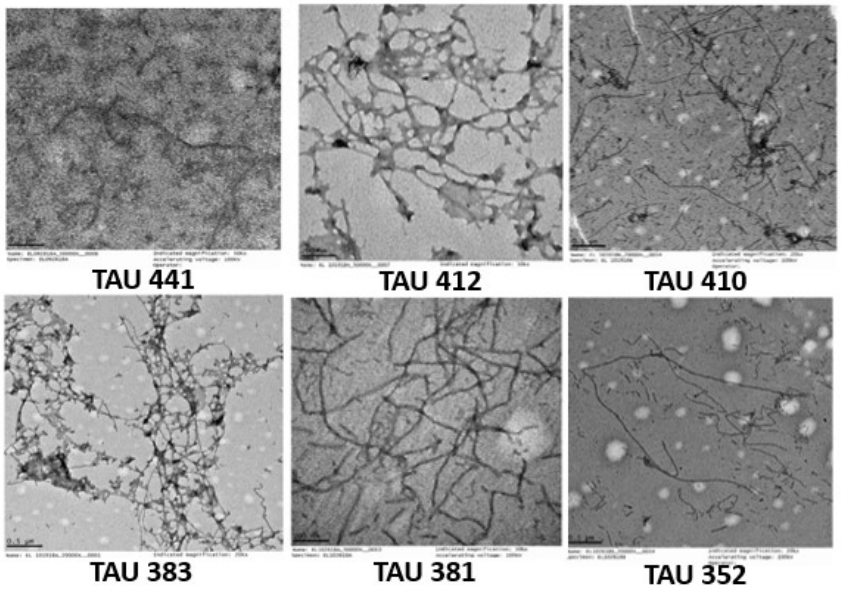

Figure 3.8: T.E.M images summary of all six Tau isoforms: Shows a summary of all the T.E.M images of the Tau isoforms at day 14.

To fully understand Tau and how it promotes proper neuronal communication, it is also imperative to know the function each domain on Tau plays. While initial work has shown that the N-terminus of Tau is vital in determining microtubule spacing in microtubule bundles within the axon, that is, the N-terminus of these MAPs may interact with each other on adjacent microtubules to determine spacing as a function of their length and reach, little or not much is known about the N-terminal imperfect repeats besides their acidic nature[142]. Other findings have also suggested that the N-terminal imperfect repeats and the N-terminal projection domain may facilitate cargo delivery in the axon[143]. However, isoform-specific differences in the aggregation behavior of Tau

based on the N-terminal imperfect repeats on the microtubule surface are not yet fully understood.

3.4.2 Aggregation of Tau based on their N-terminal repeats

The study by Amadoro *et al*. (2004) established the physiological role of the N-terminal imperfect repeats in the N-terminal domain. Their study indicated the potential toxic action these repeats may undergo whenever Tau undergoes a proteolytic attack leading to the cytoplasmic dispersion of some of its shorter N-terminal fragments[109]. However, the ability of the N-terminal repeats to co-exist and also their role in Tau aggregation promoting neuronal cell death has not been well studied and is not fully understood.

Here, the Tau isoforms were aggregated based on their number of N-terminal imperfect acidic repeats (i.e., after it has been established that all the six isoforms shown above are able to aggregate individually after 14 days of incubation). This incubation of the Tau isoforms as a function of their N-terminal repeats they were done over a 14-day period.

Aggregation was observed for all three pooled Tau isoforms with different N-terminal repeats after 14 days of incubation. The least F.I was observed in the pooled 0N (Tau 383 and Tau 352) Tau isoforms. The isoforms with 1N terminal (Tau 412 and 381) and 2N terminal repeats (Tau 441 and Tau 410) pooled together showed increased F.I readings on the 14^{th} day. The calculated p-value of 0.8232 showed the difference between the pooled 1N and 2N isoforms on day 14 was not statistically significant. This indicates the presence of the N-terminal imperfect repeats for both the 1N and 2N isoforms may

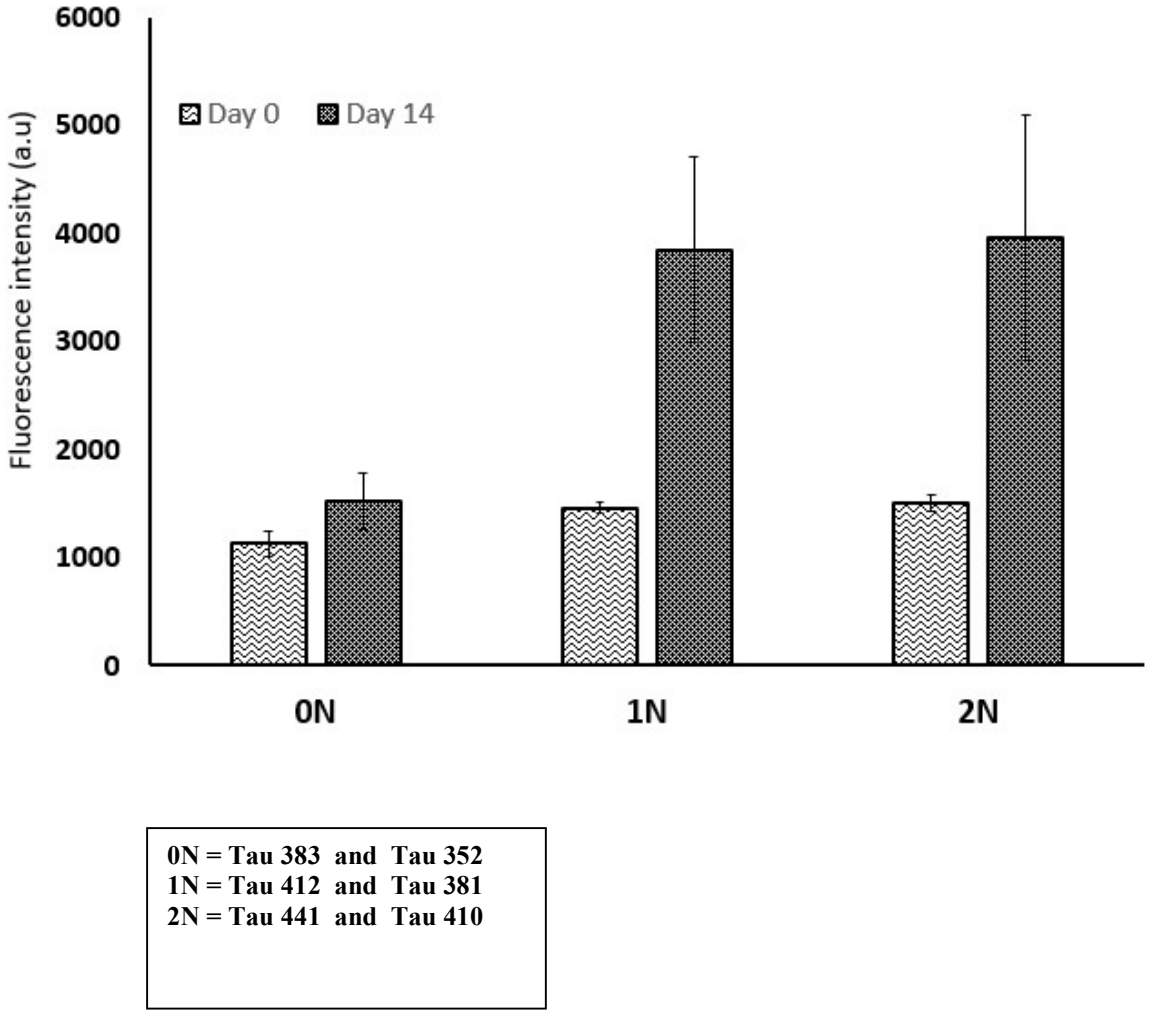

Figure 3.9: Aggregation plot of the Tau isoforms based on their N-repeats (0N,1N and 2N): Aggregation plot of Tau isoforms based on their N repeats (0N, 1N, and 2N): Tau isoforms pooled together based on their N-terminal repeats were aggregated. Proteostat aggregation assays of aliquots from days 0 and 14 were run. Although an increase in F.I was seen in the 0N Tau isoforms from Day 0 to Day 14, it showed the least aggregation. The Tau isoforms with 2N terminal repeats showed the highest FI, hence the highest aggregation over time, with the highest FI observed on the 14^{th} day. {Graph = Mean ± SD, n value = 9, unpaired t test : 1N vs 2N Day 14 (p value = 0.8232)}.

potentially play a role in aggregating Tau causing a disruption in neuronal communication.

3.5 Conclusions

The aggregation of Tau into fibrils and filaments in all the six isoforms was evaluated in this chapter. This was to establish the ability of Tau to aggregate in the presence of heparin, an inducer. While fluorescence studies showed an increase in aggregation for all the various isoforms of Tau over time, the T.E.M. images further confirmed the aggregates formed were fibrils and filaments consistent with what is observed in A.D. brains. Tau 352 showed the least F.I. readings as well as the least formation of fibrils and filament. This can be attributed to its predominance in neonates.

The aggregation of the Tau isoforms based on the number of N-terminal repeats they each have was also evaluated to establish their ability to co-exist and their role in aggregation. The order of aggregation after 14 days of incubation from the highest to the lowest of the Tau isoforms aggregations based on the N-terminal repeats were 2N > 1N > 0N. The T.E.M images further conformed the aggregates observed by the F.S were fibrils and filaments, also observed in AD brains.

Gamblin, Berry & Binder *et al.* (2000) also observed that performing these reactions in oxidizing or reducing conditions (i.e., with or without DTT) can change aggregate morphology observed earlier[144]. Combs *et al.* (2017), observed that after increasing the arachidonic acid to Tau ratio, a homogenous population of Tau oligomers was formed[141]. For my future work, I would aggregate all the isoforms in different Tau to heparin ratios and follow if this also leads to the formation of oligomeric Tau. I would

further induce these reactions with Dithiothreitol (DTT) to observe if there would be changes to aggregate morphologies observed in the absence of DTT for all the isoforms. I would also test out the ability of the pooled 2N, 1N and 0N N-terminal repeats to aggregate *in vivo* since the earlier results are based on *in vitro* analysis.

CHAPTER FOUR

IN VITRO TAU 441 PHOSPHORYLATION AND PHOSPHORYLATION INDUCED AGGREGATION ANALYSIS

4.0 Introduction

The commonest post-translational modification observed in eukaryotic cells is phosphorylation. This biochemical process in biological systems is vital for the cellular storage and transfer of free energy. Adenosine 5'-triphosphate (ATP), the most abundant energy carrier molecule, has two high-energy phosphate-phosphate bonds broken. The energy released from this process is used to drive the phosphorylation reaction. The phosphoryl group released is attached to the organic molecule be phosphorylated; in this context, Tau 441. Tau plays a crucial role in stabilizing neuronal cytoskeleton, regulating microtubule dynamics, axonal transport, and neurite outgrowth, and all these functions of Tau are modulated by site-specific phosphorylation[145]. Although several protein kinases phosphorylate Tau *in vitro*, it is still unclear how many phosphorylate Tau *in vivo* and how the various kinases work to induce hyperphosphorylation leading to Tau aggregation. Identification of the protein kinases that phosphorylate Tau and the specific phosphor-sites implicated in both physiological and pathological processes could provide potential therapeutic targets for the treatment of AD and other tauopathies.

Although hyperphosphorylation has been identified as the commonest cause of Tau aggregation, the mechanism by which it induces aggregation is not well understood. In an Alzheimer's disease patient's brain, Tau protein is invariably found in a hyperphosphorylated and aggregated form. Whether (hyper)phosphorylation of Tau can

drive aggregation is still not clear. Several kinases are being investigated to understand how phosphorylation induces Tau aggregation, including MARK4, Fyn, and GSK-3β. These kinases were carefully selected because of their biological relevance and the specific sites each phosphorylates on Tau. MARK4 is a non-proline-directed serine-threonine protein kinase, and it phosphorylates the serine and threonine residues on Tau in the microtubule-binding region (MTBR). GSK-3β is a proline-directed serine-threonine kinase, and it phosphorylates the serine and threonine residues in the PRD with the PXXP motif and Fyn is a protein tyrosine kinase phosphorylates responsible for phosphorylating the tyrosine residues on Tau. Several studies have also confirmed phosphorylation of Tau using GSK-3β, MARK4, or Fyn and they further confirmed their role in Tau pathology[146][147][148][149][150][151][152]. 40 out of the 85 putative phosphor-sites on Tau 441 have been identified as sites that can potentially be phosphorylated by GSK-3β, making it the most prolific kinase to phosphorylate Tau protein.

Although there is no conclusive evidence showing how an up-regulated Tau kinase activity can cause hyperphosphorylation of Tau in AD brains leading to enhanced Tau aggregation, there is evidence that suggests that the loss of Tau normal function due to hyperphosphorylation is sufficient to cause neurodegeneration[153][154]. Research has also shown that both the abnormally hyperphosphorylated Tau isolated from AD brains and *in vitro* hyperphosphorylated Tau become toxic enough to sequester normal Tau and other MAPs, such as MAP1 and MAP2, and this in turn causes microtubule disassembly[155][156][157].

In this chapter, I studied the differentially phosphorylated states of human recombinant Tau 441 *in vitro* to better understand whether an upregulated kinase activity can cause (hyper)phosphorylation promoting Tau aggregation. This I did by evaluating the ability of the differentially phosphorylated Tau forms to aggregate when phosphorylated using single or multiple kinase combinations. Aggregation properties of phosphorylated Tau protein was also evaluated in the presence of heparin, an anionic polymer that induces protein aggregation.

4.1 Materials

Tau-441 protein (recombinant tau-441, 2N4R) was expressed and purified from the Wu laboratory (Oakland University, MI). Commercial Tau used as control was also purchased from rPeptide (GA, USA). MARK4, Fyn or GSK-3β protein kinases at a concentration of 0.1 mg/mL were purchased from SignalChem (Richmond, British Columbia, Canada). ATP was purchased from Sigma-Aldrich (St. Louis, MO, USA). The stock solution of phosphate buffer (pH 7.0) was prepared using 60 mM sodium phosphate monobasic (anhydrous) obtained from Fisher Scientific (NJ, USA) and 60 mM sodium phosphate dibasic, anhydrous, obtained from J. T. Baker (NJ, USA). The pH was adjusted using sodium hydroxide (NaOH) obtained from Fisher Scientific (NY, USA). The stock solution of kinase buffer was a mixture of 50 mM 4-(2-hydroxyethyl)-1-piperazineethanesulfonic acid (HEPES) from Sigma-Aldrich, 100 mM sodium chloride (NaCl) from Fischer Scientific, 1 mM dithiothreitol (DTT) obtained from Thermo Scientific Pierce (Rockford, IL, USA), and 10 mM magnesium chloride ($MgCl_2$) from Amresco (Solon, OH, USA). The pH was adjusted to 7.4 using sodium hydroxide (NaOH).

Anti–Tau antibody D8 (Santa Cruz Biotech, USA) was used to detect total Tau 441. Rabbit polyclonal anti-Tau pS262 (Abcam, Cambridge, USA), rabbit monoclonal anti-Tau p-tyrosine (Santa Cruz Biotech, USA) and rabbit monoclonal anti - Tau pS199 (Life Technologies, CA, USA) were used to detect phosphorylation by MARK4, Fyn and GSK-3β.

The samples used as controls for the aggregation studies included [a] non-phosphorylated Tau 441 (1mg/mL) incubated at 37^0C with kinase buffer (pH 7.4) and phosphate buffer (pH 7.0) [b] Tau - Heparin control prepared from 1mg/mL Tau 441 and 53.54 μM heparin [c] MARK4 and GSK-3β (No heparin) was prepared with 5μL of Tau 441 at 1mg/mL, 1μL of the protein kinase at 0.1mg/mL (MARK4 and GSK-3β), 0.5μL of ATP at 50mM, 3.5μL of kinase buffer pH 7.4 and 0.5μL of phosphate buffer pH 7.0 [d] MARK4 and GSK-3β (No Tau) contained of 1μL of the protein kinase at 0.1mg/mL (MARK4 and GSK-3β), 0.5μL of ATP at 50mM, 6.5μL of kinase buffer pH 7.4, 2.5μL of phosphate buffer pH 7.0 and 1.5μL of 53.54 μM [e] MARK4 and GSK-3β (No ATP) contained of 1μL of the protein kinase at 0.1mg/mL (MARK4 and GSK-3β), 7.0μL of kinase buffer pH 7.4, 2.5μL of phosphate buffer pH 7.0 and 1.5μL of 53.54 μM [f] MARK4 and GSK-3β (No heparin, No ATP) contained of 1μL of the protein kinase at 0.1mg/mL (MARK4 and GSK-3β), 7.0μL of kinase buffer pH 7.4 and 2.5μL of phosphate buffer pH 7.0 [g] MARK4 and GSK-3β (No heparin) comprised was of 5μL of Tau 441 at 1mg/mL, 1μL of the protein kinase at 0.1mg/mL (MARK4 and GSK-3β), 0.5μL of ATP at 50mM, 6.5μL of kinase buffer pH 7.4 and 2.5μL of phosphate buffer pH 7.0.

4.2 Methods

4.2.1 Single kinase phosphorylation of Tau 441

5µL of Tau 441 at 1mg/mL, 1µL of the protein kinase at 0.1mg/mL (MARK4, Fyn or GSK-3β) (SignalChem, Richmond, British Columbia, Canada), 0.5µL of ATP at 50mM (Sigma-Aldrich, St. Louis, MO, USA), 0.5µL of phosphate buffer pH 7.0 and 3.5µL of kinase buffer pH 7.4 were mixed and incubated at 37ºC for 2 h.

4.2.2. SDS-PAGE and Western Blots

Following 2 hours of phosphorylation at 37ºC, 10µL of the phosphorylated Tau 441 protein samples were loaded on 10% sodium dodecyl sulfate-polyacrylamide gel and electrophoresis gel (SDS - PAGE) and was run for 50 minutes at 180 mA. The gel was equilibrated in Towbin transfer buffer for 60 minutes. The proteins on the SDS – PAGE was transferred from the gel to Immobilon®- FL PVDF membrane (Millipore Sigma, USA) at 15mA for 45 minutes using Bio-Rad trans-blot turbo system. After transferring the proteins onto the membrane, the remaining protein-binding sites were blocked with Odyssey® Blocking Buffer (Li-Cor Biosciences, Nebraska, USA) for 1 hour at room temperature.

4.2.3 MARK4 phosphorylation:

After blocking the protein binding sites with blocking buffer, the membrane was incubated overnight at 4 °C in rabbit polyclonal anti-Tau pS262 (Abcam, Cambridge, USA); in a 1:1000 dilution, and anti - Tau D8 antibody (Santa Cruz Biotech, USA); in a 1:1000 dilution. After washing the PVDF membrane three times with 1x TBS containing 2% Tween 20, the blot was incubated with IRDye® 800 Conjugated Affinity Purified Goat anti-rabbit IgG (Li-Cor Biosciences, Nebraska, USA); in a 1:5000 dilution and

IRDye® 650 Goat anti-mouse IgG (Li-Cor Biosciences, Nebraska, USA); in a 1:5000 for 45 minutes at room temperature. After the 45 minutes incubation, the membrane was washed three times with 1x TBS containing 2% Tween 20 and three times with 1x TBS. After, the Blot was visualized with Li-Cor's Odyssey Infrared Imaging System and Li-Cor's Image Studio 2.0 software to capture images and for densitometric analysis.

4.2.4 Fyn phosphorylation:

After blocking the protein binding sites with blocking buffer, the membrane was incubated overnight at 4 °C in rabbit monoclonal anti-Tau p-tyrosine (1:1000 dilution) and anti-Tau D8 antibody (1:1000 dilution) {(Santa Cruz Biotech, USA)}. After washing three times with 1x TBS containing 2% Tween 20, the blot was incubated with IRDye® 800 Conjugated Affinity Purified Goat anti-rabbit IgG (Li-Cor Biosciences, Nebraska, USA); 1:5000 dilution and IRDye® 650 Goat anti-mouse IgG (Li-Cor Biosciences, Nebraska, USA); 1:5000 for 45 minutes at room temperature. After washing three times with 1x TBS containing 2% Tween 20 and three times with 1x TBS, the Blot was visualized with Li-Cor's Odyssey Infrared Imaging System and Li-Cor's Image Studio 2.0 software to capture images and for densitometric analysis.

4.2.5 GSK-3β phosphorylation:

After blocking the protein binding sites with blocking buffer, the membrane was incubated overnight at 4°C in rabbit monoclonal anti - Tau pS199 (Life Technologies, CA, USA) in 1:1000 dilution and anti - Tau D8 antibody (Santa Cruz Biotech, USA); 1:1000 dilution. After washing three times with 1x TBS containing 2% Tween 20, the blot was incubated with IRDye® 800 Conjugated Affinity Purified Goat anti-rabbit IgG (Li-Cor Biosciences, Nebraska, USA); 1:5000 dilution and IRDye® 650 Goat anti-mouse

IgG (Li-Cor Biosciences, Nebraska, USA); 1:5000 for 45 minutes at room temperature. After washing three times with 1x TBS containing 2% Tween 20 and three times with 1x TBS, the Blot was visualized with Li-Cor's Odyssey Infrared Imaging System and Li-Cor's Image Studio 2.0 software to capture images and for densitometric analysis.

After phosphorylation of Tau 441 by MARK4, Fyn and GSK-3β were confirmed via Western blot using epitope-specific antibodies, the aggregation properties of the various phosphorylated Tau samples were evaluated. Single kinase aggregation properties and multiple kinase phosphorylation aggregation properties were all assessed.

4.2.6 Multiple kinase phosphorylation of Tau 441

50µL of Tau 441 at 1mg/mL, 10µL of the first protein kinase at 0.1mg/mL (either MARK4, Fyn or GSK-3β based on the multi-kinase combination been evaluated) (SignalChem, Richmond, British Columbia, Canada), 5µL of ATP at 50mM (Sigma-Aldrich, St. Louis, MO, USA), 5µL of phosphate buffer pH 7.0 and 35µL of kinase buffer pH 7.4 were mixed and incubated at 37 ºC for 24 h. After 24 h incubation with the first kinase, this was followed by addition of 10µL of the second kinase also at 0.1mg/mL (either MARK4, Fyn, or GSK-3β based on the multi-kinase combination been evaluated). The reaction was allowed to go for another 24 h, totaling 48 h.

4.2.7 Heparin induced aggregation of phosphorylated Tau 441:

To assess the effect of heparin (the polyanionic polymer) on phosphorylated Tau samples, the single and sequentially phosphorylated Tau samples were induced with heparin in the Tau to heparin ratio 4:1. Aliquots of the samples were collected at the designated times for analysis. Experiments were done in triplicates.

4.2.8 Proteostat aggregation assay

10µL aliquots of the phosphorylated Tau samples, single or multiple kinases (with or without heparin) from days 0, 3, 5, 7, and 14 were mixed with 1µL of Proteostat fluorescence dye and incubated at room temperature for 15 minutes in the dark. 3µL of the samples were spotted on the H1 Synergy TAKE – 3 Bio-Tek plate reader (Bio-Tek Instruments Inc., VT, USA). The fluorescence measurements were then taken (Emission 550nM, Excitation 600nM, 25^0C). Experiments were done in triplicates.

4.2.9 Turbidity assay measurements

Turbidity assay measurements were carried out using a Synergy H1 Take 3 reader, and data was generated using the Gen5 program (Bio-Tek Instruments Inc., VT, USA). 3µL (days 0, 3, 5, 7 and 14) each of the phosphorylated Tau samples, single or multiple kinases (with or without heparin) were loaded onto the Take 3 Bio-Tek plate (Bio-Tek Instruments Inc., VT, USA) and the turbidity intensities determined at a wavelength 360 nm at 25^0C. All measurements were done in triplicates.

4.3 Results and Discussion

4.3.1 Phosphorylation of Tau 441 with GSK-3β, MARK4, or Fyn

Phosphorylation regulates the binding of Tau to microtubules. There is significant evidence to show that abnormal phosphorylation events in Tau result in Tau aggregation. Hyperphosphorylation has been identified as a significant contributing factor to the Tau protein pathogenic process. Therefore, the phosphorylation process is being studied widely to understand how the several kinases that may hyperphosphorylate Tau can promote Tau aggregation and microtubule disassembly.

Herein, recombinant Tau 441 was phosphorylated using GSK-3β, MARK4, or Fyn in the presence of kinase-specific epitopes. Western blots (WB) confirmed phosphorylation of Tau and the phosphorylation patterns of the various kinases (WB).

In Figure 4.1, Tau 441 was phosphorylated with MARK4 *in vitro*. The primary antibody used was rabbit monoclonal anti-Tau pS262 antibody, which recognizes and binds to phosphorylated Ser262 on Tau protein, and mouse monoclonal anti-Tau D8, which recognizes N-terminus on Tau (amino acids 1-150).

Commercially procured Tau 441 was used as a control to confirm the phosphorylation in the expressed and purified Tau 441 from our laboratory (Wu laboratory). The Tau 441 expressed from the Wu laboratory here was labeled cleaved Tau 441. Anti–Tau antibody D8 bound and recognized the presence of total Tau 441 in both phosphorylated Tau (pTau) and non-phosphorylated Tau (nTau) (Figure 4.1A) as expected. This confirmed the protein was Tau since antibody D8 binds only Tau. Phosphorylation was detected in Tau 441 with the secondary antibody, 800 GAM (Green channel) and non-phosphorylated Tau 441 was also detected with another secondary antibody, 680 GAR (Red channel). pS262 antibody-bound and also recognized phosphorylated S262 in commercial pTau and cleaved pTau (Figure 4.1B). The observance of an intense signal in both pTau/commercial and pTau/cleaved lanes (i.e., not in nTau/commercial and nTau/cleaved lanes) showed Tau was phosphorylated by MARK4. Besides this confirming the phosphorylation of Tau 441 by MARK4, this further confirmed S262 as a MARK4 phosphosite.

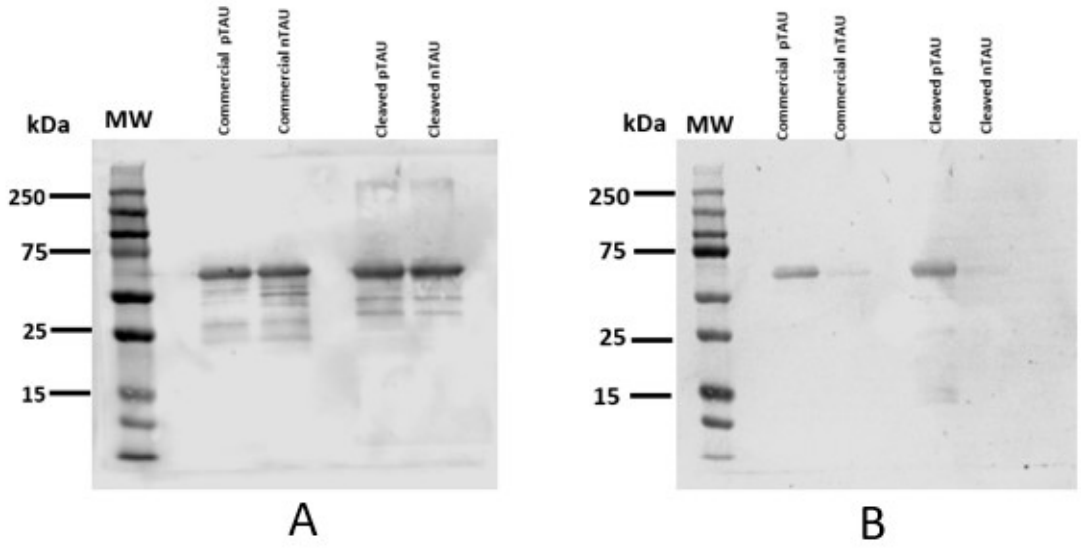

Figure 4.1: Tau 441 phosphorylation by MARK4 protein kinase: Phosphorylation of Tau 441 by MARK4 was assessed using Tau-specific epitope S262. Commercial Tau was used as a control in this experiment. Figure 4.1A shows the detection of total Tau in commercial pTau 441, commercial nTau, cleaved pTau, and cleaved nTau using antibody D8. Figure 4.1B shows the detection of phosphorylation by MARK4 at S262 only in commercial pTau and cleaved pTau. This shows MARK4 successfully catalyzed the phosphorylation of S262 in both commercial and cleaved Tau 441 from our laboratory.

Cleaved Tau 441 was further phosphorylated using Fyn and GSK-3β protein kinases. WB confirmed phosphorylation. With Fyn being a protein tyrosine kinase, anti-Tau pTyr antibody recognizes and binds to phosphorylated tyrosine residues on Tau protein. Mouse monoclonal anti-Tau D8 antibody (antibody to total Tau) was used as the primary antibody. Anti–Tau antibody D8 bound and recognized the presence of total Tau 441 in both phosphorylated Tau (pTau) and non-phosphorylated Tau (nTau).

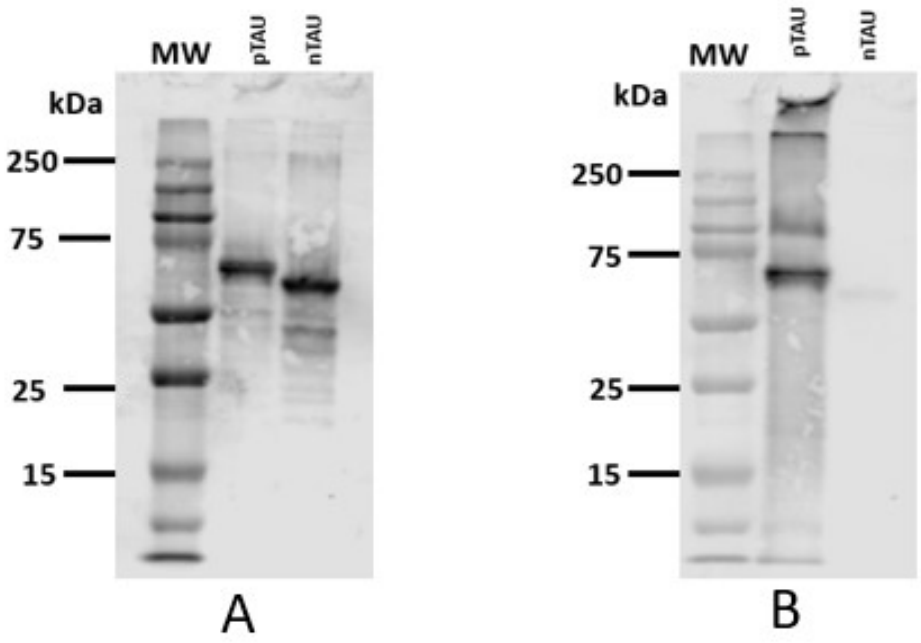

Figure 4.2: Tau 441 phosphorylation by Fyn protein kinase: Tau 441 was phosphorylated using Fyn kinase. Phosphorylation was detected with Tau-specific epitope anti-pTyr. Total Tau 441 was detected using Tau antibody D8 (binds amino acids 341 – 360 on Tau). Fig 4.2A shows the detection of total Tau 441 in both cleaved pTau and cleaved nTau while Fig 4.2B shows detection of phosphorylation by Fyn (pTyr) in cleaved pTau.

Simultaneously, rabbit monoclonal anti-Tau pS199 antibody, which recognizes and binds to phosphorylated S199 on Tau protein, and mouse monoclonal anti-Tau D8 (antibody to total Tau) were used as the primary antibodies for GSK-3β. Anti – Tau pTyr antibody bound and recognized all phosphorylated tyrosine residues in pTau (Figure 4.2B) as expected, confirming the phosphorylation of all the tyrosine residues on Tau 441 by Fyn.

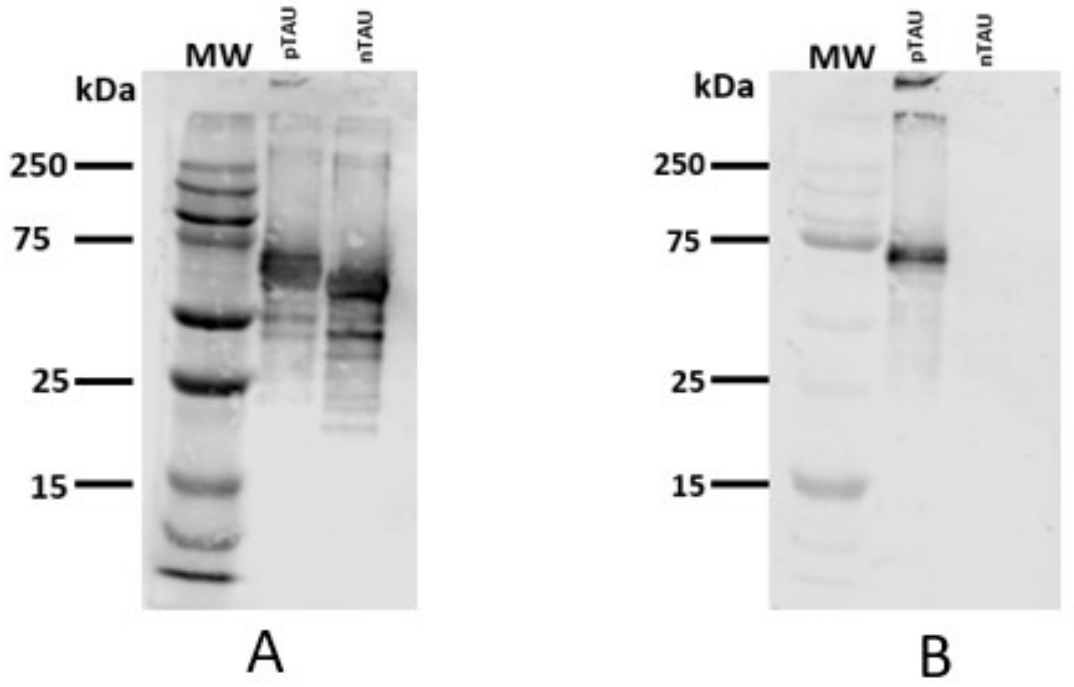

Figure 4.3: Tau 441 phosphorylation by GSK- 3β protein kinase: Tau 441 was phosphorylated with GSK-3β in this experiment. In Figure 4.3A, total Tau 441 was detected in both cleaved pTau and cleaved nTau. And the phosphorylation capability of Tau 441 was also assessed in Figure 4.3B using S199, a GSK-3β specific phosphosite.

Here, anti–Tau antibody pS199 bound and recognized phosphorylated Ser199 in only the cleaved pTau lane (Figure 4.3B). This confirmed the phosphorylation of Tau 441 by GSK-3β and further confirmed Ser199 as a GSK-3β phosphosite.

4.3.2 Phosphorylated Tau 441 (with and without heparin) aggregation data analysis

The in vitro fluorescence spectroscopy and turbidity absorbance assays were used to probe the structural changes upon Tau 441 phosphorylation by the protein kinases. While fluorescence spectroscopy gave more information on the extent of Tau fibril and filament formation after phosphorylation, the turbidity assay was used to access the

formation of other insoluble precipitates that may not be fibrils and filaments in solution after extensive phosphorylation. The composition of the buffers the kinases were in versus the MES buffer/kinase buffers used for the phosphorylation reactions had the same composition. This was to ensure that the buffers had no effect on the reading recorded when the fluorescence and turbidity assays were done. All the assays were also done in triplicates for reproducibility of the results.

Single kinase phosphorylation of Tau 441 (full length Tau 441) by GSK-3β (proline directed protein kinase), Fyn (protein tyrosine kinase) and MARK4 (Non-proline directed protein kinase) were evaluated. Figure 4.4A shows that the fluorescence intensities remained unchanged between non-phosphorylated and phosphorylated Tau 441 (Fyn), indicating lack of protein aggregation via β-pleated sheet formation. At day 7 , the phosphorylation by GSK-3β and MARK4 protein kinases resulted in a slightly greater fluorescence compared to the non-phosphorylated Tau 441, with MARK4 spotting the highest F.I. An unpaired t test (p-value = 0.0219) showed there was a significant difference between pTau/GSK3β and pTau/MARK4 F.I at day 7, indicating the differences observed is statistically significant. Although the F.I generally remained unchanged, 1-way ANOVA confirmed differences existed in F.I readings observed at day 7 for pTau/GSK3β, pTau/MARK4 and pTau/Fyn (p-value = 0.00468).

Due to the biological relevance of heparin on Tau aggregation, the heparin-induced aggregation propensities of differentially phosphorylated Tau 441 were analyzed for β-sheet formation after the protein was aged at 37°C.

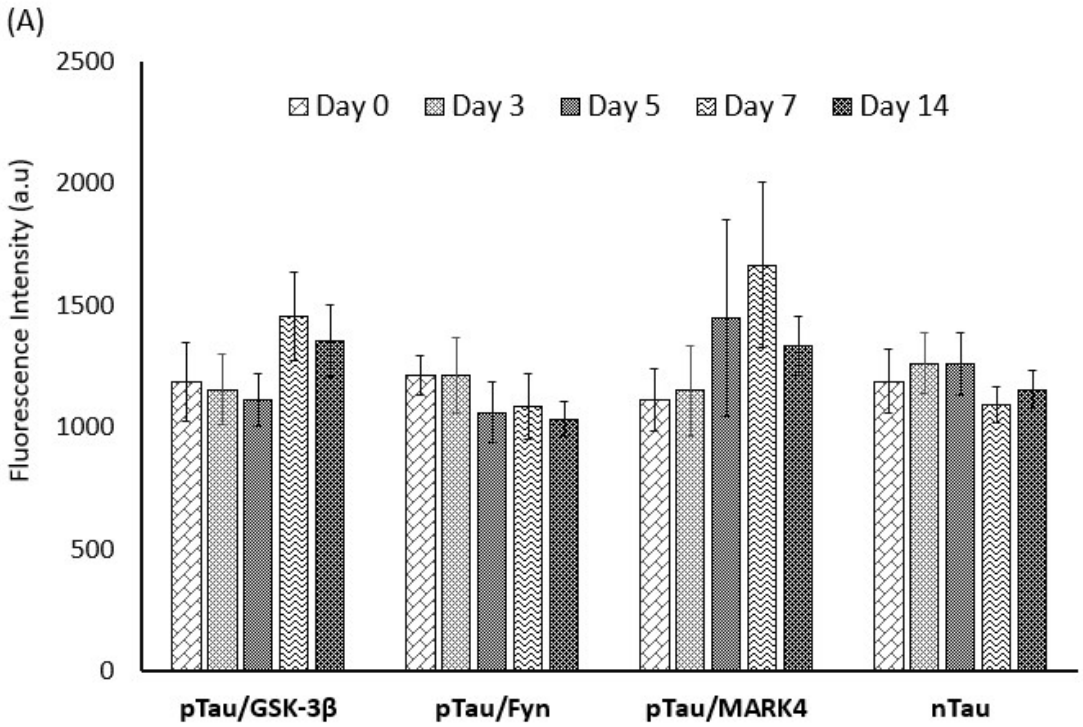
(A)
Day 0
Day 3
Day 5
Day 7
Day 14
Fluorescence Intensity (a.u)
2500
2000
1500
1000
500
0
pTau/GSK-3β
pTau/Fyn
pTau/MARK4
nTau

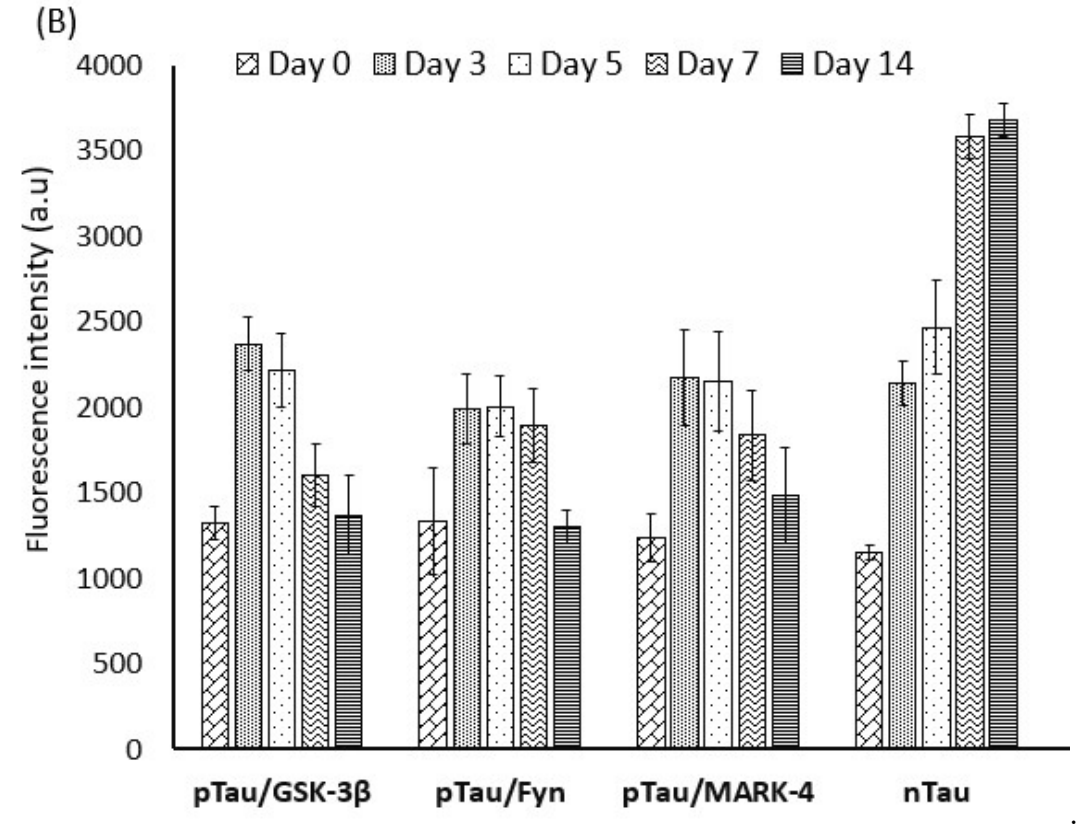
(B)
Day 0
Day 3
Day 5
Day 7
Day 14
Fluorescence intensity (a.u)
4000
3500
3000
2500
2000
1500
1000
500
0
pTau/GSK-3β
pTau/Fyn
pTau/MARK-4
nTau

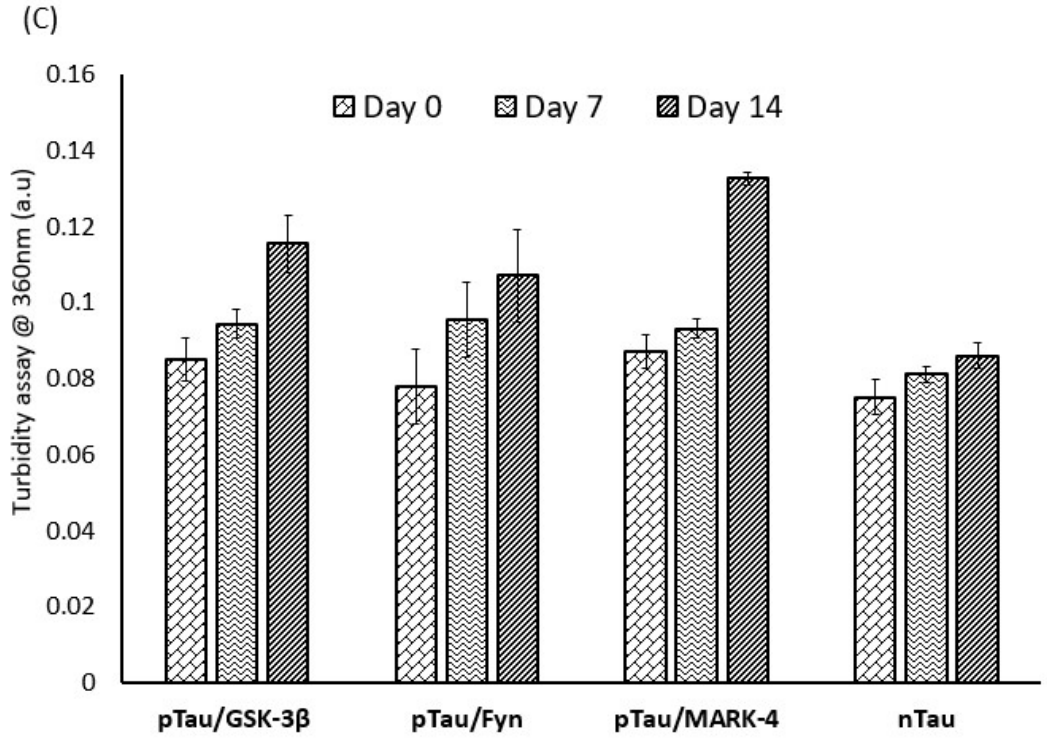

Figure 4.4: Single kinase proteostat and turbidity assays: (A) Proteostat aggregation assay fluorescence intensities as a function of Tau 441 phosphorylation by using single kinases in the absence of heparin; (phosphorylation time = 24 h; phosphorylation temperature = 37 °C; ageing time = 0, 3, 5, 7 or 14 days; ageing temperature = 37 °C), (Graph = Mean ± SD, n value = 9) (B) Proteostat aggregation assay fluorescence intensities as a function of Tau 441 phosphorylation using single kinases and aging in the presence of heparin; (phosphorylation time = 24 h; phosphorylation temperature = 37 °C; ageing time = 0, 3, 5, 7 and 14 days; ageing temperature = 37 °C), (Graph = Mean ± SD, n value = 9) (C) Turbidity assay as a function of Tau 441 phosphorylation using single kinases and aging in the presence of heparin (phosphorylation time = 24 h; phosphorylation temperature = 37 °C; ageing time = 0, 7 and 14 days; ageing temperature = 37 °C). {Graph = Mean ± SD, n value = 9).

Heparin, the polyanionic co-factor used to induce Tau aggregation into fibrils and filaments *in vitro* has also been used by several laboratories including the Martic laboratory [120][138]. The fluorescence aggregation assay (Proteostat) was used to monitor Tau 441 aggregation. During the first 3 days of ageing of GSK-3β, Fyn and

MARK4 phosphorylated Tau 441, the fluorescence intensity remained unchanged indicating no aggregation.

A significant increase in fluorescence intensity at day 5 maintained through day 7 was observed for all 3 kinases with the highest recorded in GSK-3β and MARK4 (Figure 4.4B). A 2-way ANOVA (p-value = 0.8981) comparing F.I for days 5 and 7 in both kinases showed the difference in readings were not statistically significant. A notable change is the drop in fluorescence intensity after 14 days of ageing for pTau samples. Therefore, the cause of the drop in the heparin induced aggregation of the phosphorylated Tau samples was also assessed as a function of ageing time. The drop in fluorescence intensity in Figure 4.4B, may be ascribed to the decrease in aggregation, and dissolution of aggregates or formation of insoluble aggregates. The solution appeared cloudy and hence, formation of insoluble aggregates was more likely reason for fluorescence intensity decrease. To determine the insoluble aggregate formation, the UV-Vis turbidity measurements were carried out. Figure 4.4C shows a slight increase in the UV-VIS turbidity measurement at day 14, with pTau MARK4 being the most turbid. The 1-way ANOVA (p-value = 0.0015) for day 14 indicates the turbidity increase observed in pTau was not due to chance although very small. This most likely confirms the presence of insoluble aggregates. The phosphorylated Tau protein samples with heparin followed similar aggregation trend with nTau, at days 3 and 5 days. However, at 7- and 14-days aggregation of pTau declined overtime but solutions became cloudy indicating increase in turbidity. The presence of heparin induced both degradation and the formation of SDS resistant aggregates in phosphorylated Tau 441 on day 7 (Figure A.1ii). Although Phosphorylated Tau 441 still formed SDS-resistant aggregates even on day 14 in the

presence of heparin, pTau was extensively degraded and this was seen via the formation of lower molecular weight fragments (Figure A.1iii). The degradation pattern was dependent on the protein kinase used for phosphorylation reaction. This phenomenon could have accounted for the decline observed in fluorescence intensity at day 14. With the increase in SDS resistant aggregates observed in Figure B.1, it is obvious the presence of heparin induced an increased formation of SDS resistant aggregates than in Tau 441 without heparin absent even after 7 days. Phosphorylation seems to be promoting the degradation of pTau with ageing of the sample. The Figure 4.4C shows an increase in turbidity in the phosphorylated Tau samples with MARK4 catalyzed phosphorylation of Tau 441 being the most and Fyn catalyzed phosphorylation of Tau 441 being the least turbid.

In the absence of ATP, there is no phosphorylation of Tau. However, the fluorescence signal was low when kinase was present, but not a co-substrate, (Figure C-1) which indicates that heparin-induced Tau aggregation was modulated by a presence of a kinase. Hence, protein kinase interferes with the formation of insoluble beta-sheet structures. Also consistent with absence of phosphorylation, was the nonexistence of cloudiness. The turbid assay also showed the absence of the formation of insoluble precipitates (Figure D.1). These findings were in stark contrast to nTau aggregation. Avila *et al* (1996) observed aggregation and filament formation when GSK-3β-catalyzed pTau 441 was aggregated in the presence of heparin[158].

The single kinase phosphorylation was followed with multi kinase phosphorylations that produced the sequential phosphorylations.

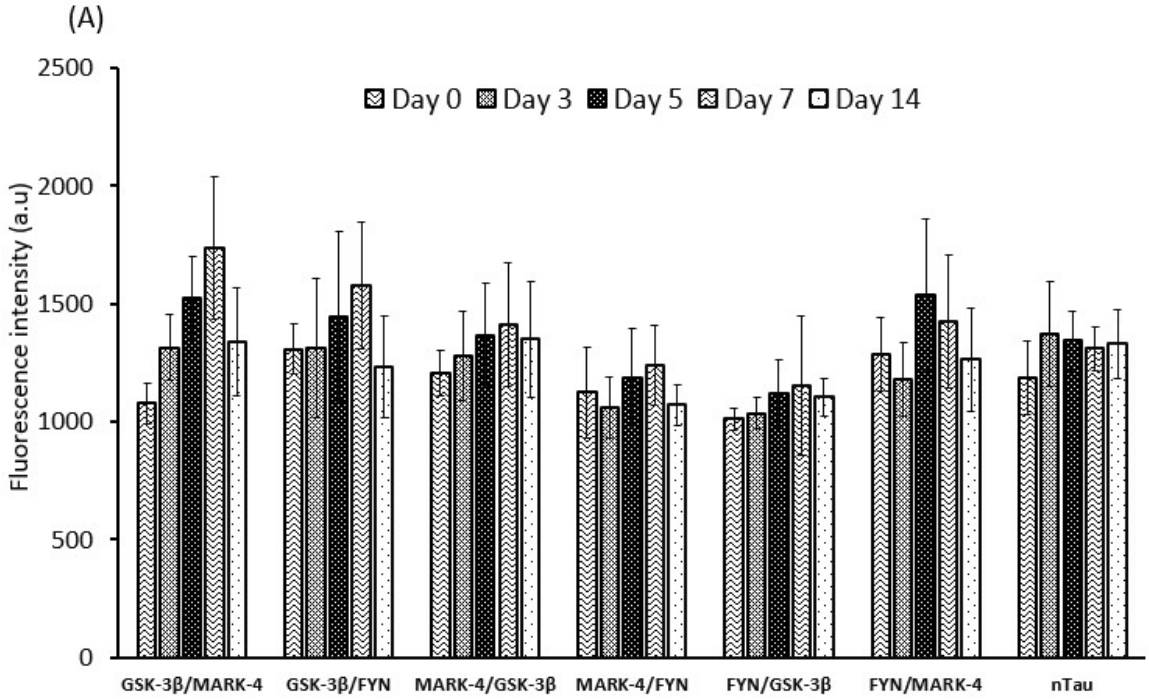
(A)
Day 0
Day 3
Day 5
Day 7
Day 14
Fluorescence intensity (a.u)
2500
2000
1500
1000
500
0
GSK-3β/MARK-4
GSK-3β/FYN
MARK-4/GSK-3β
MARK-4/FYN
FYN/GSK-3β
FYN/MARK-4
nTau

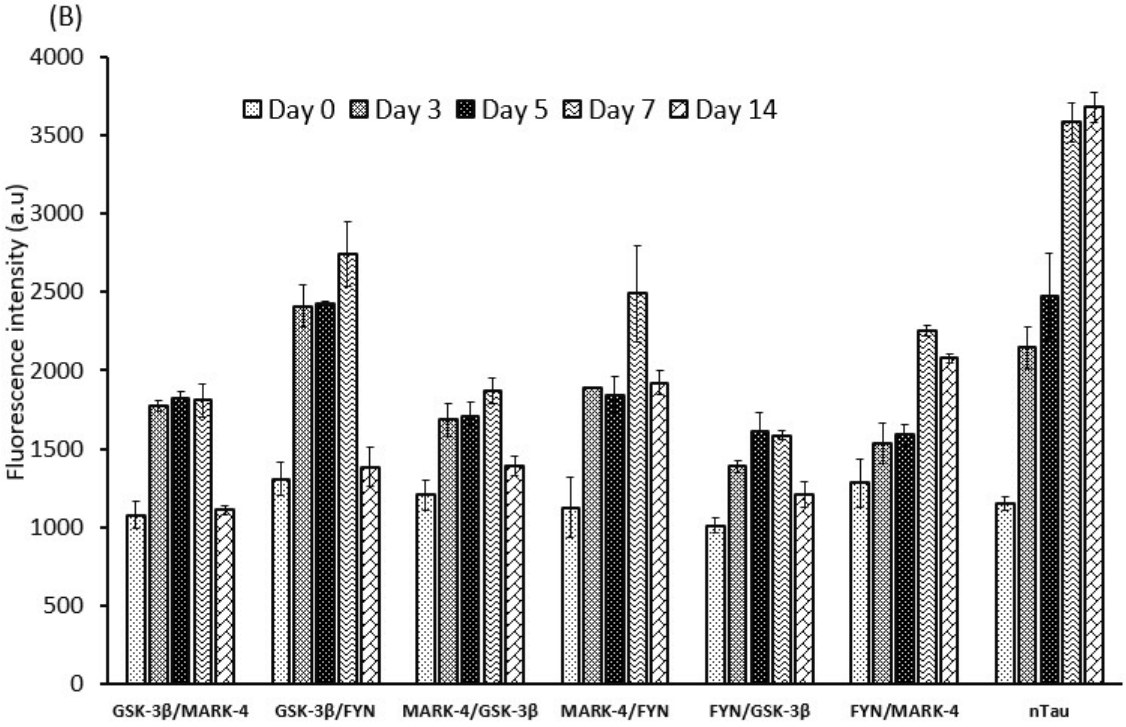
(B)
Day 0
Day 3
Day 5
Day 7
Day 14
Fluorescence intensity (a.u)
4000
3500
3000
2500
2000
1500
1000
500
0
GSK-3β/MARK-4
GSK-3β/FYN
MARK-4/GSK-3β
MARK-4/FYN
FYN/GSK-3β
FYN/MARK-4
nTau

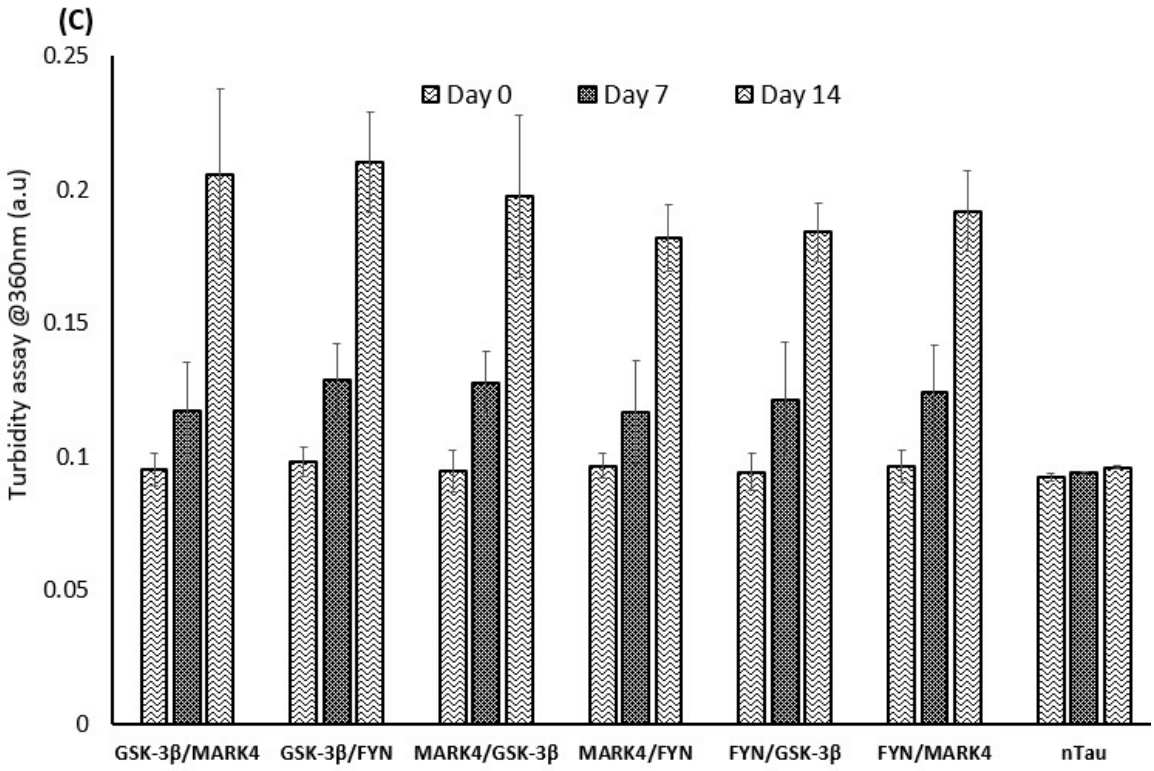

Figure 4.5: Multiple kinase proteostat and turbidity assays: (A) Proteostat aggregation assay fluorescence intensities as a function of Tau 441 phosphorylation using multiple kinases; (phosphorylation time = 48 h; phosphorylation temperature = 37 °C; ageing time = 14 days; ageing temperature = 37 °C). {Graph = Mean ± SD, n value = 9} (B) Proteostat aggregation assay fluorescence intensities as a function of Tau 441 phosphorylation using multiple kinases in the presence of heparin; (phosphorylation time = 48 h; phosphorylation temperature = 37 °C; ageing time = 14 days; ageing temperature = 37 °C). {Graph = Mean ± SD, n value = 9}. (C) Turbidity assay as a function of Tau 441 phosphorylation using multiple kinases and aging in the presence of heparin (phosphorylation time = 48 h; phosphorylation temperature = 37 °C; ageing time = 0 - 14 days; ageing temperature = 37 °C). {Graph = Mean ± SD, n value = 9}.

The following kinase combinations: GSK3β/MARK4, GSK3β/Fyn, MARK4/GSK3β, MARK4/Fyn, Fyn/ GSK3β and Fyn/MARK4 were used to produce sequentially phosphorylated Tau protein samples that were investigated.

The proteostat assay was used to measure the aggregation propensities of the sequentially phosphorylated Tau proteins. Regardless of the phosphorylation sequence, the fluorescence intensities remained below ~1500 a.u. indicating negligible aggregation. A slight increase in the fluorescence intensity (~1700 a.u.) was observed for GSK-3β/MARK4 phosphorylation sequence after 7 days, compared to other kinase combinations (Figure 4.5A). The 1-way ANOVA (p-value = 0.00653) confirmed the observed increment in F.I readings at day 7 for pTau/GSK3β/MARK4 was statistically significant although negligible. Also, at day 14, the fluorescence intensity decreased as it was observed for the prolonged aggregation of singly phosphorylated Tau in the absence of heparin (Figure 4.4A). The sequentially phosphorylated Tau showed a slight increase in the turbidity assay which could be indicative of the insoluble precipitates not detectable by fluorescence, accounting for the drop in fluorescence intensity observed (Figure E.1). Hence, the phosphoproteins formed insoluble structures in the absence of heparin, but nTau did not (Figure E.1). The insoluble structures were similar for all protein kinase combinations tested.

Sequentially phosphorylated Tau 441 aggregation with heparin, as was done in singly phosphorylated Tau 441, was also investigated. As was observed on day 14 in the singly phosphorylated Tau samples, there was a drastic decline in aggregation in the sequentially phosphorylated Tau samples following a gradual increase in aggregation after 7 days. The sequentially phosphorylated Tau sample GSK-3β/Fyn showed the highest fluorescence intensity above ~2700 a.u (Figure 4.5B). A 1-way ANOVA p-value of < 0.01 shows the increment observed in GSK-3β/Fyn F.I readings at day 7 is statistically significant.

As was expected, there was an increment in aggregation overtime with the sequentially phosphorylated Tau samples induced with heparin (Figure 4.5B), and also a significantly higher reading in the turbidity assays observed (Figure 4.5C) at day 14.

However, the role of phosphorylation in these increments in fluorescence and turbidity readings observed remained unknown. The MARK4/GSK-3β sequentially phosphorylated samples were investigated to identify the role of phosphorylation in the increased fluorescence intensities and increased turbidity readings seen. In the absence of ATP, sequential phosphorylation of Tau is not expected to occur. With both the MARK4/GSK-3β sequentially phosphorylated Tau samples without heparin and ATP showing fluorescence intensity below ~1500 a.u (Figure F.1), then the sequential phosphorylation of the Tau sample did not increase aggregation, as was observed in Gamblin *et al* (2007) phosphorylation of Tau with GSK-3β[119]. The presence of heparin in sequentially phosphorylated MARK4/GSK-3β Tau samples with and without ATP all showed fluorescence intensity above ~1700 a.u till 5 days after which there was a decline in fluorescence intensity (Figure F.1). Notably, phosphoprotein resulted in more β-sheet than non-phosphorylated Tau protein when kinase was present during the heparin-induced aggregation. Again, the protein kinase promoted Tau aggregation into insoluble structures. This indicates phosphorylation of Tau increased fluorescence intensity in the case of sequentially phosphorylated Tau samples in Figure 4.5B. Turbidity assays for the MARK4/GSK-3β sequentially phosphorylated Tau samples with and without ATP showed high turbidity reading after 14 days (Figure G.1). The calculated 1-way ANOVA p-value of 0.14943 for day 14 indicated that the increase in turbidity observed for the other sequentially phosphorylated Tau samples on day 14 was not statistically significant.

Again, the phosphorylated protein forms more insoluble structures than the protein when kinase was present, without a co-substrate. Data indicates that the phosphoprotein and mixtures of protein and kinase exhibit propensity for formation of insoluble structures. This could be attributed to the formation of other insoluble precipitates other than fibrils and filaments or protein degradation. The presence of the kinases after also promoted the cloudiness observed as this was not observed when Tau 441 only was aggregated with heparin (Figure 4.5C).

The SDS-PAGE analysis indicated greater formation of HMW aggregates for phosphorylated protein than the non-phosphorylated protein (Figure H-1). The presence of heparin induced both degradation and the formation of SDS resistant aggregates in the sequentially phosphorylated Tau 441 on day 7 (Figure H.1), as was observed with the single phosphorylated samples assessed . Even though sequentially phosphorylated Tau 441, on day 14 still formed SDS-resistant aggregates. pTau further degraded (Figure H.1iii), analogous to the observation made in the single kinase phosphorylated Tau 441.

To confirm by SDS-PAGE the formation of SDS-resistant aggregates in the absence of phosphorylation when Tau 441 was aggregated in the presence of heparin, and to also establish the role of phosphorylation in the observed was insignificant, Tau 441 was incubated in the presence of the kinases (GSK-3β, MARK4 and Fyn) and heparin with no ATP and the gels run. The SDS-PAGE for the single kinases, GSK-3β, MARK4 and Fyn additions to Tau 441 in the absence of ATP at day 7 (Figure 4.6Aii) showed the formation of SDS-resistant aggregates that gradually degraded by day 14 (Figure 4.6Aiii).

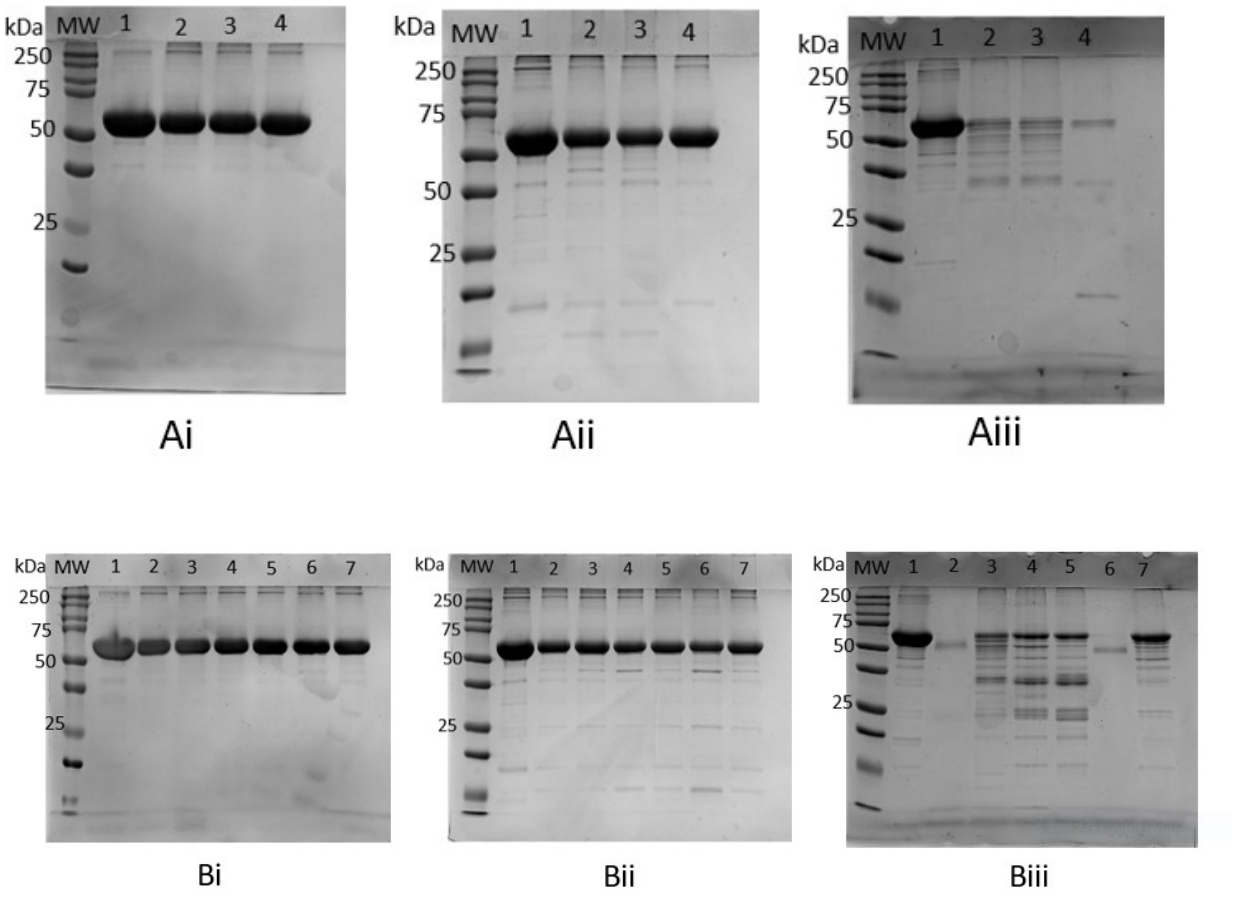

A
1 – nTau 411
2 – Tau 441 (GSK-3β)
3 – Tau 441 (MARK4)
4 - Tau 441 (Fyn)

B
1 – nTau 411
2 – Tau 441 (GSK-3β followed by MARK4)
3 – Tau 441 (GSK-3β followed by Fyn)
4 - Tau 441 (MARK4 followed by GSK-3β)
5 – Tau 441 (MARK4 followed by Fyn)
6 – Tau 441 (Fyn followed by GSK-3β)
7 – Tau 441 (Fyn followed by MARK4)

Figure 4.6: SDS-PAGE of single and multiple kinases in the presence of Tau 441 and heparin (No ATP): (A) SDS-PAGES of Tau 441 with kinases in the presence of heparin with no ATP; (incubation time = 24 h; incubation temperature = 37 °C; ageing time = 14 days; ageing temperature = 37 °C). (B) SDS-PAGES of Tau 441 with kinases in the presence of heparin with no ATP; (incubation time = 48 h; incubation temperature = 37 °C; ageing time = 14 days; ageing temperature = 37 °C).

Hence, protein kinase being co-present with Tau protein promoted degradation. There was also an extensive formation of lower molecular products at day 14 than in day 7. This is synonymous to the observation made when Tau was aggregated with heparin only in the Tau-heparin-buffers aggregation study (Figure B.1). This indicates phosphorylation had no role to play in the SDS-resistant aggregates observed but that protein kinase being co-present with Tau did contribute. The multi-kinase combinations where the protein kinases were co-present with Tau protein, without ATP, showed the same trend observed in the single kinase experiments. There was the formation of HMW SDS-resistant aggregates at day 7 (Figure 4.6Bii) which also gradually degraded at day 14 (Figure 4.6Biii).

Although day 7 was characterized by the formation of lower molecular products, there was an extensive formation of lower molecular products at day 14 (Figure 4.6Biii), also analogous to the observation made in Figure 4.6A and Figure B-1. Figure 4.6Biii clearly depicts that protein degradation was highly dependent on the protein/enzyme composition. For example, lanes 2 and 6 (GSK-3β followed by MARK4 and Fyn followed by GSK-3β phosphorylations) resulted in a complete degradation of protein, or formation of insoluble structures which did not enter the gel. By contrast, lanes 4 and 5 (MARK4 followed by GSK-3β and MARK4 followed by Fyn phosphorylations) are similar in terms of protein loading and fragmentation. The nTau, lane 1, without any protein kinase clearly shows minimal protein degradation. Notably, lane 7 (Fyn followed by MARK4 phosphorylation), gel behaviour was similar to that of nTau.

4.4 Conclusions

The aggregation properties of *in vitro* phosphorylated single or multi-kinase Tau 441 were evaluated in this chapter. Proteostat assay, turbidity assay and SDS-PAGES were employed for these assessments. The proteostat assay of the single kinase phosphorylation of Tau 441 without heparin showed no aggregation over time. However, when heparin, a polyanionic co-factor that induces aggregation, was added to the singly phosphorylated Tau samples, the presence of the inducer caused significantly higher aggregation of the phosphorylated Tau 441 samples. The drop in fluorescence intensity (F.I) observed at day 14 could be attributed to visible cloudiness observed which was also confirmed by turbidity assays. The SDS-resistant aggregates seen on the SDS-PAGE at day 7 corroborated the increased fluorescence intensity observed by proteostat assay when heparin was added as an inducer of aggregation in the single kinase proteostat assays. This observation also confirms the ability of heparin to co-localize with Tau leading to Tau fibrillization as observed by Goedert *et al*, 1996[159].

With Tau phosphorylated *in vivo* by several kinases, the role of sequential phosphorylation on Tau aggregation was evaluated. The multi-kinase combinations assessed were the GSK-3β/MARK4, GSK-3β/Fyn, MARK4/GSK-3β, MARK4/Fyn, Fyn/GSK-3β and Fyn/MARK4. This was done to establish which kinase combination would yield the most aggregation of phosphorylated Tau 441. Like in the single kinase phosphorylations, the sequentially phosphorylated Tau 441 combinations without heparin showed no aggregation overtime. There was no significant increase in the F.I's when heparin was added, with the highest F.I recorded in the GSK-3β/Fyn combination on day

7. There was a drop in F.I on day 14 just was seen with the single kinase with heparin proteostat assay.

To further confirm phosphorylation played no role in high F.I recorded, an SDS-PAGE confirmed the formation of SDS-resistant aggregates and extensive formation of lower molecular degradation products in the absence of Tau phosphorylation. This is synonymous to the observation made when Tau was induced with only heparin and no kinases.

CHAPTER FIVE

MASS SPECTROMETRY ANALYSIS OF PHOSPHORYLATED TAU

5.0 Introduction

A fascinating way to study posttranslational modifications is via 'proteomics.' Proteomics being extremely sensitive, can be used to identify the specific amino acid sites on a protein that undergo posttranslational modifications. Phosphorylation, the most prevalent posttranslational modification (PTM) in eukaryotic cells has been found to play a vital role in numerous cellular processes, including cell differentiation, proliferation, and migration. Tau, one of the proteins implicated in AD, also undergoes several PTMs, including phosphorylation. When Tau is hyperphosphorylated in the human brain, it forms NFTs. With hyperphosphorylation being the primary cause of Tau fibrillization, it is imperative to study and identify the phosphosites on Tau that contribute to the conformational changes that promote Tau aggregation.

Significant advancements have been made in the development of analytical techniques designed to measure protein structure and dynamics. Over the last two decades NMR has been used to decipher the pattern of tau phosphorylation both qualitatively and quantitatively [160][161]. However, in recent times, coupling of electrospray ionization mass spectrometry (ESI-MS) to HDX has rapidly gained popularity[162][163].

To understand and identify the phosphorylation patterns that lead to the structural changes that cause Tau aggregation, we characterized differentially phosphorylated states of full-length Tau 441 using tandem mass spectrometry and Time-resolved electrospray

Mass spectrometry - Hydrogen deuterium exchange (TRESI-MS HDX). Tandem mass spectrometry was used to identify all the amino acid sites phosphorylated by GSK-3β, MARK4, and Fyn, either singly or with multiple kinases combinations. TRESI-MS HDX was also used to give a detailed account of the conformational shifts that occurred when Tau 441 was phosphorylated. The structural changes in TRESI MS-HDX are observed when the hydrogens on protein amide, hydroxyl, or thiol groups in the protein backbone undergo exchange with deuterium from the solvent used (usually water).

In this chapter, the structural changes observed via phosphorylation were rationalized as the cause of increasing amyloidogenic propensity, suggesting that GSK-3β, MARK4, and Fyn mediated hyperphosphorylation observed in Tau 441 at specific sites could be a causative event of Tau amyloidogenesis.

5.1 Experimental section

5.1.1 Materials and equipments

Tau-441 protein (recombinant tau-441, 2N4R) was expressed and purified from the Wu laboratory (Oakland University, MI). MARK4, Fyn or GSK-3β protein kinases at a concentration of 0.1 mg/mL were purchased from SignalChem (Richmond, British Columbia, Canada). ATP was purchased from Sigma-Aldrich (St. Louis, MO, USA). The stock solution of phosphate buffer, pH 7.0, was prepared using 60 mM sodium phosphate monobasic, anhydrous, obtained from Fisher Scientific (NJ, USA) and 60 mM sodium phosphate dibasic, anhydrous, obtained from J. T. Baker (NJ, USA). The pH was adjusted using sodium hydroxide (NaOH) obtained from Fisher Scientific (NY, USA). The stock solution of kinase buffer was a mixture of 50 mM 4-(2-hydroxyethyl)-1-piperazineethanesulfonic acid (HEPES) from Sigma-Aldrich, 100 mM sodium chloride

(NaCl) from Fischer Scientific, 1 mM dithiothreitol (DTT) obtained from Thermo Scientific Pierce (Rockford, IL, USA), and 10 mM magnesium chloride ($MgCl_2$) from Amresco (Solon, OH, USA). The pH was adjusted to 7.4 using sodium hydroxide (NaOH).

The phosphorylated sample were separated by reverse phase chromatography and analyzed on a Orbitrap Fusion™ Tribrid mass spectrometer (Thermo scientific). QStar Elite Hybrid Q-TOF Mass Spectrometer coupled with HDX (AB SCIEX) was used for the conformational studies of phospho-Tau.

5.1.2 Phosphorylation of Tau 441 by MARK4, Fyn or GSK-3β

Single and multi-kinase phosphorylated Tau 441 samples were generated as described in chapter 4 for tandem mass spectrometry and Time-resolved electrospray (TRESI) – Mass spectrometry (MS) – Hydrogen deuterium exchange (HDX).

5.1.3 Liquid Chromatography/Mass spectrometry/Mass Spectrometry (LC/MS/MS)

Single and multi-kinase phosphorylated Tau 441 samples were analyzed with Orbitrap Fusion™ Tribrid mass spectrometer (Thermo scientific) at Wayne State University (WSU). 25 μg of each sample was reduced with DTT and alkylated with iodoacetamide, and then digested with 0.5 μg of either trypsin or chymotrypsin overnight at 37ºC. Samples were acidified with formic acid and dried. Phosphopeptides were enriched using TiO2 tips with a Bravo automated liquid handling platform (Agilent), acidified with formic acid, and dried. Samples were resuspended in 15 μl of 5% acetonitrile, 0.1% formic acid and 0.005% trifluoroacetic acid (TFA). Half the sample was separated by reverse-phase chromatography and analyzed on a Fusion Orbitrap mass spectrometer (Thermo Scientific, WSU). MS1 scans were performed with a 375 – 1600

m/z range in the Orbitrap at 240,000 resolution. MS2 Ions were scanned in the ion trap. Peptides with +2 or +3 charges were fragmented by CID (32% collision energy), and those with +3 to +7 were fragmented by ETD.

5.1.4 LC/MS/MS data Analysis:

Data were analyzed using PEAKS Studio software (Build 8.5). Data were filtered to 10 ppm and 0.6 Da tolerances for parent and fragment ions, respectively. Spectra were searched against a human protein database from Uniprot (downloaded 2018-05-06; 20,260 sequences), which contained the 441 isoform for Tau protein (accession P10636-8). 4 search engines were used in the search (De Novo, Peaks DB, Peaks PTM, and Spider). The results from 2 enzymes were combined into one search result. Data were filtered to a 1% FDR level for peptides, at least 2 unique peptides, and a score of >20 (i.e., at least 99% confidence in PTM localization). For the Peaks DB search, carbamidomethylation of C was included, variable modifications for oxidation of M, deamidation for NQ, and phosphorylation of STY. Peaks PTM search had 313 built-in mutations.

5.2 Time-resolved electrospray – Mass spectrometry – Hydrogen deuterium exchange (TRESI-MS-HDX)

Phospho-Tau samples were analyzed with QStar Elite Hybrid Q-TOF Mass Spectrometer coupled with HDX (AB SCIEX) at the Wilson laboratory (York University, Canada)

1. Acquisition of Pepsin and Tau Protein Only Spectra: Samples were Electrospray-ionization (ESI)-MS was carried out in positive ion mode with a voltage of +4,500 to +5,000, 60-V declustering potential, and 250-V focusing potential. The spectra for both

pepsin and native Tau 441 are acquired over a range of 350-1,500 m/z with a scanning rate of 1 s^{-1}.

After acquiring a pepsin-only spectrum, any other peaks appearing in this spectrum are subtracted once the protein is added, and this is identified as the spectrum for native Tau 441.

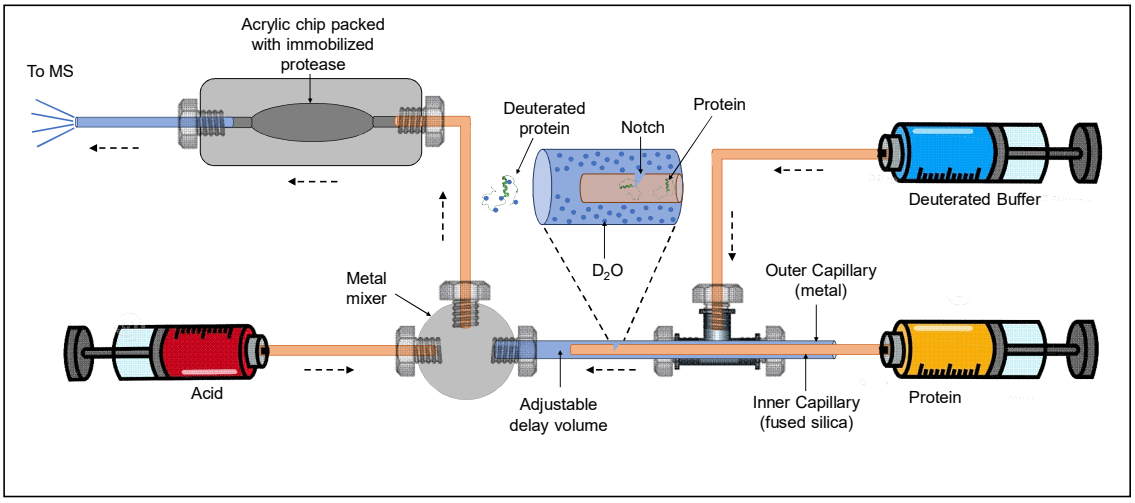

Figure 5.1: TRESI-HDX MS apparatus:

The conformation of the Tau samples (phosphorylated and non-phosphorylated) was evaluated by introducing the samples into the fused silica in the inner capillary of the TRESI – MS HDX apparatus after it was buffered with D_2O.

2. HDX-MS analysis of non-phosphorylated Tau and phosphorylated Tau 441 (single and multi-kinase combinations): 50-100 µM Tau or phospho-Tau protein (Tau expressed/purified as described in chapter 2 and phosphorylated Tau as described in chapter 4) was introduced at a rate of 1 µL/min where the 50 mM ammonium acetate

buffer was previously flowing. After a complete equilibration of the Tau samples with the D_2O, the proteins exposed to the deuterated solvent for a variable 'labeling time', resulted in isotopic exchange of unprotected labile protons on the amide backbone and amino acid side chains. The spectrum at the end of the analysis was an indication of phosphorylation and conformational change.

3. Acquiring a Tau or phospho-Tau protein only spectrum (Acquisition of Time Points): While 100 μM Tau/phospho-Tau protein was flowing at 1 μL/min, D_2O was introduced at a rate of 3 μL/min via a tee connector and allowed to react in the kinetic mixer. The system was allowed to equilibrate for at least 10 min before acquiring the spectrum. It is crucial to note that, after the exchange of hydrogen for deuterium, the labeling reaction was quenched by the flow of acetic acid pH 2.4 at 10 μL/min, and digestion of the labeled protein occurs in the proteolytic chamber. To increase the labeling time, the inner glass capillary was manually mixing 42 m/s to 8s. The system was allowed to equilibrate for at least 10 mins in between each pull-back. The structure of (hyper)phosphorylated Tau was generated using FRODAN simulation with subsequent refinement using VADAR. The Wilson laboratory (York University, Canada) did all HDX-MS analysis, kinetic plots, FRODAN simulations, and VADAR refinements used in this chapter

5.3 Results and discussion

5.3.1 LC/MS/MS characterization of phosphosites on Tau 441

Site-specific phosphorylation causes a distinct conformational change. Tau-specific phosphosite identification could lead to recognizing phospho-sites that promote Tau detachment from microtubule or its aggregation into fibrils and filaments.

As expected, the Liquid chromatography (LC) in tandem with mass spectrometry data showed no phosphorylation when non-phosphorylated Tau 441 was characterized. In contrast to what was observed in non-phosphorylated Tau, kinase-specific phosphorylation sites were observed when specific kinases were employed to phosphorylate Tau 441. *In vitro* phosphorylation of Tau 441 by GSK-3β showed significant phosphorylation in the proline-rich (190-240 aa) and C-terminus (390-441aa) domains. The most abundant phospho-sites observed were specifically pSer199, pSer396, pSer400, and pSer404 (Figure 5.2).

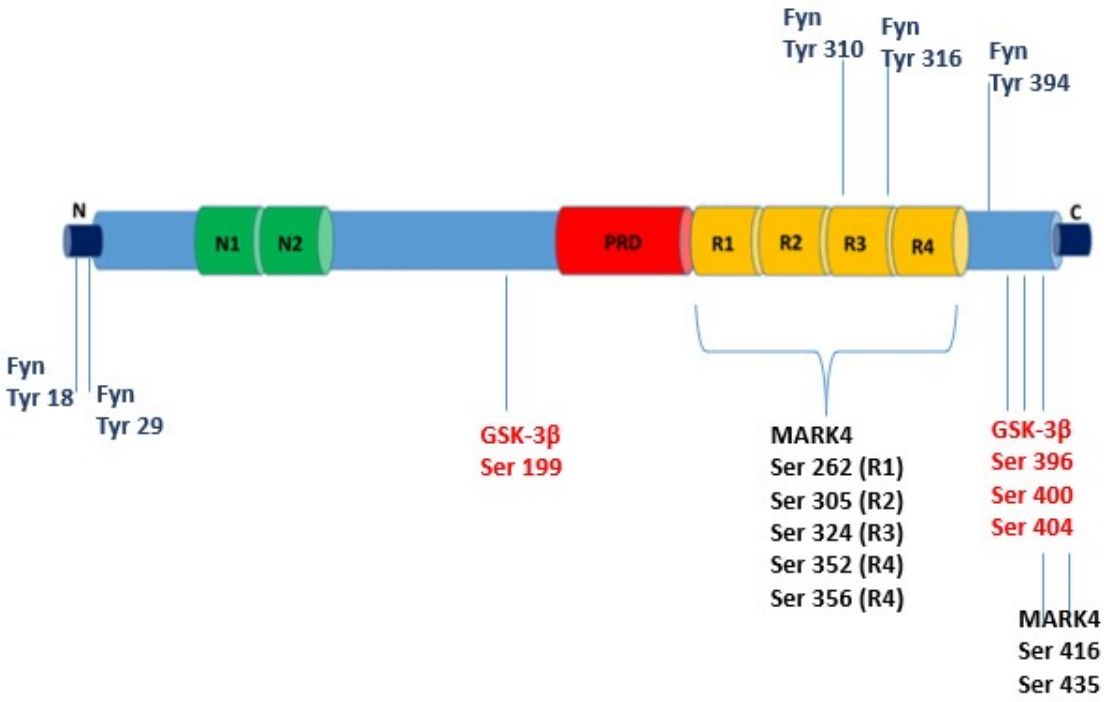

Figure 5.2: Schematic of Tau 441 showing phosphosites detected after in vitro phosphorylation using specific kinases

The tandem mass spectrometry analysis of Fyn-phosphorylated Tau 441 indicated phosphorylation at pTyr18, pTyr29, pTyr310, pTyr316 and pTyr394, with the most significant phospho-sites being pTry310 and pTyr394 (Figure 29). But in the case of the *in vitro* phosphorylation of Tau 441 by MARK4, phosphorylation was observed at pSer262, pSer305, pSer324, pSer352, pSer356, pSer416, and pSer435, but the greatest intensities were seen pSer262, pSer258, pSer324, and pSer356 (Figure 29).

With Tau being phosphorylated *in vivo* by several kinases, Tau was sequentially phosphorylated with multiple kinases to examine the role they play in changing the conformation of Tau imparting its ability to aggregate. Tau 441 phosphorylated using different kinase combinations were also analyzed using LC in tandem with MS. The *in vitro* phosphorylation of Tau 441 using GSK-3β followed by MARK4 showed significant phosphorylation in the proline-rich region (175–235aa), the MTBRs R1 - R2 (262–305aa), and the C-terminal region (324–422aa), with pSer396, pSer400, and pSer404 being the most phosphorylated sites. These commonly phosphorylated sites in GSK-3β followed by MARK4 phosphorylation of Tau were similar to the commonly observed sites in the GSK-3β only phosphorylation. Similarly, MARK4 followed by GSK-3β phosphorylation of Tau 441 also showed significant phosphorylation in the proline-rich region (175–235aa), the MTBRs (262–324aa and 352–361aa), and the C-terminal region (396–435aa). The most phosphorylated sites observed here were pSer352 and pSer356.

Tau 441, sequentially phosphorylated by GSK-3β followed by Fyn, was also analyzed. Like the GSK-3β and MARK4 sequentially phosphorylated Tau samples, most phospho-sites were also found in the proline-rich region (149–235aa), the MTBRs R2 – R4 (285–356aa), and the C-terminal region (394–422aa).

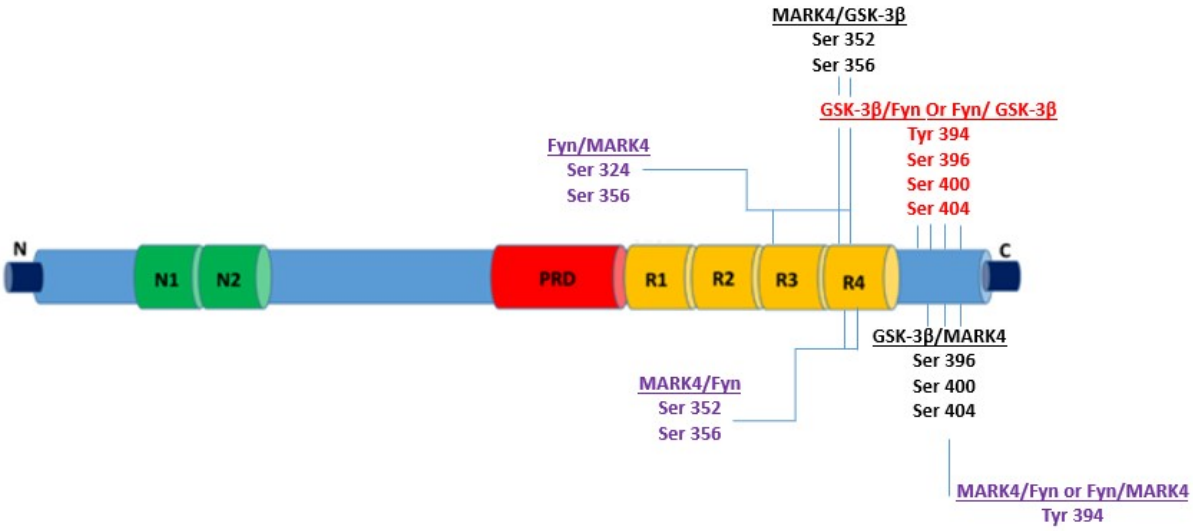

Figure 5.3: Schematic showing phosphosites detected after multi-kinase in vitro phosphorylation of Tau 441

Besides the Ser's and Thr's, some Tyr residues were among the phosphorylated sites observed, and this is because Fyn is a protein Tyr kinase. The frequently encountered phosphosites here included pTyr394, pSer396, pSer400 and pSer404. Likewise, the Fyn followed by GSK-3β phosphorylated samples also showed significant phosphorylation in the proline-rich region (169–235aa and 289–324aa) and the C-terminal region (356–416aa), with a few of the phosphosites identified in the N-terminal region (pTyr18, pTyr29, and pSer46). The most abundant phosphosites observed with the Fyn followed by GSK-3β *in vitro* phosphorylation were pTyr394, pSer396, pSer400 and pSer404. The last kinase combinations analyzed were that of MARK4 and Fyn. The *in vitro* MARK4 followed by Fyn phosphorylation of Tau 441 showed significant phosphorylation in the MTBRs R1 – R3 (262–324aa) and the C-terminal region (352–416aa).

Table 5.1: Phosphorylated domains of sequentially phosphorylated Tau 441: Table of Tau 441 shows the domains where the most phosphosites were detected after the in vitro phosphorylation of Tau 441 by specific sequential kinases.

Phosphorylation sequence	**Phosphosites**
GSK-3β/MARK4	PRD (175 - 235), MTBR R1 – R2 (262 - 305), CTD (324 - 422)
MARK4/GSK-3β	PRD (175 - 235), MTBR (262 – 324 and 352 - 361), CTD (396 - 435)
GSK-3β/Fyn	PRD (149 - 235), MTBR R2 – R4 (285 - 356), CTD (392 - 422)
Fyn/GSK-3β	NTD (pTyr18, pTyr29, pSer46), PRD (169 – 235 and 289 - 324), CTD (356 - 416).
MARK4/Fyn	NTD (pTyr18), PRD (pSer208, pSer237), MTBR R1 – R3 (262 - 324), CTD (352 - 361)
Fyn/MARK4	NTD (pTyr18, pTyr29), MTBR R1 – R3 (262 - 324), CTD (352 - 416

Other sites phosphorylated that fell outside the above listed groups were pTyr18 in the N-terminal region, and pSer208 along with pSer237 in the proline-rich region. The most abundant phosphosites observed with the MARK4 followed by Fyn *in vitro* phosphorylation were pSer262, pSer352, pSer356 and pTyr394 all in the MTBRs. The reverse, which is Fyn followed by MARK4 phosphorylation of Tau also exhibited significant phosphorylation in the MTBRs R1 – R3 (262–324aa) and the C-terminal region (352–416aa). The Fyn followed by MARK4 combination also showed phosphorylation of pTyr18 and pTyr29 in the N-terminal region. The most abundant phosphosites observed with the Fyn followed by MARK4 *in vitro* phosphorylation were pSer324, pSer356 and pTyr394.

5.3.2 Conformational analysis of phosphoproteins

Conformational changes play a crucial role in protein dynamics and are often intimately related to protein functions. Before Tau protein aggregates, it assumes a particular conformational state that promotes its clustering. Hyperphosphorylation, identified as the primary cause of Tau fibrillization, gives rise to different conformational changes in Tau, resulting in the formation of oligomers, pair helical filaments, or straight filaments, and then neurofibrillary tangles (NFTs). Over the years, the most comprehensive structural description of Tau protein was first achieved by NMR. Mukrasch *et al*, in 2009 building on resonance data was able to describe the structure of the full-length Tau protein[164]. This was the most challenging prospect ever to be achieved for any large IDP due to their low spectral dispersion. NMR measurements was afterwards used to predict the locations of residual secondary structures in Tau and has also been used to identify site-specific mapping of ϕ/φ angle 'conformational potentials' in a Tau fragment that may promote aggregation. Other approaches after Mukrasch *et al*., 2009 findings have been used to achieved even better results[165]. Wilson *et al.*, 2015 using TRESI-MS-HDX, gave a detailed view of GSK-3β hyperphosphorylation-driven conformational shifts in the full-length Tau 441[121]. The global and local structural changes identified by Wilson and his group were rationalized as the cause of increasing amyloidogenic propensity in the GSK-3β hyperphosphorylated Tau monomer. However, little is known about how other phosphosites modulate Tau protein conformation and they were evaluated next.

The conformational changes in Tau 441 phosphorylated with GSK-3β, Fyn, and MARK4 were evaluated. By assessing the various phosphorylated ensembles, the

ensemble that promotes the most aggregation can be identified. The exchange of the hydrogens in the amide, hydroxyl, or thiol groups in the protein backbone with deuterium are used to monitor the conformational changes if any. The TRESI-MS HDX data for GSK-3β phosphorylated Tau 441 showed the most significant deuterium uptake in the R3 region (326 – 336aa) of Tau 441. Other areas with considerable deuterium uptake were in the proline rich region (226 – 230aa) and the MTBR (300 – 317aa and 331 – 360aa)(Figure 5.4). These regions showing high deuterium uptake is consistent with the phosphosites observed in the tandem MS data on phosphorylation collected for GSK-3β. Due to the consistency between the HDX-MS data (Figure 5.4) and the tandem MS data (Figure 5.2), the conformational change observed in the GSK-3β phosphorylated Tau 441 ensemble can be attributed solely to phosphorylation.

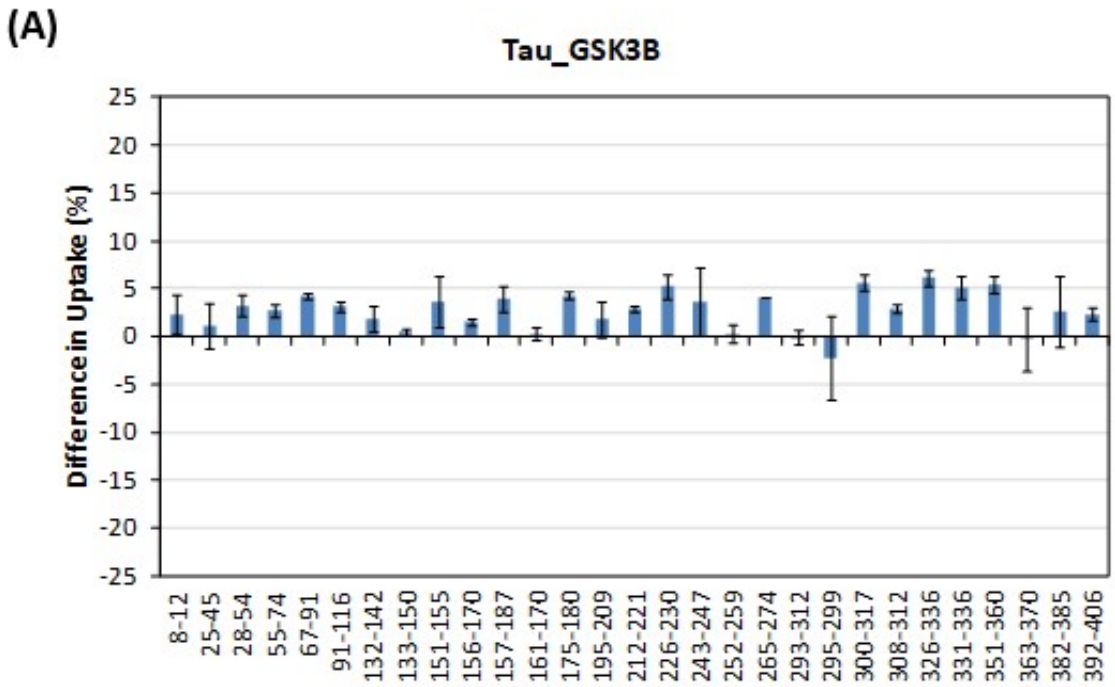

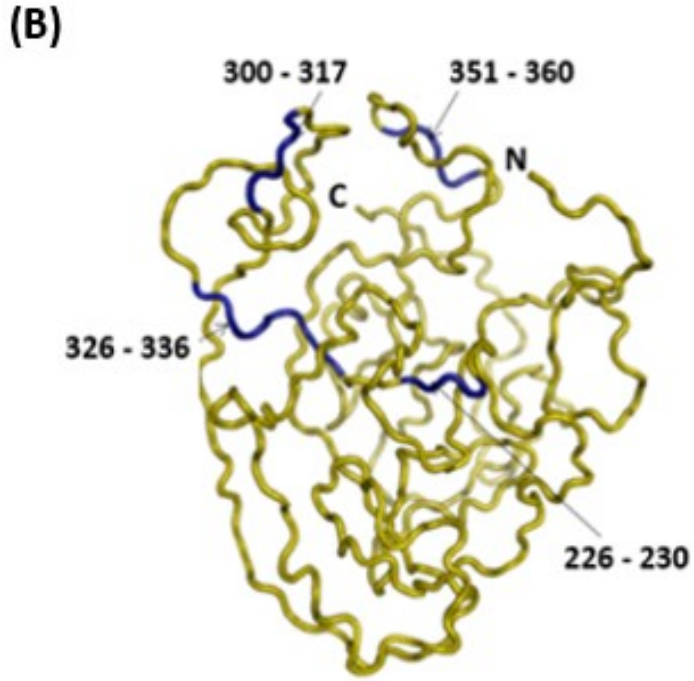

Figure 5.4: HDX-MS data and predicted conformation of GSK3β phosphorylated Tau 441 protein: (A) After the phosphorylation of Tau 441 by GSK-3β, the sample was subjected to TRESI – MS HDX. Deuterium uptake in Tau 441, which is a mark of conformational change observed in Tau 441 showed the most significant deuterium uptake in R3 region (326 – 336aa) of Tau 441. There was also extensive deuterium uptake in the proline rich region (226 – 230aa) and the MTBR (300 – 317aa and 331 – 360aa). (B) A predicted conformation showing deuterium uptake in Tau 441 phosphorylated by GSK-3β**:** The predicted conformation shows regions on Tau 441 that have their hydrogens in the amide backbone and amino acid side chains replaced by deuterium. The deuterium uptake after the pTau Fyn sample was analyzed by MS-HDX is indicative of Tau phosphorylation by GSK-3β. The regions marked blue on the Tau cartoon (226 – 230aa, 300 – 317aa, 326 – 336aa, and the 351 and 360aa) were the regions that showed high deuterium uptake. The conformational change observed in Tau after phosphorylation was easily detected via the deuterium location on Tau.

Figure 5.4B shows the global structure observed after the deuterium uptake in GSK3 phosphorylated Tau 441. Here, there were observable new intramolecular interactions in the MTBR, with the hexapeptide repeats (H2) which have been identified to be largely implicated in amyloidogenesis shown to be exposed in the global structure of the GSK-3β phosphorylated Tau. This indicates that, GSK-3β phosphorylated Tau could be a probable cause of observable Tau aggregation. This is similar to the finding by Wilson *et al,* 2015[121].

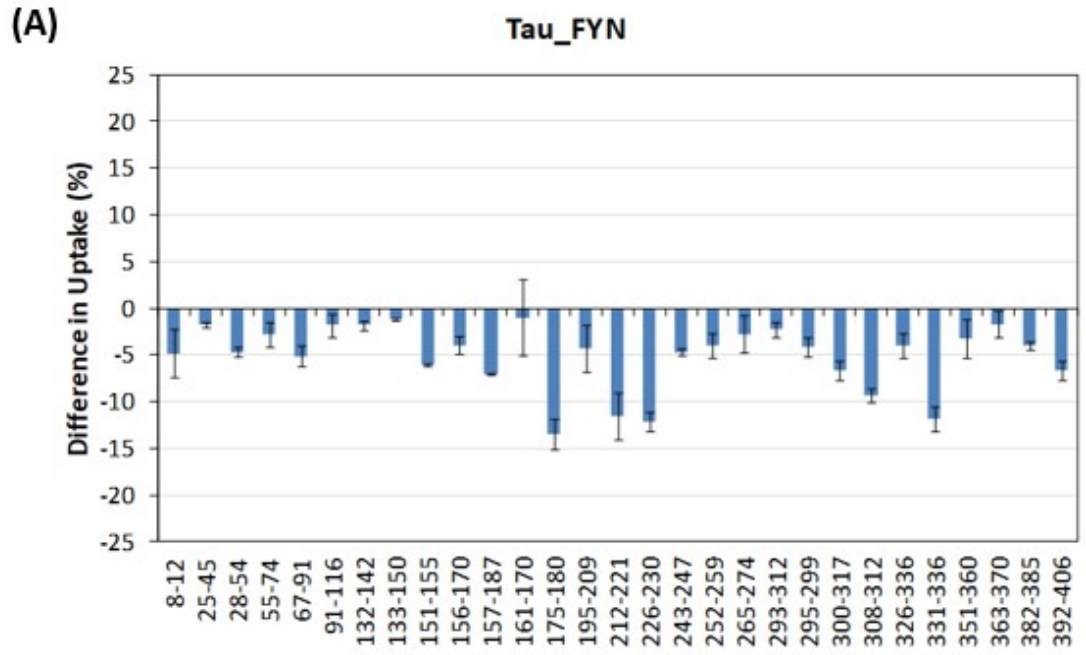

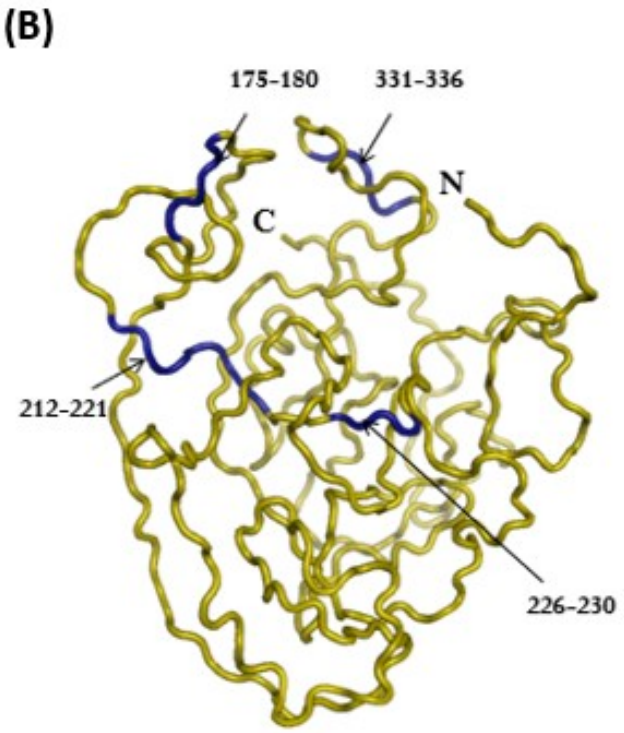

Figure 5.5: HDX-MS data and predicted conformation of Fyn phosphorylated Tau 441 protein : (A) Fyn phosphorylated Tau 441 was subjected to TRESI – MS HDX. The isotopic exchange of unprotected labile protons on the amide backbone and amino acid side chains with deuterium which marked the conformational change observed in Fyn was observed in the Proline rich region (175 – 180aa, 212 – 221aa, and 226 – 230aa) and the MTBR R3 region (331 and 336aa). (B) A predicted conformation showing deuterium uptake in Tau 441 phosphorylated by Fyn**:** The cartoon shows the regions on Tau 441 that have their hydrogens in the amide backbone and amino acid side chains replaced by deuterium. The deuterium uptake after the pTau Fyn sample was analyzed by MS-HDX is indicative of Tau phosphorylation by Fyn. The regions marked blue on the Tau cartoon (175 – 180aa, 212 – 221aa, 226 – 230aa, and the 331 and 336aa) were the regions that showed high deuterium uptake. The conformational change observed in Tau after phosphorylation was easily detected via the deuterium location on Tau.

In AD, Fyn has been shown to bind and co-localize with Tau directly[166]. Dawn *et al*. (2016) demonstrated that the proline residues P213, P216, P219 are critical for Tau: Fyn interactions[167]. The HDX-MS data for Fyn phosphorylated Tau 441 validated Fyn binding and co-localizing with Tau.

The highest deuterium uptake following Fyn phosphorylation of Tau 441 was observed in 175 – 180aa, 212 – 221aa, and 226 – 230aa all in the proline rich domain and 331 and 336aa also in the R3 region of the MTBD.

Here, the data from the TRESI – MS HDX for phosphorylated Tau by Fyn also showed high deuterium uptake in this region, indicative of the increased Tau /Fyn interactions (Figure 5.5A).

As was observed in GSK-3β phosphorylated Tau 441, even though there were observable intramolecular interactions in the PRD and the R3 region, the hexapeptide repeats were again sequestered in the Fyn phosphorylated conformation (Figure 5.5B).

MARK4 phosphorylated Tau 441 was also subjected to TRESI – MS HDX. Like the other kinases, specific regions showed high uptake of deuterium. While MARK4 showed different deuterium uptake in the different regions of Tau 441, the proline-rich regions, specifically between 151 – 221aa, showed the highest amount of deuterium uptake.

The R3 region amino acid sequence of 331 – 336 also showed considerable uptake of deuterium uptake when Tau 441 was phosphorylated with MARK4.

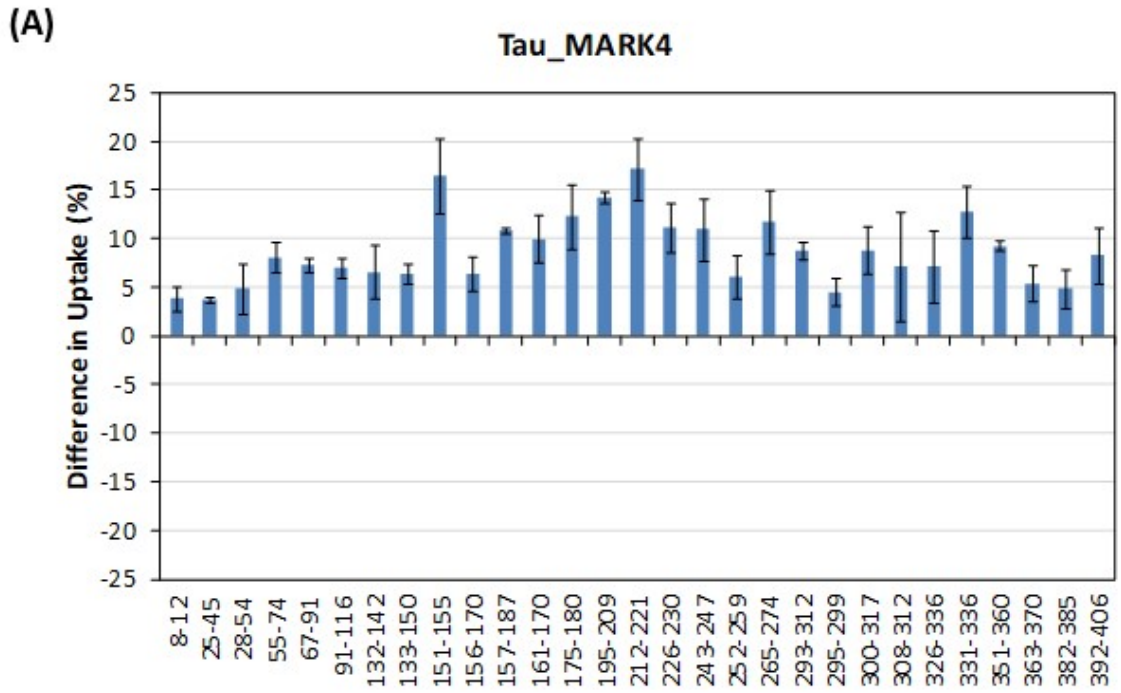

Even though the tandem MS data showed increased phosphorylation in pSer262, pSer305, pSer324, pSer352, pSer356, pSer416, and pSer435, with the most significant intensities seen in pSer262, pSer258, pSer324, and pSer356 (Figure 5.2), the increased uptake of deuterium in 151 – 221aa could be attributed to the change in conformation that resulted when the sites above in Tau were phosphorylated.

The conformational changes led to the hydrogen in amide, hydroxyl, or thiol groups in these regions being more prone to deuterium uptake. As it was observed in the GSK-3β and Fyn phosphorylated Tau ensembles, the hexapeptide repeats that promote Tau aggregation were here again sequestered despite the intramolecular interactions observed in the PRD and the MTBR (Figure 5.6B).

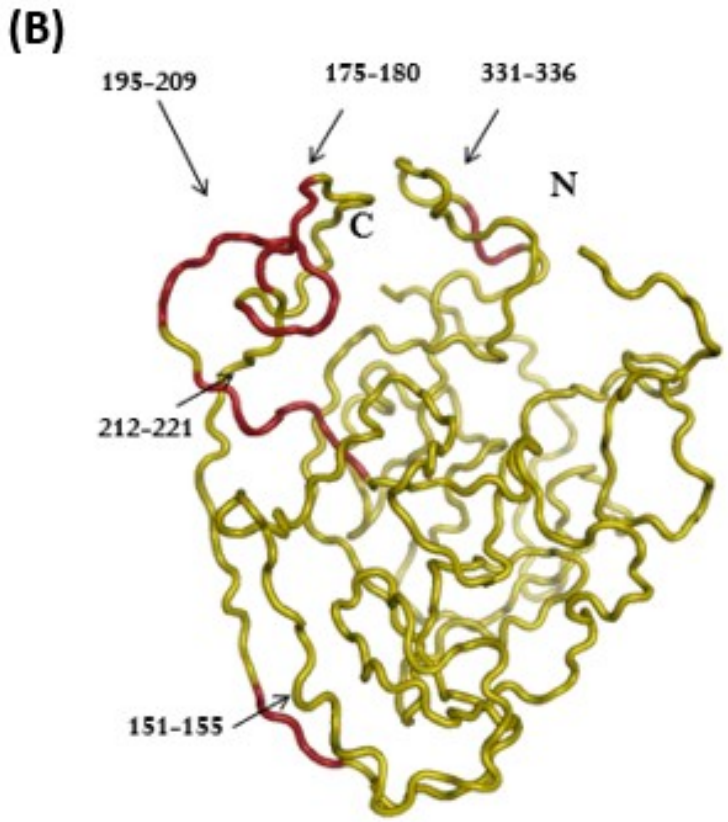

Figure 5.6: HDX-MS data and predicted conformation of MARK4 phosphorylated Tau 441 protein: (A) The HDX-MS data shows the distribution of deuterium uptake in MARK4 phosphorylated Tau 441 subjected to MS - HDX. The proline rich domain (151 – 155aa, 175 – 180aa, 195 – 209aa and 212 – 221aa) and the MTBR R3 (331 and 336aa) showed high deuterium uptake in Tau phosphorylated by MARK4. (B) A predicted conformation showing deuterium uptake in Tau 441 phosphorylated by MARK4**:** After Tau 441 was phosphorylated with MARK4, the phosphorylated Tau sample was subjected to TRESI – MS HDX. The Tau 441 cartoon regions marked red (151 – 155aa, 175 – 180aa, 195 – 209aa, 212 – 221aa, and the 331 and 336aa) were the regions that showed high deuterium uptake, which is an indicator of conformational change in Tau after phosphorylation by MARK4.

Protein phosphorylation is a post-translational modification process that involves a series of sequence-specific kinases and occurs on specific residues. In eukaryotes the amino acid phosphorylated are the serine(s), threonine(s), and tyrosine(s).

Hence, after the single kinase phosphorylated samples were subjected to TRESI MS – HDX, multiple kinases phosphorylated Tau 441 deuterium uptake data, and their predicted conformational changes were also evaluated. That is, the same multi-kinase phosphorylated samples subjected to LC/MS/MS.

Since it has been established that different kinases phosphorylate Tau in the human brain, it is imperative that possible specific kinase combinations that could lead to conformational changes triggering the most aggregation in Tau protein be known.

For the purposes of this experiments, one kinase was first utilized to phosphorylate Tau, after which a second kinase was also introduced to phosphorylate the protein further.

Equal phosphorylation times were allotted to each kinase introduced so they have the same time period to induce conformation changes if any.

The initial set to be investigated were the GSK-3β and Fyn kinase combinations. The GSK-3β followed by Fyn sequentially phosphorylated Tau was the first to be evaluated, i.e., GSK-3β was added to native Tau to phosphorylate it for 24 hours and after Fyn was also introduced into the same reaction to further phosphorylate Tau for another 24 hours.

(A)

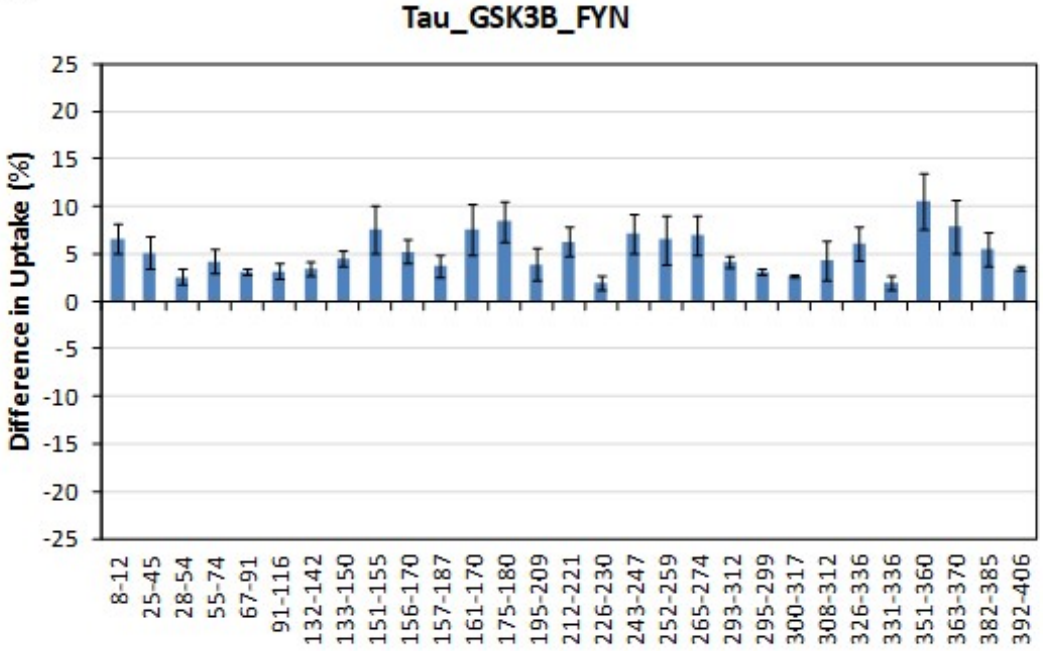
Tau_GSK3B_FYN
Difference in Uptake (%)
25
20
15
10
5
0
-5
-10
-15
-20
-25
8-12
25-45
28-54
55-74
67-91
91-116
132-142
133-150
151-155
156-170
157-187
161-170
175-180
195-209
212-221
226-230
243-247
252-259
265-274
293-312
295-299
300-317
308-312
326-336
331-336
351-360
363-370
382-385
392-406

(B)

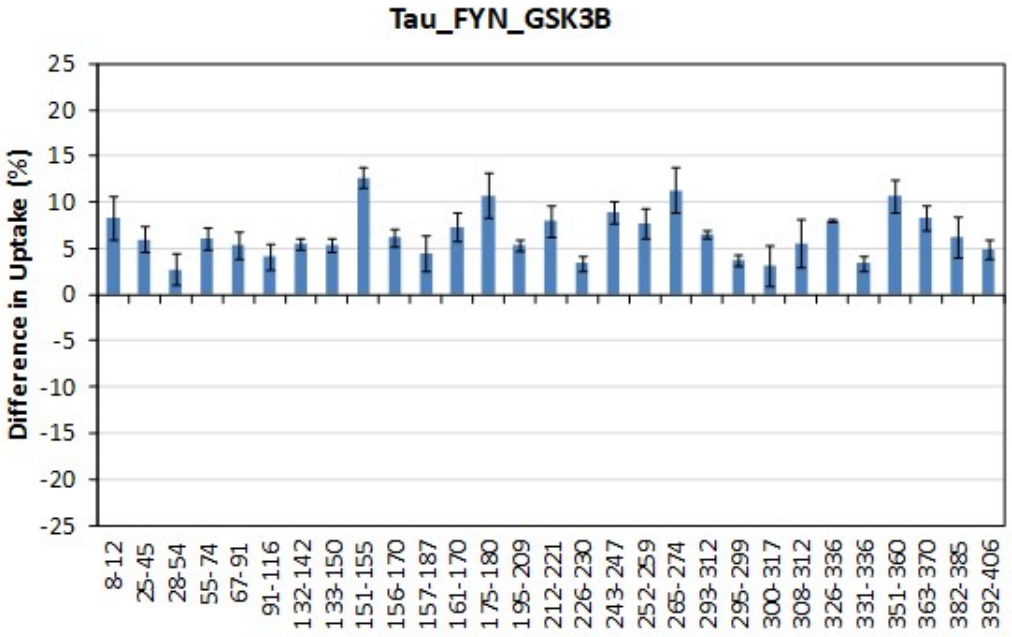
Tau_FYN_GSK3B
Difference in Uptake (%)
25
20
15
10
5
0
-5
-10
-15
-20
-25
8-12
25-45
28-54
55-74
67-91
91-116
132-142
133-150
151-155
156-170
157-187
161-170
175-180
195-209
212-221
226-230
243-247
252-259
265-274
293-312
295-299
300-317
308-312
326-336
331-336
351-360
363-370
382-385
392-406

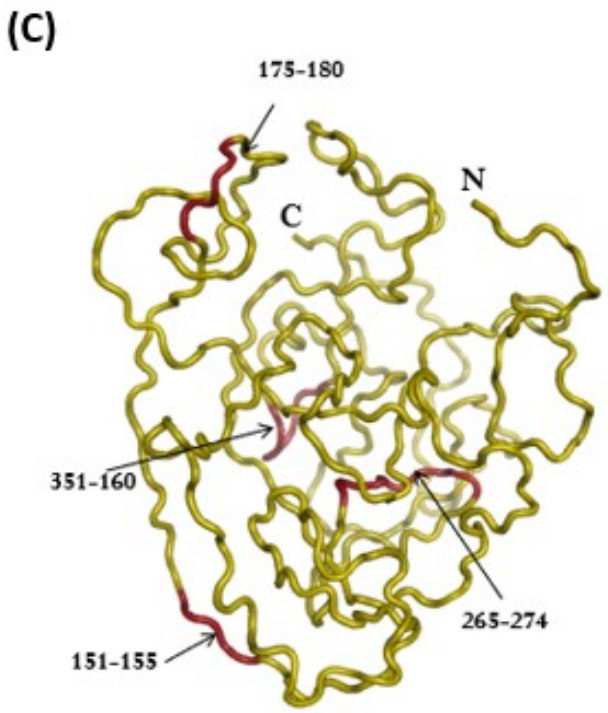

Figure 5.7: HDX-MS data and predicted conformation of GSK3β and Fyn sequentially phosphorylated Tau 441: (A) Tau 441 was phosphorylated with GSK-3β followed by Fyn. The phosphorylated Tau sample was subjected to HDX-MS to assess the phosphorylation patterns and conformational changes using the deuterium incorporated in the protein. Amino acids spanning from 151 – 155aa, 175 – 180aa, 265 – 274aa in the proline rich region and 351 – 360aa in the MTBR R4 which showed the highest deuterium uptake in the GSK-3β followed by Fyn Tau 441 phosphorylation indicated the phosphosites on Tau 441 following the GSK-3β followed by Fyn kinase phosphorylation. (B) HDX-MS data showing the deuterium uptake in Tau 441 phosphorylated with Fyn followed by GSK-3β**:** Once Tau 441 was phosphorylated with Fyn followed by GSK-3β, the phosphorylated Tau sample was evaluated by HDX-MS. Amino acids 151 – 155aa, 175 – 180aa, 265 – 274aa in the proline rich region and 351 – 360aa in the MTBR R4 showed the highest deuterium uptake, indicating the phosphosites on Tau 441 following the GSK-3β followed by Fyn kinase phosphorylation. (C) A predicted conformation showing deuterium uptake in Tau 441 phosphorylated by GSK-3β and Fyn**:** The cartoon of Tau 441 phosphorylated with GSK-3β and Fyn shows the regions on Tau with high deuterium uptake. The amino acids marked red (151 – 155aa, 175 – 180aa, 265 – 274aa, and 351 – 360aa).

After the GSK-3β followed by Fyn sequential phosphorylation as shown above, it was observed that the deuterium uptake was high in 151 – 155aa, 175 – 180aa, 265 – 274aa, and 351 – 360aa regions of Tau 441, with the highest observed uptake seen at 351 – 360aa 90 (Figure 5.7A). The next to be evaluated in the GSK-3β and Fyn kinase combination was the Fyn followed by GSK-3β sequentially phosphorylated Tau sample. The Fyn followed by GSK-3β sequential phosphorylation of Tau sample showed the same deuterium uptake pattern (151 – 155aa, 175 – 180aa, 265 – 274aa, and 351 – 360aa, with the highest observed uptake seen between 351 – 360aa) (Figure 5.7B) as sequentially phosphorylated Tau using GSK-3β followed by Fyn. It is important to note that irrespective of the GSK-3β and Fyn kinase order used to phosphorylation Tau, the regions that showed an increase deuterium uptake were similar in both cases. The deuterium uptake detection is equivalent to phosphorylation which is the cause of the conformational changes observed in Tau due to phosphorylation by GSK-3β and Fyn. The deuterium uptake observed in GSK-3β/Fyn and Fyn/GSK-3β phosphorylated Tau ensembles showed considerable intramolecular interactions in the PRD and MTBR. Here, the H1 hexapeptide repeat was partially exposed, indicating the potential of this kinase combination to aggregate Tau (Figure 5.7C).

The next set that was assessed were the MARK4 and Fyn kinase combination. Here, the first phosphorylation pattern to be evaluated was the MARK4 followed by Fyn sequentially phosphorylation of Tau.

(A)

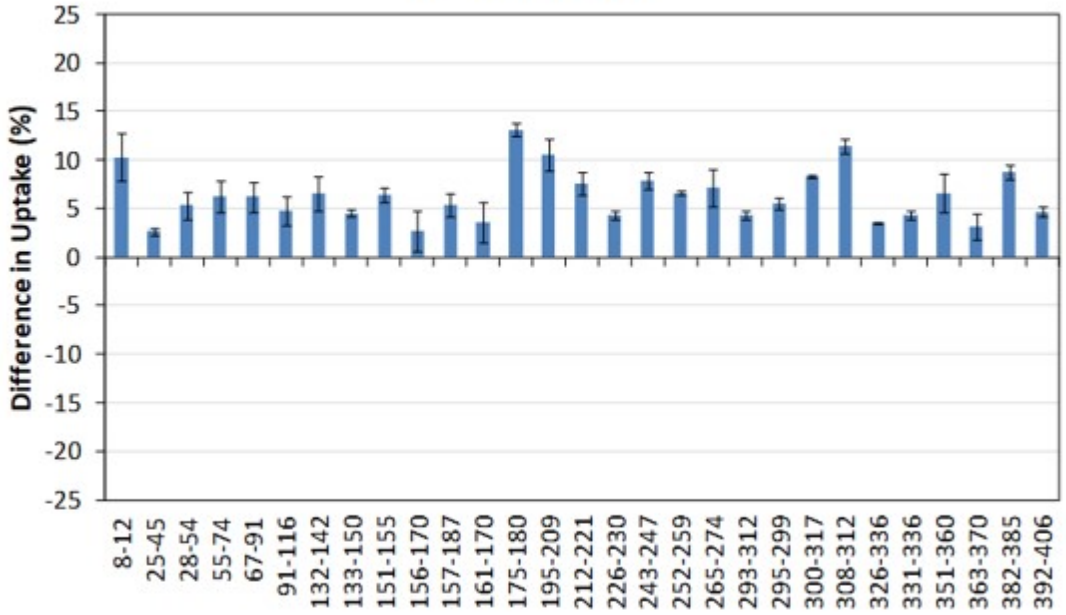
Tau_MARK4_FYN
Difference in Uptake (%)
25
20
15
10
5
0
-5
-10
-15
-20
-25
8-12
25-45
28-54
55-74
67-91
91-116
132-142
133-150
151-155
156-170
157-187
161-170
175-180
195-209
212-221
226-230
243-247
252-259
265-274
293-312
295-299
300-317
308-312
326-336
331-336
351-360
363-370
382-385
392-406

(B)

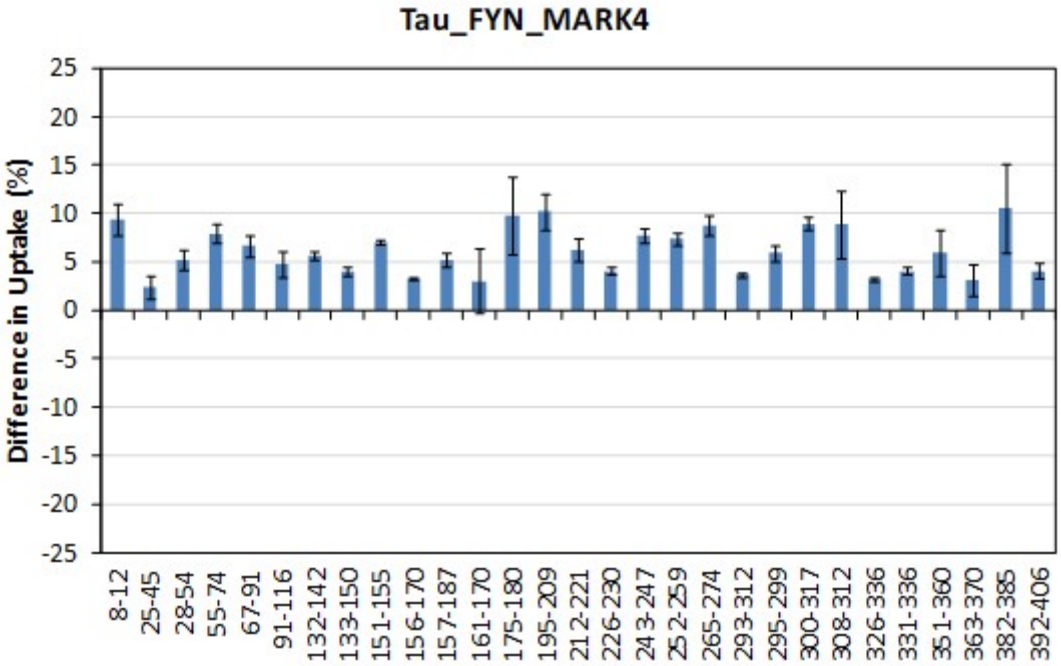
Tau_FYN_MARK4
Difference in Uptake (%)
25
20
15
10
5
0
-5
-10
-15
-20
-25
8-12
25-45
28-54
55-74
67-91
91-116
132-142
133-150
151-155
156-170
157-187
161-170
175-180
195-209
212-221
226-230
243-247
252-259
265-274
293-312
295-299
300-317
308-312
326-336
331-336
351-360
363-370
382-385
392-406

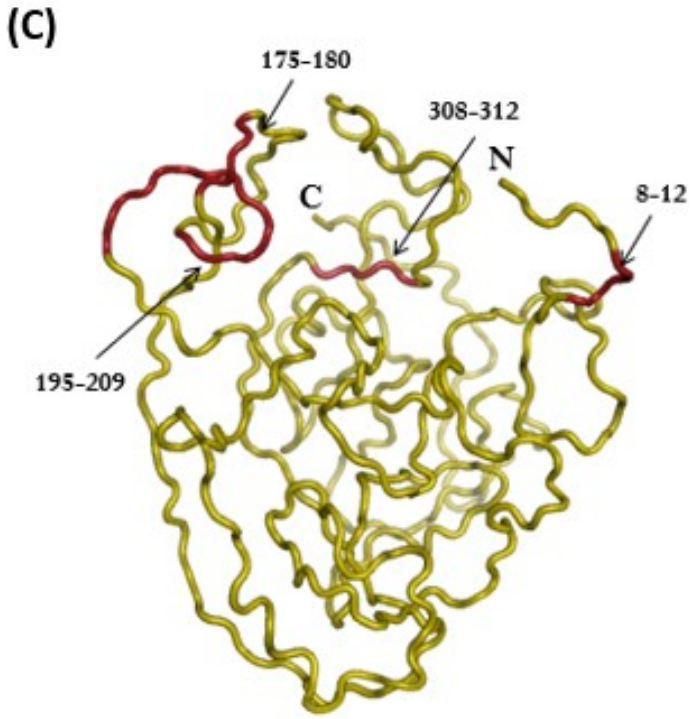

Figure 5.8: HDX-MS data and predicted conformation of MARK4 and Fyn phosphorylated Tau 441: (A) MS HDX evaluated phosphorylated Tau sample (MARK4 followed by Fyn kinase phosphorylation) showed that amino acids 8 – 12aa, 175 – 180aa, 195 – 209aa in the proline-rich region, and 308 – 312aa in the MTBR R3 showed the highest deuterium uptake, indicating the phosphosites on Tau 441 following the MARK4 followed by Fyn kinase phosphorylation. (B) HDX-MS data showing the deuterium uptake in Tau 441 phosphorylated with Fyn followed by MARK4:When Tau 441 was phosphorylated with Fyn followed by MARK4, the phosphorylated Tau sample was assessed by MS HDX. Amino acids 8 – 12aa, 175 – 180aa, 195 – 209aa in the proline rich region and 308 – 312aa in the MTBR R3 showed the highest deuterium uptake, matching the phosphosites on Tau 441 following Fyn followed by MARK4 phosphorylation of Tau. (C) A predicted conformation showing deuterium uptake in Tau 441 phosphorylated with MARK4 and Fyn**:** Tau 441 was phosphorylated with MARK4, after which the phosphorylated Tau sample was subjected to TRESI – MS HDX.

HDX-MS data showed increased deuterium uptake in Tau 441 at 8 – 12aa, 175 – 209aa, 195 – 209aa, and 308 – 312aa. The highest deuterium uptake was observed at 175 – 180aa (Figure 5.8A). This was followed by the Fyn and MARK4 phosphorylation evaluation. When Tau 441 was phosphorylated by Fyn followed by MARK4 combination, the deuterium uptake was high in exactly the same regions (8 – 12aa, 175 – 180aa, 195 – 209aa, and 308 – 312aa regions, with the highest observed at 195 – 209aa and 308 – 312aa) (Figure 5.8B) as it was observed in the MARK4 followed by Fyn sequential phosphorylation order. With the regions of high deuterium uptake not changing irrespective of the order in which the kinases were used to phosphorylate Tau, it could be said that the phosphosites observed when specific kinases are used to phosphorylate Tau 441 is dependent on the kinases used not on the order in which they are used to phosphorylate the protein. Just as it was observed in the single kinase phosphorylation of Tau, the hexapeptide repeats H1 and H2 were all sequestered in the global structure of the phosphorylated ensembles of the MARK4 and Fyn kinase combinations (Figure 5.8C). Thus, making this sequential kinase combination less prone to initiating Tau aggregation.

5.4 Conclusions

A change in Tau protein conformation has strongly been linked to Tau phosphorylation, and this is essential for the study of pathology[125][126]. While the phosphorylation of some sites on Tau promoted Tau detachment from microtubules, phosphorylation of some other sites also promotes Tau aggregation[170]. In recent years, diverse techniques have been employed to identify specific conformational changes that are associated with certain phosphosites. Here, single, and sequentially phosphorylated

Tau 441 were evaluated with LC in tandem with MS and TRESI MS-HDX. The phosphosites from the singly or sequentially phosphorylated Tau using LC/MS/MS coupled with data from the HDX-MS were used to identify the phosphosites on Tau and also to describe the structure, conformational dynamics, and aggregation proneness of Tau.

All the single kinase phosphorylated Tau samples showed phosphosites unique to only the kinase used. On the other hand, the multiple kinase phosphorylated Tau combinations evaluated showed irrespective of the kinase that was used in the 2-way kinase sequence explored, the phosphosites observed were not affected. Also, the TRESI MS-HDX also showed the two hexapeptide repeats, H1 and H2 largely sequestered in the single kinase phosphorylated Tau samples. However, the GSK-3β/Fyn and Fyn/GSK-3β sequential phosphorylated Tau samples showed the partial exposure of the first hexapeptide repeat (H1), indicating the ability of this kinase sequential combination promoting amyloidogenesis in Tau.

CHAPTER SIX

CONCLUSIONS AND FUTURE WORK

6.1 Conclusions

Since Alzheimer's disease still has no cure, there is the need to identify the phosphorylation patterns which causes conformational changes in Tau, an intrinsically disordered protein which is at the center of this neurodegenerative disease. Although aggregated and/or hyperphosphorylated Tau forms are considered potential therapeutic targets for Alzheimer's disease and other tauopathies, there is still more work to be done to determine the Tau epitopes and Tau forms to target. GSK-3β, MARK4, and Fyn from the three main classes of kinases that phosphorylate Tau on several sites had their phosphorylation patterns and conformational changes evaluated to confirm which kinase or kinase combination promoted the most aggregation. I hypothesized specific phosphoproteins exbibit preferential aggregation properties and conformational changes. This hypothesis was tested out by first phosphorylating Tau using GSK-3β, MARK4, and Fyn, confirming phosphorylation with western blots and LC/MS/MS, and then assessing the ability of pTau to aggregate after incubation with fluorescence assays. Phosphorylated Tau conformational changes for the various pTau samples were evaluated with HDX-MS.

After the expression and purification of all 6 Tau isoforms from *E. Coli* cells (Chapter 2), their aggregation properties were evaluated in the presence of heparin, a polyanionic polymer. All 6 isoforms showed aggregation, with the highest F.I recorded in Tau 412 and the least in Tau 352. TEM analysis also showed the formation of fibrils and

filaments in all six isoforms, confirming the aggregates formed were β-pleated sheets. The ability of each isoform to aggregate confirmed the involvement of all the isoforms in Tau fibrillization in different tauopathies. This proof of principle was critical as the recombinantly expressed and purified Tau must mimic the properties human Tau has *in vivo*. Tau protein plays a key role in axonal transport, tubulin assembly and microtubule stabilization. The detachment of Tau and its aggregation disrupts these functions. MTBR, a domain on Tau's role on Tau aggregation and deposition has been studied extensively. However, the role of the N-terminal acidic repeats in Tau aggregation is not known. With the Tau isoforms been developmentally synthesized, their ability to co-exist and aggregate based on the number of N-terminal acidic repeats each has was investigated. The 1N and 2N N-Terminal acidic repeats showed the most aggregation with time, with the p -value (0.8232) showing no statistical difference between F.I readings at day 14. Their aggregation into fibrils and filaments was confirmed using transmission electron microscopy (Chapter 3). This finding may support the involvement of the N-terminal repeats in Tau aggregation since the isoforms without N repeats did not show any increased aggregation at day 14.

With hyperphosphorylated identified as the major cause of Tau fibrillization, the role of kinase activity to upregulate Tau aggregation overtime via extensive fibril and filament formation was also evaluated. Sulfated aminoglycans including heparin have also been shown to co-localize with Tau causing Tau aggregation. Hence, the phosphorylation patterns and aggregation properties of phosphorylated full-length Tau with and without heparin was assessed in Chapter 4. The aggregation studies of single and multi-kinase were assessed after phosphorylation of Tau by GSK-3β, MARK4, and

Fyn was confirmed by immunostaining. Although single kinase phosphorylated Tau 441 did not show aggregation over time in the absence of heparin, the reverse was observed when phosphorylated Tau was induced with heparin. The highest fluorescence intensity was observed in GSK-3β and MARK4 phosphorylated Tau 441 on the 5^{th} day maintained through the 7^{th} day (p-value = 0.8981). A drop in F.I was observed on day 14. This can be attributed to the apparent cloudiness that made the samples turbid. SDS-PAGE also confirmed the formation of SDS-resistant aggregates characteristic of Tau aggregation. The multi-kinase phosphorylated Tau showed similar trends. There was no aggregation observed in the Tau samples sequentially phosphorylated in the absence of heparin. Although the increase observed for GSK-3β/MARK4 at day 7 was very little, it was statistically significant (p-value = 0.00653). As expected, the presence of heparin-induced significantly higher F.I readings in the multi-kinase samples. Here, the highest F.I was observed in the GSK-3β/Fyn combination on also on day 7. Likewise, a drop in F.I was also observed on day 14, and there was noticeable cloudiness that also made the samples turbid. SDS-PAGE also confirmed the formation of insoluble aggregates. Phosphorylation was observed to not contribute to the increase in F.I observed in both single and multi-kinase phosphorylated Tau 441 but rather contributed to the formation of lower molecular weight products in the presence of heparin.

To further confirm phosphorylation and characterize the phosphorylated sites in the single and sequentially phosphorylated Tau 441, the samples were subjected to LC/MS/MS (Chapter 5). Tandem MS detected the phosphorylated sites of GSK-3β to be S199, S396, S400, and S404. For MARK4, the sites characterized were S262, S305, S324, S325, S356, S416, and S435. While in Fyn, all the tyrosine residues on Tau, Y18,

Y29, Y310, Y316, and Y394 were phosphorylated. In the sequentially phosphorylated Tau, GSK-3β/Fyn and Fyn/GSK-3β presented with the same sites, Y394, S396, S400, and S404 as the same sites mainly phosphorylated. The MARK4/Fyn and Fyn/MARK4 phospho-combination also mainly phosphorylated S356 and Y394. Also, the MARK4/ GSK-3β sites were characterized as S352and S356 awhile that of GSK-3β/MARK4 was characterized as S396, S400 and S404.

The conformational changes that were observed via phosphorylation with TRESI MS – HDX were used to describe the amyloidogenic properties of Tau (Chapter 5). Although all 3 kinases, in the single kinase phosphorylated Tau 441 adopted conformational changes distinct from each other, the hexapeptide repeats H1 and H2, identified as the promoter of aggregation in Tau 441 remained largely sequestered in pTau/MARK4 and pTau/Fyn. The second hexapeptide repeat (H2) remained exposed in pTau/GSK-3β, indicating GSK-3β phosphorylated Tau could be a probable cause of Tau aggregation. Although the single kinase phosphorylation did not show Tau aggregation overtime as it was hypothesized, different conformational changes were observed for the differentially phosphorylated single pTau samples. There observed Tau fibrillization as proposed to be due to hyperphosphorylation may be due to several kinase activities rather than just one as observed. In the multi-kinase phosphorylations, the conformation observed for any 2 specific kinases combinations used were the same irrespective of the order in which the kinases were employed to phosphorylate Tau. was added to phosphorylate the protein. Similarly, the same conformation was also observed irrespective of the order in which the kinase was added to induce phosphorylation. The GSK-3β/Fyn and Fyn/GSK-3β sequential phosphorylated Tau combination showed the

partial exposure of the first hexapeptide repeat (H1), indicating the ability of this kinase combination to promote amyloidogenesis in Tau. Here too, even though multi-kinase in the absence of heparin did not also show increased F.I readings, conformational changes observed were based on the kinase used for the phosphorylation. Confirming the hypothesis that specific kinase phosphorylated proteins exhibit a preferred conformation.

However, the given these findings, the structural and functional investigations of Tau protein as a function of hyperphosphorylation pattern by multiple protein kinases needs to be further investigated extensively and the study must be designed so as to mimic the biological setting more closely.

6.2 Future work

Many neurodegenerative conditions, including Alzheimer's disease (AD) are characterized by intracellular aggregation of pathogenic proteins. Tau, one of the two proteins implicated in AD gets modified at several sites via hyperphosphorylation and this promotes the formation of neurofibrillary tangles (NFTs).

For my future work, to further probe the phosphorylation patterns, aggregation properties and morphological changes of Tau 441, I would phosphorylate Tau with all 3 kinases sequentially, characterize their phosphosites and their corresponding conformational changes. The selected protein kinases and the order of phosphorylation may be important and that is why there is the need to investigate this further. Isoform-specific studies would also be done because of their biological relevance. In addition, cell toxicity assays would also be done to provide information on toxicity of the various aggregated isoforms on neuronal cells.

Besides phosphorylation, which is the commonest post translational modification (PTM) process that promote protein aggregation in eukaryotic cells, caspase cleavage of Tau at specific sites on Tau have also been identified to promote Tau aggregation. With most aggregation studies done being in vitro, the ability to track how hyperphosphorylation occurs in intact cells in a quantitative manner using a high-throughput system would give more cellular and molecular insights into AD disease pathogenesis.

Thus, I would transfect full length Tau 441 and caspase cleaved Tau 441 into human embryonic kidney (HEK) cells. I would then examine the cell - based fluorescence resonance energy transfer (FRET) efficiency in the presence of constitutively active kinase or kinase dead MARK4, Fyn and GSK-3β. This will be done to assess the aggregation propensity and morphological changes induced in Tau in vivo.

APPENDIX

PROTEOSTAT ASSAYS, TURBIDITY ASSAYS AND SDS-PAGES

SUPPLEMENTARY DATA

(A)

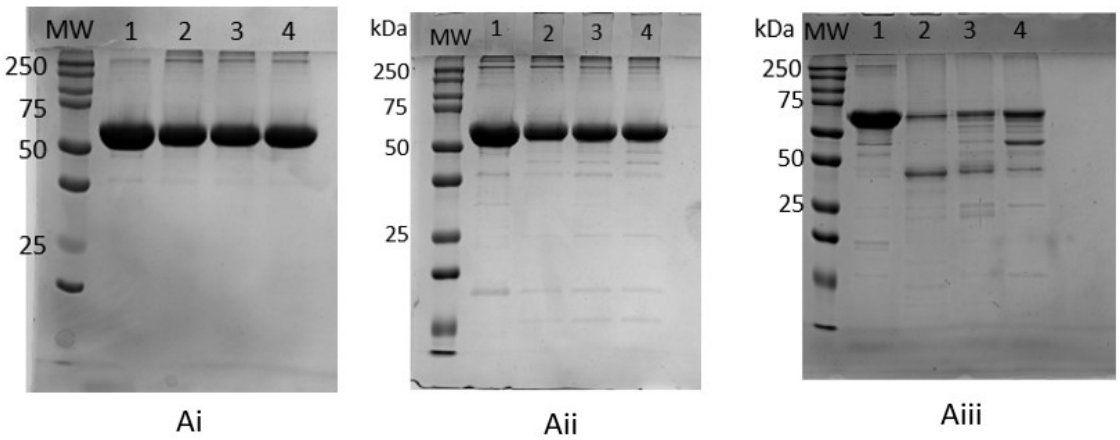

1 – nTau (non-phosphorylated Tau)
2 - pTau (phosphorylation by GSK-3β)
3 - pTau (phosphorylation by MARK4)
4 - pTau (phosphorylation by Fyn)

Figure A.1: SDS-PAGE of single phosphorylated Tau with heparin: (Ai) SDS-PAGE of phosphorylated Tau 441 in the presence of heparin (phosphorylation time = 24 h; phosphorylation temperature = 37 °C; ageing time = 0 days; ageing temperature = 37 °C (Aii) SDS-PAGE of phosphorylated Tau 441 in the presence of heparin (phosphorylation time = 24 h; phosphorylation temperature = 37 °C; ageing time = 7 days; ageing temperature = 37 °C; (Aiii) SDS-PAGE of phosphorylated Tau 441 in the presence of heparin (phosphorylation time = 24 h; phosphorylation temperature = 37 °C; ageing time = 14 days; ageing temperature = 37 °C.

(B)

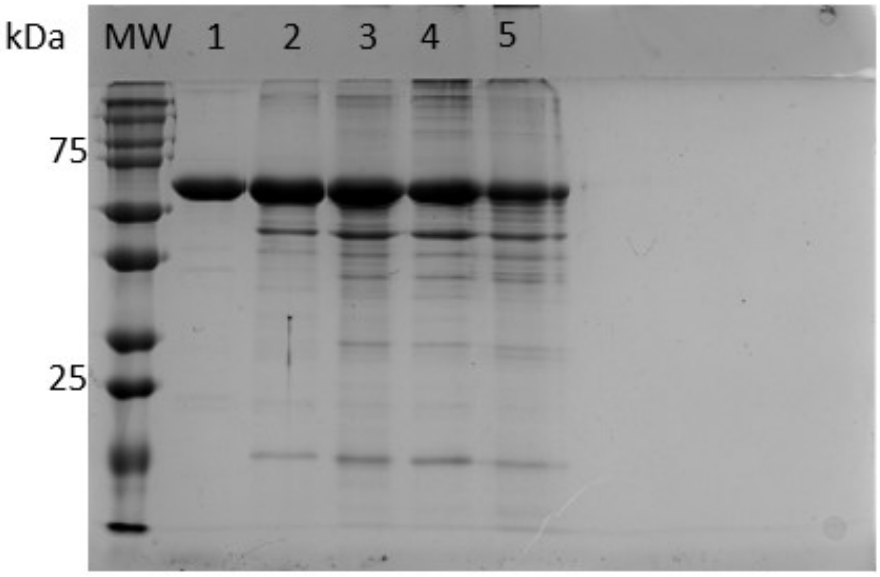

1 – Tau 441 (No heparin, Day 0)
2 – Tau 441 (No heparin, Day 7)
3 - Tau 441 (No heparin Day 14)
4 - Tau 441 (Heparin, Day 7)
5 - Tau 441 (Heparin, Day 14)

Figure B.1: SDS-PAGE of Tau with and without heparin: SDS-PAGE of non-phosphorylated Tau 441 with and without heparin aged overtime (ageing time = 14 days; ageing temperature = 37 °C.

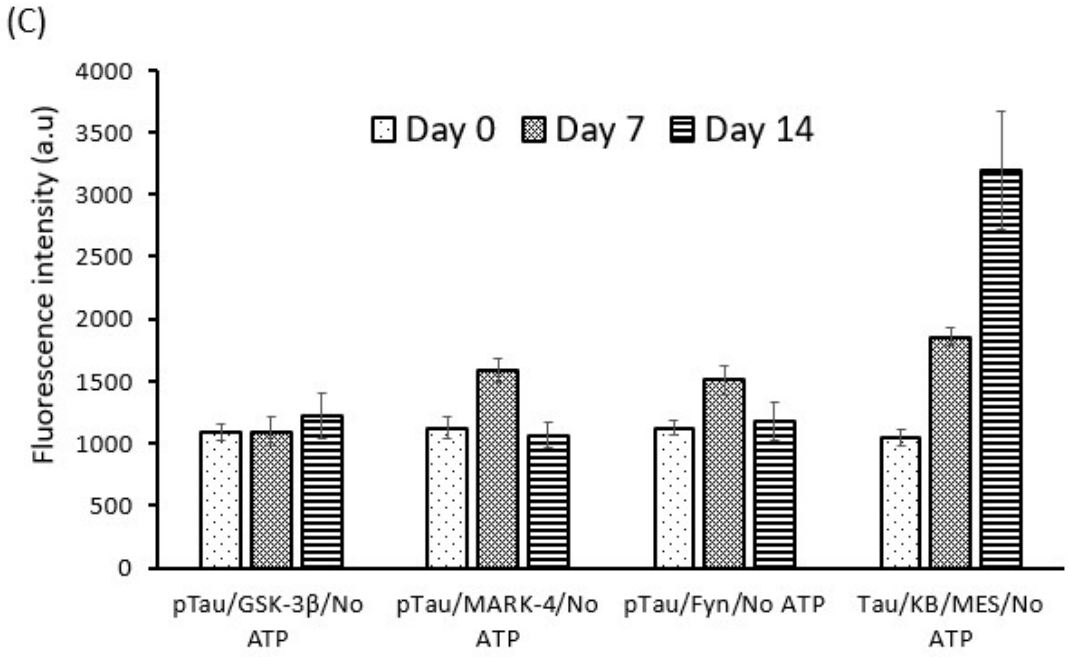

Figure C.1: Proteostat assay of single phosphorylated Tau in the absence of ATP: A proteostat aggregation fluorescence intensity plot showing the absence of ATP in a phosphorylation reaction for GSK, MARK4 and Fyn with heparin. {Graph = Mean ± SD, n value = 9}.

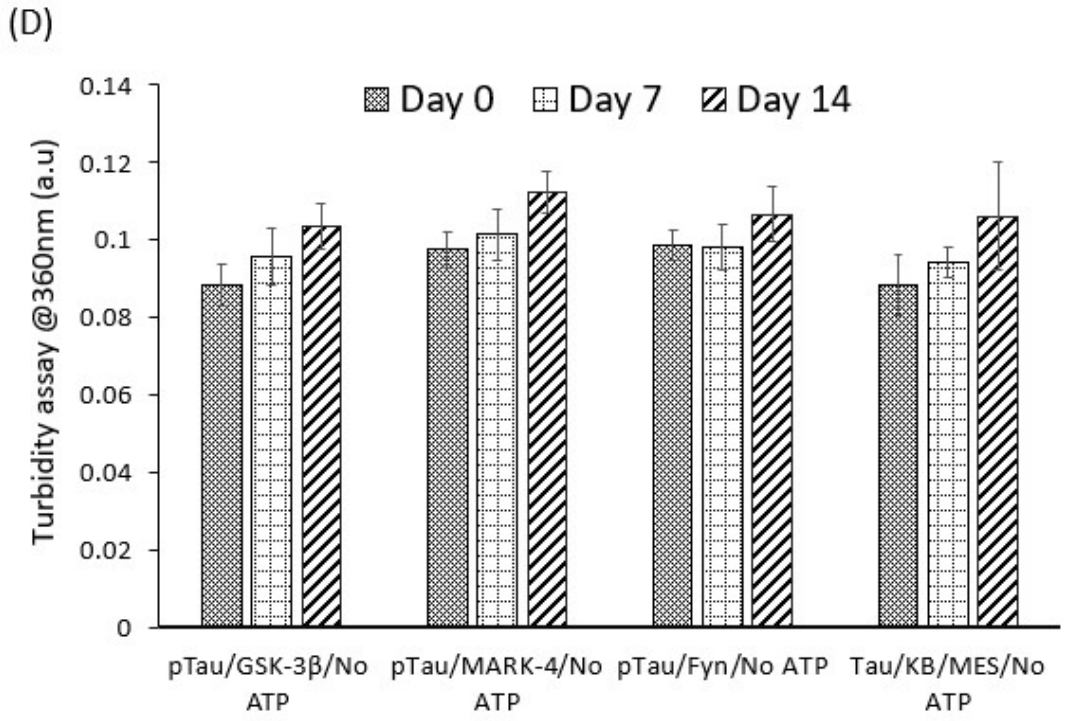

Figure D.1: Turbidity assay of single phosphorylated Tau in the absence of ATP: A turbidity plot showing the absence of ATP in a phosphorylation reaction for GSK3β, MARK4 and Fyn in the presence of heparin. {Graph = Mean ± SD, n value = 9}.

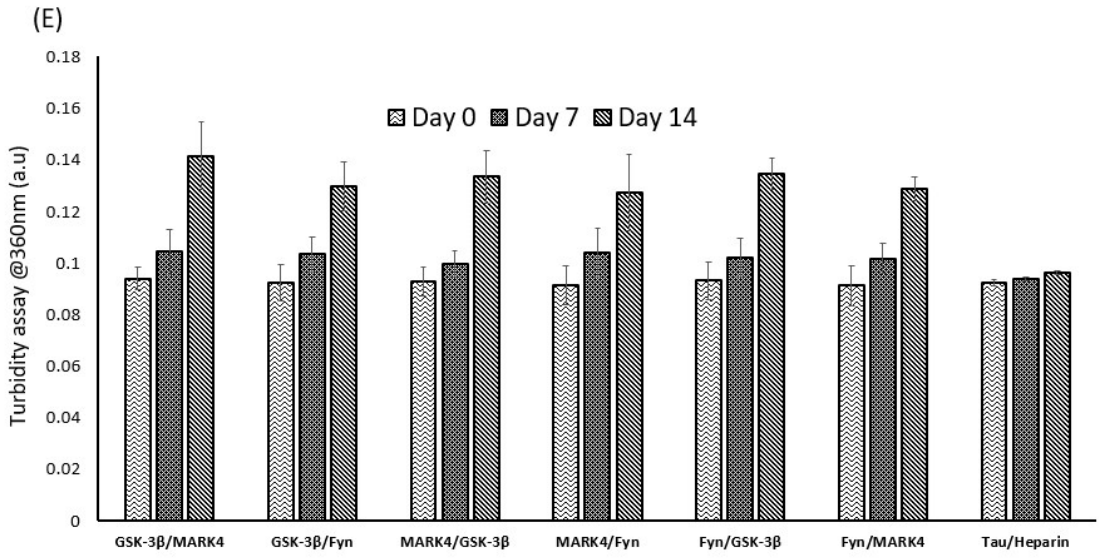

Figure E.1: Turbidity assay of sequentially phosphorylated Tau: Turbidity assay as a function of Tau 441 phosphorylation using multiple kinases in the absence of heparin; (phosphorylation time = 48 h; phosphorylation temperature = 37 °C; ageing time = 14 days; ageing temperature = 37 °C, wavelength = 360nm). {Graph = Mean ± SD, n value = 9}.

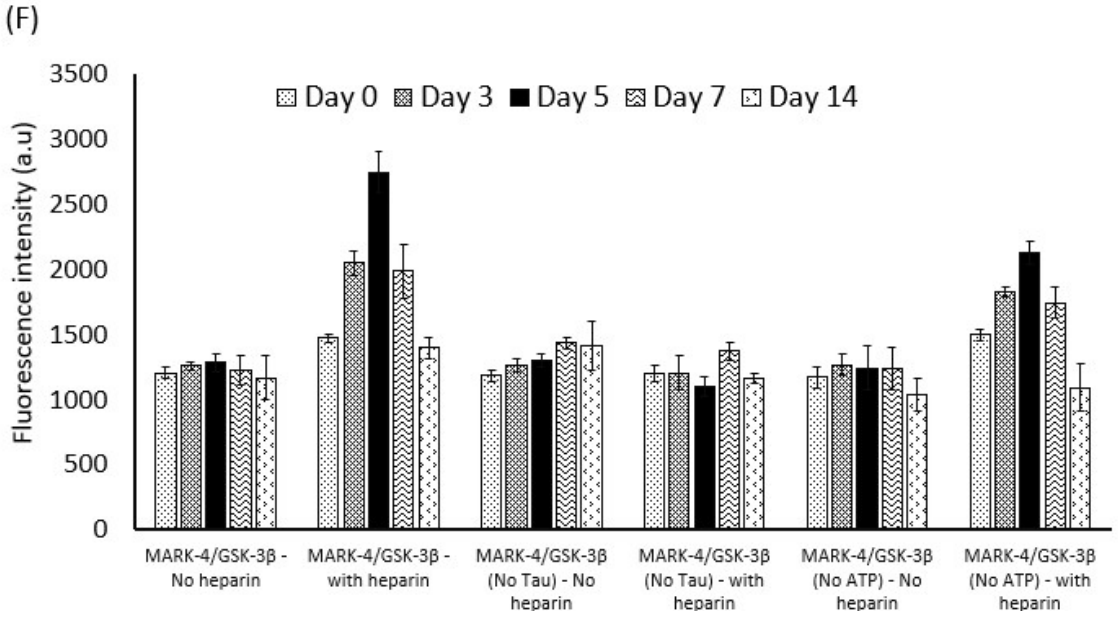

Figure F.1: Proteostat assay of MARK4 and GSK3(with and without heparin, with and without ATP and with and without substrate): Proteostat aggregation assay fluorescence intensities as a function of Tau 441 phosphorylation using multiple kinases: with and without heparin, with and without substrate and with and without ATP; (phosphorylation time = 48 h; phosphorylation temperature = 37 °C; ageing time = 14 days; ageing temperature = 37 °C). {Graph = Mean ± SD, n value = 9}.

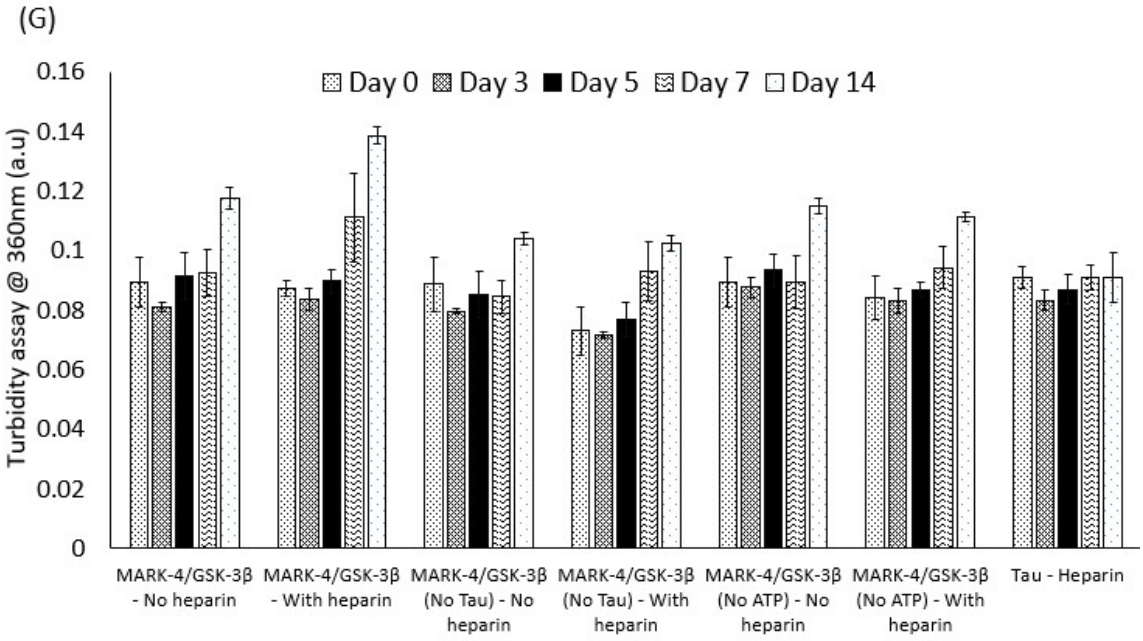

Figure G.1: Turbidity assay of MARK4 and GSK (with and without heparin, with and without ATP and with and without substrate): Turbidity assay as a function of Tau 441 phosphorylation using multiple kinases with and without heparin, with and without substrate and with and without ATP; (phosphorylation time = 48 h; phosphorylation temperature = 37 °C; ageing time = 14 days; ageing temperature = 37 °C, wavelength = 360nm). {Graph = Mean ± SD, n value = 9}.

(H)

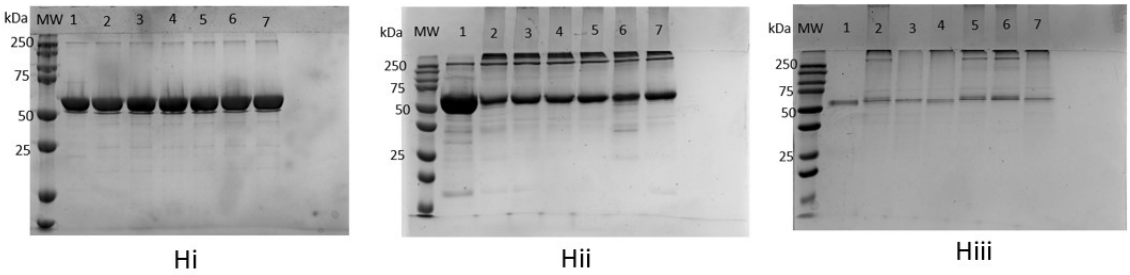

1 - nTau (Non-phosphorylated Tau 441, No heparin)
2 - pTau (phosphorylation by GSK-3β followed by MARK4)
3 - pTau (phosphorylation by GSK-3β followed by Fyn)
4 - pTau (phosphorylation by MARK4 followed by GSK-3β)
5 - pTau (phosphorylation by MARK4 followed by Fyn)
6 - pTau (phosphorylation by Fyn followed by GSK-3β)
7 - pTau (phosphorylation by Fyn followed by MARK4)

Figure H.1: SDS-PAGE of sequentially phosphorylated Tau with heparin: (Hi) SDS-PAGE of sequentially phosphorylated Tau 441 in the presence of heparin (phosphorylation time = 48 h; phosphorylation temperature = 37 °C; ageing time = 0 days; ageing temperature = 37 °C (Hii) SDS-PAGE of phosphorylated Tau 441 in the presence of heparin (phosphorylation time = 48 h; phosphorylation temperature = 37 °C; ageing time = 7 days; ageing temperature = 37 °C; (Hiii) SDS-PAGE of phosphorylated Tau 441 in the presence of heparin (phosphorylation time = 48 h; phosphorylation temperature = 37 °C; ageing time = 14 days; ageing temperature = 37 °C.

REFERENCES

[1] Y. Yang and J. Z. Wang, "Nature of Tau-Associated Neurodegeneration and the Molecular Mechanisms," *Journal of Alzheimer's Disease*. 2018.

[2] B. Choudhury, P. Saytode, and V. Shah, "NEURODEGENRATIVE DISORDERS: PAST, PRESENT AND FUTURE.," *Int. J. Appl. Pharm. Biotechnol.*, 2014.

[3] J. Gao, L. Wang, J. Liu, F. Xie, B. Su, and X. Wang, "Abnormalities of mitochondrial dynamics in neurodegenerative diseases," *Antioxidants*. 2017.

[4] K. Cherry, "An Overview of the Different Parts of a Neuron," *VERYWELL mind*, 2018.

[5] J. Wang, W. W. Hu, Z. Jiang, and M. J. Feng, "Advances in treatment of neurodegenerative diseases: Perspectives for combination of stem cells with neurotrophic factors," *World J. Stem Cells*, 2020.

[6] K. J. De Vos and M. Hafezparast, "Neurobiology of axonal transport defects in motor neuron diseases: Opportunities for translational research?," *Neurobiology of Disease*. 2017.

[7] M. P. Sheetz, K. K. Pfister, J. C. Bulinski, and C. W. Cotman, "Mechanisms of trafficking in axons and dendrites: Implications for development and neurodegeneration," *Prog. Neurobiol.*, 1998.

[8] N. Villain and B. Dubois, "Alzheimer's Disease Including Focal Presentations," *Semin. Neurol.*, 2019.

[9] M. Zvěřová, “Clinical aspects of Alzheimer’s disease,” *Clinical Biochemistry*. 2019.

[10] K. L. Leenders and W. H. Oertel, “Parkinson’s disease: Clinical signs and symptoms, neural mechanisms, positron emission tomography, and therapeutic interventions,” *Neural Plast.*, 2001.

[11] L. Crews and E. Masliah, “Molecular mechanisms of neurodegeneration in Alzheimer’s disease,” *Hum. Mol. Genet.*, 2010.

[12] S. Tu, S. ichi Okamoto, S. A. Lipton, and H. Xu, “Oligomeric Aβ-induced synaptic dysfunction in Alzheimer’s disease,” *Molecular neurodegeneration*. 2014.

[13] E. Shi and A. Kyung, “Study on the biochemical nanoparticles for bio-imaging and molecular diagnostics of alzheimer’s disease,” in *IEMTRONICS 2020 - International IOT, Electronics and Mechatronics Conference, Proceedings*, 2020.

[14] R. Tarawneh and D. M. Holtzman, “The clinical problem of symptomatic Alzheimer disease and mild cognitive impairment,” *Cold Spring Harb. Perspect. Med.*, 2012.

[15] A. Caruso, F. Nicoletti, D. Mango, A. Saidi, R. Orlando, and S. Scaccianoce, “Stress as risk factor for Alzheimer’s disease,” *Pharmacological Research*. 2018.

[16] J. J. Breunig, M. V. Guillot-Sestier, and T. Town, “Brain injury, neuroinflammation and Alzheimer’s disease,” *Frontiers in Aging Neuroscience*. 2013.

[17] D. L. Tudorascu *et al.*, “Comparison of longitudinal Aβ in nondemented elderly and Down syndrome,” *Neurobiol. Aging*, 2019.

[18] A. Tagarelli, A. Piro, G. Tagarelli, P. Lagonia, and A. Quattrone, “Alois Alzheimer: a hundred years after the discovery of the eponymous disorder.,” *Int. J. Biomed. Sci.*, 2006.

[19] G. Cipriani, C. Dolciotti, L. Picchi, and U. Bonuccelli, “Alzheimer and his disease: A brief history,” *Neurol. Sci.*, 2011.

[20] M. Da Mota Gomes, “Franz Nissl (1860-1919), noted neuropsychiatrist and neuropathologist, staining the neuron, but not limiting it,” *Dement. e Neuropsychol.*, 2019.

[21] M. MH, “The Decrease of Amyloid-Beta Deposit, Increase of Brain-Derived Neurotrophic Factor and Decrease of C-Reactive Protein Levels in the Rat Model of Dementia, Related to the Physical Exercises,” *BAOJ Neurol.*, 2016.

[22] R. Macleod, E. K. Hillert, R. T. Cameron, and G. S. Baillie, “The role and therapeutic targeting of α-, β-and γ-secretase in Alzheimer’s disease,” *Future Science OA*. 2015.

[23] C. Nordstedt, S. Lake, and B. Winblad, “Alzheimer’s disease--an amyloid disease of the brain,” *Läkartidningen*. 1992.

[24] G. Konig *et al.*, “Identification and differential expression of a novel alternative splice isoform of the βA4 amyloid precursor protein (APP) mRNA in leukocytes and brain microglial cells,” *J. Biol. Chem.*, 1992.

[25] J. Nunan and D. H. Small, “Regulation of APP cleavage by alpha-, beta- and gamma-secretases.,” *FEBS Lett.*, 2000.

[26] T. Bittner *et al.*, “Amyloid plaque formation precedes dendritic spine loss,” *Acta Neuropathol.*, 2012.

[27] D. Chen, Z. S. Martin, C. Soto, and C. H. Schein, “Computational selection of inhibitors of Aβ aggregation and neuronal toxicity,” *Bioorganic Med. Chem.*, 2009.

[28] M. Citron, T. S. Diehl, G. Gordon, A. L. Biere, P. Seubert, and D. J. Selkoe, “Evidence that the 42- and 40-amino acid forms of amyloid β protein are generated from the β-amyloid precursor protein by different protease activities,” *Proc. Natl. Acad. Sci. U. S. A.*, 1996.

[29] Y. Zhou, L. Liu, Y. Hao, and M. Xu, “Detection of Aβ Monomers and Oligomers: Early Diagnosis of Alzheimer’s Disease,” *Chem. - An Asian J.*, 2016.

[30] B. Penke, M. Szucs, and F. Bogár, “Oligomerization and conformational change turn monomeric β-amyloid and tau proteins toxic: Their role in Alzheimer’s pathogenesis,” *Molecules*. 2020.

[31] M. Manczak and P. H. Reddy, “Abnormal interaction of oligomeric amyloid-β with phosphorylated tau: Implications to synaptic dysfunction and neuronal damage,” *J. Alzheimer’s Dis.*, 2013.

[32] T. Guo, W. Noble, and D. P. Hanger, “Roles of tau protein in health and disease,” *Acta Neuropathologica*. 2017.

[33] J. Miao *et al.*, “Pathological Tau From Alzheimer’s Brain Induces Site-Specific Hyperphosphorylation and SDS- and Reducing Agent-Resistant Aggregation of Tau in vivo,” *Front. Aging Neurosci.*, 2019.

[34] N. Musi *et al.*, “Tau protein aggregation is associated with cellular senescence in the brain,” *Aging Cell*, 2018.

[35] “2020 Alzheimer’s disease facts and figures,” *Alzheimer’s Dement.*, 2020.

[36] "Alzheimer's Kills More People Than Breast And Prostate Cancer Combined, So Why Is It So Underfunded?" [Online]. Available: https://www.medicaldaily.com/alzheimers-kills-more-people-breast-and-prostate-cancer-combined-so-why-it-so-underfunded-282090. [Accessed: 24-Feb-2022].

[37] Alzheimer's Association, "2018 Alzheimer's Disease Facts and Figures. Alzheimers Dement 2018;14(3):367-429," 2018.

[38] Alzheimer's Association, "2021 Alzheimer's disease facts and figures special report Race, Ethnicity and Alzheimer's in America," 2021.

[39] L. I. Binder, A. Frankfurter, and L. I. Rebhun, "The distribution of tau in the mammalian central nervous central nervous," *J. Cell Biol.*, 1985.

[40] K. Iqbal, F. Liu, and C. X. Gong, "Tau and neurodegenerative disease: The story so far," *Nature Reviews Neurology*. 2016.

[41] S. Schraen-Maschke *et al.*, "Tau as a biomarker of neurodegenerative diseases," *Biomark. Med.*, vol. 2, no. 4, p. 363, 2008.

[42] N. Sibille *et al.*, "Structural characterization by nuclear magnetic resonance of the impact of phosphorylation in the proline-rich region of the disordered Tau protein," *Proteins Struct. Funct. Bioinforma.*, 2012.

[43] N. Kalcheva, J. S. Albala, L. I. Binder, and B. Shafit-Zagardo, "Localization of Specific Epitopes on Human Microtubule-Associated Protein 2," *J. Neurochem.*, 2002.

[44] E. M. Mandelkow and E. Mandelkow, "Tau in Alzheimer's disease," *Trends Cell Biol.*, 1998.

[45] M. Kolarova, F. García-Sierra, A. Bartos, J. Ricny, and D. Ripova, "Structure and pathology of tau protein in Alzheimer disease," *International Journal of Alzheimer's Disease*. 2012.

[46] K. W. Drombosky *et al.*, "Native tau structure is disrupted by disease-associated mutations that promote aggregation," *bioRxiv*, 2018.

[47] M. Stefani and C. M. Dobson, "Protein aggregation and aggregate toxicity: New insights into protein folding, misfolding diseases and biological evolution," *Journal of Molecular Medicine*. 2003.

[48] A. S. M. Hung *et al.*, "Mutated tau, amyloid and neuroinflammation in Alzheimer disease-A brief review," *Progress in Histochemistry and Cytochemistry*. 2016.

[49] Y. Raz and Y. Miller, "Interactions between Aβ and Mutated Tau Lead to Polymorphism and Induce Aggregation of Aβ-Mutated Tau Oligomeric Complexes," *PLoS One*, 2013.

[50] P. Poorkaj *et al.*, "Tau is a candidate gene for chromosome 17 frontotemporal dementia," *Ann. Neurol.*, 1998.

[51] T. Sposito *et al.*, "Developmental regulation of tau splicing is disrupted in stem cell-derived neurons from frontotemporal dementia patients with the 10 + 16 splice-site mutation in MAPT," *Hum. Mol. Genet.*, 2015.

[52] R. Rademakers *et al.*, "Tau negative frontal lobe dementia at 17q21: Significant finemapping of the candidate region to a 4.8 cM interval," *Mol. Psychiatry*, 2002.

[53] H. Kadavath *et al.*, "Tau stabilizes microtubules by binding at the interface between tubulin heterodimers," *Proc. Natl. Acad. Sci. U. S. A.*, 2015.

[54] M. Goedert and R. Jakes, “Expression of separate isoforms of human tau protein: Correlation with the tau pattern in brain and effects on tubulin polymerization,” *EMBO J.*, 1990.

[55] S. J. Adams, M. A. de Ture, M. McBride, D. W. Dickson, and L. Petrucelli, “Three repeat isoforms of tau inhibit assembly of four repeat tau filaments,” *PLoS One*, 2010.

[56] E. Majounie *et al.*, “Variation in tau isoform expression in different brain regions and disease states,” *Neurobiol. Aging*, 2013.

[57] S. G. Kang, G. Eskandari-Sedighi, L. Hromadkova, J. G. Safar, and D. Westaway, “Cellular Biology of Tau Diversity and Pathogenic Conformers,” *Front. Neurol.*, vol. 11, Nov. 2020.

[58] K. McKibben and E. Rhoades, “Regulation of tau’s proline rich region by its N-terminal domain,” *bioRxiv*, 2019.

[59] T. J. Hausrat, J. Radwitz, F. L. Lombino, P. Breiden, and M. Kneussel, “Alpha- and beta-tubulin isotypes are differentially expressed during brain development,” *Dev. Neurobiol.*, 2021.

[60] E. Nogales, S. G. Wolf, and K. H. Downing, “Structure of the αβ tubulin dimer by electron crystallography,” *Nature*, 1998.

[61] M. Knossow, V. Campanacci, L. A. Khodja, and B. Gigant, “The Mechanism of Tubulin Assembly into Microtubules: Insights from Structural Studies,” *iScience*. 2020.

[62] G. Tian, A. Bhamidipati, N. J. Cowan, and S. A. Lewis, “Tubulin folding cofactors as GTPase-activating proteins. GTP hydrolysis and the assembly of the α/β-tubulin heterodimer,” *J. Biol. Chem.*, 1999.

[63] G. Tian, A. Bhamidipati, N. J. Cowan, and S. A. Lewis, “Tubulin Folding Cofactors as GTPase-activating Proteins,” *J. Biol. Chem.*, 1999.

[64] S. B. Horwitz and T. Fojo, “Microtubule Stabilizing Agents,” in *The Role of Microtubules in Cell Biology, Neurobiology, and Oncology*, 2009.

[65] R. M. Buey *et al.*, “Microtubule interactions with chemically diverse stabilizing agents: Thermodynamics of binding to the paclitaxel site predicts cytotoxicity,” *Chem. Biol.*, 2005.

[66] F. Carubbi, A. Alunno, R. Gerli, and R. Giacomelli, “Post-Translational Modifications of Proteins: Novel Insights in the Autoimmune Response in Rheumatoid Arthritis,” *Cells*, 2019.

[67] M. Kokkinidis, N. M. Glykos, and V. E. Fadouloglou, “Catalytic activity regulation through post-translational modification: the expanding universe of protein diversity,” *Adv. Protein Chem. Struct. Biol.*, 2020.

[68] “Posttranslational modifications of proteins – Cell Physiology.” [Online]. Available: https://uta.pressbooks.pub/cellphysiology/chapter/posttranslational-modifications-of-proteins/. [Accessed: 24-Feb-2022].

[69] A. Burkle, “Posttranslational Modification Predator ± Prey and Parasite ± Host Interactions,” in *Encyclopedia of Genetics*, 2001.

[70] L. Shi *et al.*, “Cross-phosphorylation of bacterial serine/threonine and tyrosine protein kinases on key regulatory residues,” *Front. Microbiol.*, 2014.

[71] P. C. Ostrovsky and S. Maloy, “Protein phosphorylation on serine, threonine, and tyrosine residues modulates membrane-protein interactions and transcriptional regulation in Salmonella typhimurium,” *Genes Dev.*, 1995.

[72] H. R. Matthews, “Protein kinases and phosphatases that act on histidine, lysine, or arginine residues in eukaryotic proteins: A possible regulator of the mitogen-activated protein kinase cascade,” *Pharmacology and Therapeutics*. 1995.

[73] I. Hadrovic, P. Rebmann, F. G. Klärner, G. Bitan, and T. Schrader, “Molecular Lysine Tweezers Counteract Aberrant Protein Aggregation,” *Frontiers in Chemistry*. 2019.

[74] A. Sharma *et al.*, “Understanding Tetrahydropyranyl as a Protecting Group in Peptide Chemistry,” *ChemistryOpen*. 2017.

[75] B. Miao, Q. Xiao, W. Chen, Y. Li, and Z. Wang, “Evaluation of functionality for serine and threonine phosphorylation with different evolutionary ages in human and mouse,” *BMC Genomics*, 2018.

[76] T. Hunter, “The Croonian Lecture 1997. The phosphorylation of proteins on tyrosine: Its role in cell growth and disease,” *Philos. Trans. R. Soc. B Biol. Sci.*, 1998.

[77] T. Hunter, “The genesis of tyrosine phosphorylation,” *Cold Spring Harb. Perspect. Biol.*, 2014.

[78] M. Schwalbe *et al.*, “Phosphorylation of human tau protein by microtubule affinity-regulating kinase 2,” *Biochemistry*, 2013.

[79] D. B. Flaherty, J. P. Soria, H. G. Tomasiewicz, and J. G. Wood, "Phosphorylation of human tau protein by microtubule-associated kinases: GSK3β and cdk5 are key participants," *J. Neurosci. Res.*, 2000.

[80] A. S. Robinson, "P1-090: Tau isoforms maintain different structural features that may impact their cytotoxicity," *Alzheimer's Dement.*, 2015.

[81] K. Mi and G. Johnson, "The Role of Tau Phosphorylation in the Pathogenesis of Alzheimers Disease," *Curr. Alzheimer Res.*, 2006.

[82] R. J. Hatch, Y. Wei, D. Xia, and J. Götz, "Hyperphosphorylated tau causes reduced hippocampal CA1 excitability by relocating the axon initial segment," *Acta Neuropathol.*, 2017.

[83] X. Zhang *et al.*, "The proline-rich domain promotes Tau liquid-liquid phase separation in cells," *J. Cell Biol.*, 2020.

[84] A. Cavallini *et al.*, "An unbiased approach to identifying tau kinases that phosphorylate tau at sites associated with alzheimer disease," *J. Biol. Chem.*, 2013.

[85] D. Tuerde *et al.*, "Isoform-independent and-dependent phosphorylation of microtubule-associated protein tau in mouse brain during postnatal development," *J. Biol. Chem.*, 2018.

[86] H. Yoshida and M. Goedert, "Phosphorylation of microtubule-associated protein tau by AMPK-related kinases," *J. Neurochem.*, 2012.

[87] S. Kumar *et al.*, "Stages and conformations of the Tau repeat domain during aggregation and its effect on neuronal toxicity," *J. Biol. Chem.*, 2014.

[88] B. Nizynski, W. Dzwolak, and K. Nieznanski, "Amyloidogenesis of Tau protein," *Protein Science*. 2017.

[89] J. Biernat and E. M. Mandelkow, “The development of cell processes induced by tau protein requires phosphorylation of serine 262 and 356 in the repeat domain and is inhibited by phosphorylation in the proline-rich domains,” *Mol. Biol. Cell*, 1999.

[90] M. Morishima-Kawashima *et al.*, “Proline-directed and non-proline-directed phosphorylation of PHF-tau,” *J. Biol. Chem.*, 1995.

[91] S. Mondragón-Rodríguez, G. Perry, X. Zhu, P. I. Moreira, M. C. Acevedo-Aquino, and S. Williams, “Phosphorylation of tau protein as the link between oxidative stress, mitochondrial dysfunction, and connectivity failure: Implications for Alzheimer’s disease,” *Oxidative Medicine and Cellular Longevity*. 2013.

[92] S. P. Wickramasinghe *et al.*, “Polyphosphate Initiates Tau Aggregation through Intra- and Intermolecular Scaffolding,” *Biophys. J.*, 2019.

[93] E. T. Lund, R. McKenna, D. B. Evans, S. K. Sharma, and W. Rodney Mathews, “Characterization of the in vitro phosphorylation of human tau by tau protein kinase II (cdk5/p20) using mass spectrometry,” *J. Neurochem.*, 2001.

[94] P. M. Horowitz, N. LaPointe, A. L. Guillozet-Bongaarts, R. W. Berry, and L. I. Binder, “N-terminal fragments of tau inhibit full-length tau polymerization in vitro,” *Biochemistry*, 2006.

[95] S. J. Shire, Z. Shahrokh, and J. Liu, “Challenges in the development of high protein concentration formulations,” *J. Pharm. Sci.*, vol. 93, no. 6, pp. 1390–1402, 2004.

[96] M. Hofmann and H. Gieseler, “Predictive Screening Tools Used in High-Concentration Protein Formulation Development,” *J. Pharm. Sci.*, vol. 107, no. 3, pp. 772–777, Mar. 2018.

[97] “The Shape and Structure of Proteins - Molecular Biology of the Cell - NCBI Bookshelf.” [Online]. Available: https://www.ncbi.nlm.nih.gov/books/NBK26830/. [Accessed: 24-Feb-2022].

[98] E. Chatani and N. Yamamoto, “Recent progress on understanding the mechanisms of amyloid nucleation,” *Biophys. Rev.*, vol. 10, no. 2, p. 527, Apr. 2018.

[99] M. Törnquist *et al.*, “Secondary nucleation in amyloid formation,” *Chem. Commun. (Camb).*, vol. 54, no. 63, pp. 8667–8684, 2018.

[100] J. Zhang and M. Muthukumar, “Simulations of nucleation and elongation of amyloid fibrils,” *J. Chem. Phys.*, vol. 130, no. 3, 2009.

[101] B. Morel, L. Varela, A. I. Azuaga, and F. Conejero-Lara, “Environmental Conditions Affect the Kinetics of Nucleation of Amyloid Fibrils and Determine Their Morphology,” *Biophys. J.*, vol. 99, no. 11, p. 3801, Dec. 2010.

[102] M. A. B. Baker *et al.*, “Domain-swap polymerization drives the self-assembly of the bacterial flagellar motor,” *Nat. Struct. Mol. Biol. 2016 233*, vol. 23, no. 3, pp. 197–203, Feb. 2016.

[103] S. Sambashivan, Y. Liu, M. R. Sawaya, M. Gingery, and D. Eisenberg, “Amyloid-like fibrils of ribonuclease A with three-dimensional domain-swapped and native-like structure,” *Nat. 2005 4377056*, vol. 437, no. 7056, pp. 266–269, Sep. 2005.

[104] A. Hassoun, A. Sahar, L. Lakhal, and A. Aït-Kaddour, “Fluorescence spectroscopy as a rapid and non-destructive method for monitoring quality and authenticity of fish and meat products: Impact of different preservation conditions,” *LWT*. 2019.

[105] S. Shaikh and C. O’Donnell, “Applications of fluorescence spectroscopy in dairy processing: a review,” *Current Opinion in Food Science*. 2017.

[106] A. L. Smoot, M. Panda, B. T. Brazil, A. M. Buckle, A. R. Fersht, and P. M. Horowitz, “The binding of bis-ANS to the isolated GroEL apical domain fragment induces the formation of a folding intermediate with increased hydrophobic surface not observed in tetradecameric GroEL,” *Biochemistry*, vol. 40, no. 14, pp. 4484–4492, Apr. 2001.

[107] D. Shen *et al.*, “Novel Cell- and Tissue-Based Assays for Detecting Misfolded and Aggregated Protein Accumulation Within Aggresomes and Inclusion Bodies,” *Cell Biochem. Biophys.*, vol. 60, no. 3, p. 173, Jul. 2011.

[108] C. A. Rankin, Q. Sun, and T. C. Gamblin, “Pre-assembled tau filaments phosphorylated by GSK-3b form large tangle-like structures,” *Neurobiol. Dis.*, vol. 31, no. 3, pp. 368–377, Sep. 2008.

[109] G. Amadoro *et al.*, “Role of N-terminal tau domain integrity on the survival of cerebellar granule neurons,” *Cell Death Differ. 2004 112*, vol. 11, no. 2, pp. 217–230, Nov. 2003.

[110] A. Bretteville and E. Planel, “Tau Aggregates: Toxic, Inert, or Protective Species?,” *J. Alzheimer’s Dis.*, vol. 14, no. 4, pp. 431–436, Jan. 2008.

[111] A. Fuster-Matanzo, M. Llorens-Martín, J. Jurado-Arjona, J. Avila, and F. Hernández, "Tau protein and adult hippocampal neurogenesis," *Front. Neurosci.*, vol. 6, no. JULY, pp. 1–6, 2012.

[112] W. Tang, N. Han, Y. Liu, Z. Li, and Y. Wei, "GSK3β expression and phosphorylation during neuronal maturation in the rat dorsal root ganglion," *Int. J. Clin. Exp. Med.*, vol. 8, no. 4, p. 5897, 2015.

[113] D. P. Hanger *et al.*, "Novel phosphorylation sites in Tau from Alzheimer brain support a role for casein kinase 1 in disease pathogenesis," *J. Biol. Chem.*, vol. 282, no. 32, pp. 23645–23654, Aug. 2007.

[114] M. L. Billingsley and R. L. Kincaid, "Regulated phosphorylation and dephosphorylation of tau protein: effects on microtubule interaction, intracellular trafficking and neurodegeneration," *Biochem. J.*, vol. 323 (Pt 3), no. Pt 3, pp. 577–591, May 1997.

[115] E. M. Hur and F. Q. Zhou, "GSK3 signaling in neural development," *Nat. Rev. Neurosci.*, vol. 11, no. 8, p. 539, Aug. 2010.

[116] F. Naz, N. Sami, A. Islam, F. Ahmad, and M. I. Hassan, "Ubiquitin-associated domain of MARK4 provides stability at physiological pH," *Int. J. Biol. Macromol.*, vol. 93, pp. 1147–1154, Dec. 2016.

[117] H. Kadavath *et al.*, "Tau stabilizes microtubules by binding at the interface between tubulin heterodimers," *Proc. Natl. Acad. Sci. U. S. A.*, vol. 112, no. 24, pp. 7501–7506, Jun. 2015.

[118] G. Marotta, F. Basagni, M. Rosini, and A. Minarini, “Role of Fyn Kinase Inhibitors in Switching Neuroinflammatory Pathways,” *Curr. Med. Chem.*, vol. 29, Dec. 2021.

[119] C. A. Rankin, Q. Sun, and T. C. Gamblin, “Tau phosphorylation by GSK-3ß promotes tangle-like filament morphology,” *Mol. Neurodegener.*, vol. 2, no. 1, pp. 1–14, Jun. 2007.

[120] M. Goedert, R. Jakes, M. G. Spillantini, M. Hasegawa, M. J. Smith, and R. A. Crowther, “Assembly of microtubule-associated protein tau into Alzheimer-like filaments induced by sulphated glycosaminoglycans,” *Nature*, vol. 383, no. 6600, pp. 550–553, 1996.

[121] S. Zhu, A. Shala, A. Bezginov, A. Sljoka, G. Audette, and D. J. Wilson, “Hyperphosphorylation of Intrinsically Disordered Tau Protein Induces an Amyloidogenic Shift in Its Conformational Ensemble,” *PLoS One*, vol. 10, no. 3, p. e0120416, Mar. 2015.

[122] G. Mitra, “Emerging Role of Mass Spectrometry-Based Structural Proteomics in Elucidating Intrinsic Disorder in Proteins,” *Proteomics*, vol. 21, no. 3–4, p. 2000011, Feb. 2021.

[123] M. Hasegawa, R. A. Crowther, R. Jakes, and M. Goedert, “Alzheimer-like Changes in Microtubule-associated Protein Tau Induced by Sulfated Glycosaminoglycans: INHIBITION OF MICROTUBULE BINDING, STIMULATION OF PHOSPHORYLATION, AND FILAMENT ASSEMBLY DEPEND ON THE DEGREE OF SULFATION *,” *J. Biol. Chem.*, vol. 272, no. 52, pp. 33118–33124, Dec. 1997.

[124] Y. K. Al-Hilaly *et al.*, "Alzheimer's Disease-like Paired Helical Filament Assembly from Truncated Tau Protein Is Independent of Disulfide Crosslinking," *J. Mol. Biol.*, vol. 429, no. 23, pp. 3650–3665, Nov. 2017.

[125] P. Barbier *et al.*, "Role of tau as a microtubule-associated protein: Structural and functional aspects," *Front. Aging Neurosci.*, vol. 10, no. JUL, p. 204, 2019.

[126] R. Morales, K. Callegari, and C. Soto, "Prion-like features of misfolded Aβ and tau aggregates," *Virus Res.*, vol. 207, pp. 106–112, Sep. 2015.

[127] B. Frost and M. I. Diamond, "Prion-like mechanisms in neurodegenerative diseases," *Nat. Rev. Neurosci. 2009 113*, vol. 11, no. 3, pp. 155–159, Dec. 2009.

[128] M. Goedert and R. Jakes, "Expression of separate isoforms of human tau protein: correlation with the tau pattern in brain and effects on tubulin polymerization.," *EMBO J.*, vol. 9, no. 13, pp. 4225–4230, Dec. 1990.

[129] Y. Xu, D. Seeman, Y. Yan, L. Sun, J. Post, and P. L. Dubin, "Effect of heparin on protein aggregation: inhibition versus promotion," *Biomacromolecules*, vol. 13, no. 5, pp. 1642–1651, May 2012.

[130] S. H. Satyal *et al.*, "Polyglutamine aggregates alter protein folding homeostasis in Caenorhabditis elegans," *Proc. Natl. Acad. Sci. U. S. A.*, vol. 97, no. 11, p. 5750, May 2000.

[131] S. H. Barage and K. D. Sonawane, "Amyloid cascade hypothesis: Pathogenesis and therapeutic strategies in Alzheimer's disease," *Neuropeptides*, vol. 52, pp. 1–18, 2015.

[132] C. N. Chirita, M. Necula, and J. Kuret, “Anionic Micelles and Vesicles Induce Tau Fibrillization in Vitro,” *J. Biol. Chem.*, vol. 278, no. 28, pp. 25644–25650, Jul. 2003.

[133] M. Goedert, M. G. Spillantini, R. Jakes, D. Rutherford, and R. A. Crowther, “Multiple isoforms of human microtubule-associated protein tau: sequences and localization in neurofibrillary tangles of Alzheimer’s disease,” *Neuron*, vol. 3, no. 4, pp. 519–526, 1989.

[134] L. Buée and A. Delacourte, “Comparative Biochemistry of Tau in Progressive Supranuclear Palsy, Corticobasal Degeneration, FTDP-17 and Pick’s Disease,” *Brain Pathol.*, vol. 9, no. 4, p. 681, 1999.

[135] M. Mulaj, J. Foley, and M. Muschol, “Amyloid Oligomers and Protofibrils, but Not Filaments, Self-Replicate from Native Lysozyme,” *J. Am. Chem. Soc.*, vol. 136, no. 25, pp. 8947–8956, Jun. 2014.

[136] C. N. Chirita, E. E. Congdon, H. Yin, and J. Kuret, “Triggers of Full-Length Tau Aggregation: A Role for Partially Folded Intermediates†,” *Biochemistry*, vol. 44, no. 15, pp. 5862–5872, Apr. 2005.

[137] J. Kuret *et al.*, “Pathways of tau fibrillization,” *Biochim. Biophys. Acta - Mol. Basis Dis.*, vol. 1739, no. 2–3, pp. 167–178, Jan. 2005.

[138] J. O. Esteves-Villanueva, H. Trzeciakiewicz, D. A. Loeffler, and S. Martić, “Effects of tau domain-specific antibodies and intravenous immunoglobulin on tau aggregation and aggregate degradation,” *Biochemistry*, 2015.

[139] F. Chiti, “Relative Importance of Hydrophobicity, Net Charge, and Secondary Structure Propensities in Protein Aggregation,” *Protein Misfolding, Aggregation, Conform. Dis.*, pp. 43–59, Nov. 2006.

[140] D. M. Wilson and L. I. Binder, “Free fatty acids stimulate the polymerization of tau and amyloid beta peptides. In vitro evidence for a common effector of pathogenesis in Alzheimer’s disease.,” *Am. J. Pathol.*, vol. 150, no. 6, p. 2181, 1997.

[141] B. Combs, C. T. Tiernan, C. Hamel, and N. M. Kanaan, “Production of recombinant tau oligomers in vitro,” *Methods Cell Biol.*, vol. 141, pp. 45–64, Jan. 2017.

[142] A. Samsonov, J. Z. Yu, M. Rasenick, and S. V. Popov, “Tau interaction with microtubules in vivo,” *J. Cell Sci.*, vol. 117, no. 25, pp. 6129–6141, Dec. 2004.

[143] M. Redmond, “The Role Of N-Terminal Acidic Inserts On The Dynamics Of The Tau Protein.,” *Grad. Coll. Diss. Theses*, Jan. 2017.

[144] T. C. Gamblin, M. E. King, J. Kuret, R. W. Berry, and L. I. Binder, “Oxidative Regulation of Fatty Acid-Induced Tau Polymerization†,” *Biochemistry*, vol. 39, no. 46, pp. 14203–14210, Nov. 2000.

[145] G. V. W. Johnson and W. H. Stoothoff, “Tau phosphorylation in neuronal cell function and dysfunction,” *J. Cell Sci.*, vol. 117, no. 24, pp. 5721–5729, Nov. 2004.

[146] J. Busciglio, A. Lorenzo, J. Yeh, and B. A. Yankner, “β-Amyloid fibrils induce tau phosphorylation and loss of microtubule binding,” *Neuron*, vol. 14, no. 4, pp. 879–888, Apr. 1995.

[147] A. Takashima, K. Noguchi, K. Sato, T. Hoshino, and K. Imahori, “Tau protein kinase I is essential for amyloid beta-protein-induced neurotoxicity,” *Proc. Natl. Acad. Sci.*, vol. 90, no. 16, pp. 7789–7793, Aug. 1993.

[148] A. Takashima *et al.*, “Exposure of rat hippocampal neurons to amyloid β peptide (25–35) induces the inactivation of phosphatidyl inositol-3 kinase and the activation of tau protein kinase I/glycogen synthase kinase-3β,” *Neurosci. Lett.*, vol. 203, no. 1, pp. 33–36, Jan. 1996.

[149] R. S. Jope and G. V. W. Johnson, “The glamour and gloom of glycogen synthase kinase-3,” *Trends Biochem. Sci.*, vol. 29, no. 2, pp. 95–102, Feb. 2004.

[150] G. Drewes, A. Ebneth, U. Preuss, E. M. Mandelkow, and E. Mandelkow, “MARK, a Novel Family of Protein Kinases That Phosphorylate Microtubule-Associated Proteins and Trigger Microtubule Disruption,” *Cell*, vol. 89, no. 2, pp. 297–308, Apr. 1997.

[151] E. M. Mandelkow, E. Thies, B. Trinczek, J. Biernat, and E. Mandelkow, “MARK/PAR1 kinase is a regulator of microtubule-dependent transport in axons,” *J. Cell Biol.*, vol. 167, no. 1, pp. 99–110, Oct. 2004.

[152] G. Lee *et al.*, “Phosphorylation of Tau by Fyn: Implications for Alzheimer’s Disease,” *J. Neurosci.*, vol. 24, no. 9, pp. 2304–2312, Mar. 2004.

[153] M. Goedert and M. G. Spillantini, “Synucleinopathies and Tauopathies,” *Basic Neurochem.*, pp. 829–843, 2012.

[154] P. Friedhoff, M. Von Bergen, E. M. Mandelkow, P. Davies, and E. Mandelkow, “A nucleated assembly mechanism of Alzheimer paired helical filaments,” *Proc. Natl. Acad. Sci. U. S. A.*, 1998.

[155] C.-X. Gong and K. Iqbal, “Hyperphosphorylation of Microtubule-Associated Protein Tau: A Promising Therapeutic Target for Alzheimer Disease,” *Curr. Med. Chem.*, vol. 15, no. 23, p. 2321, Sep. 2008.

[156] K. Iqbal, A. D. C. Alonso, and I. Grundke-Iqbal, “Cytosolic Abnormally Hyperphosphorylated Tau But Not Paired Helical Filaments Sequester Normal MAPs and Inhibit Microtubule Assembly,” *J. Alzheimers. Dis.*, vol. 14, no. 4, p. 365, 2008.

[157] A. Schneider and E. Mandelkow, “Tau-Based Treatment Strategies in Neurodegenerative Diseases,” *Neurotherapeutics*, vol. 5, no. 3, pp. 443–457, Jul. 2008.

[158] M. Pérez, J. M. Valpuesta, M. Medina, E. Montejo De Garcini, and J. Avila, “Polymerization of τ into Filaments in the Presence of Heparin: The Minimal Sequence Required for τ - τ Interaction,” *J. Neurochem.*, vol. 67, no. 3, pp. 1183–1190, Sep. 1996.

[159] M. Goedert, R. Jakes, M. G. Spillantini, M. Hasegawa, M. J. Smith, and R. A. Crowther, “Assembly of microtubule-associated protein tau into Alzheimer-like filaments induced by sulphated glycosaminoglycans,” *Nat. 1996 3836600*, vol. 383, no. 6600, pp. 550–553, 1996.

[160] H. Qi *et al.*, “Characterization of Neuronal Tau Protein as a Target of Extracellular Signal-regulated Kinase.,” *J. Biol. Chem.*, vol. 291, no. 14, pp. 7742–7753, Feb. 2016.

[161] C. Despres *et al.*, “Major Differences between the Self-Assembly and Seeding Behavior of Heparin-Induced and in Vitro Phosphorylated Tau and Their Modulation by Potential Inhibitors,” *ACS Chem. Biol.*, vol. 14, no. 6, pp. 1363–1379, Jun. 2019.

[162] C. S. Ho *et al.*, “Electrospray Ionisation Mass Spectrometry: Principles and Clinical Applications,” *Clin. Biochem. Rev.*, vol. 24, no. 1, p. 3, 2003.

[163] J. R. Engen and D. L. Smith, “Investigating protein structure and dynamics by hydrogen exchange MS.,” *Anal. Chem.*, vol. 73, no. 9, pp. 256A-265A, May 2001.

[164] M. D. Mukrasch, J. Biernat, M. Von Bergen, C. Griesinger, E. Mandelkow, and M. Zweckstetter, “Sites of tau important for aggregation populate {beta}-structure and bind to microtubules and polyanions,” *J. Biol. Chem.*, vol. 280, no. 26, pp. 24978–24986, Jul. 2005.

[165] M. D. Mukrasch *et al.*, “Structural Polymorphism of 441-Residue Tau at Single Residue Resolution,” *PLOS Biol.*, vol. 7, no. 2, p. e1000034, Feb. 2009.

[166] E. D. Roberson *et al.*, “Amyloid-β/Fyn-induced synaptic, network, and cognitive impairments depend on tau levels in multiple mouse models of Alzheimer’s disease,” *J. Neurosci.*, vol. 31, no. 2, pp. 700–711, Jan. 2011.

[167] D. H. W. Lau *et al.*, “Critical residues involved in tau binding to fyn: Implications for tau phosphorylation in Alzheimer’s disease,” *Acta Neuropathol. Commun.*, vol. 4, no. 1, 2016.

[168] M. M. Mocanu *et al.*, “The Potential for β-Structure in the Repeat Domain of Tau Protein Determines Aggregation, Synaptic Decay, Neuronal Loss, and Coassembly with Endogenous Tau in Inducible Mouse Models of Tauopathy,” *J. Neurosci.*, vol. 28, no. 3, pp. 737–748, Jan. 2008.

[169] A. Al Mamun, M. S. Uddin, B. Mathew, and G. M. Ashraf, “Toxic tau: structural origins of tau aggregation in Alzheimer’s disease,” *Neural Regen. Res.*, vol. 15, no. 8, p. 1417, Aug. 2020.

[170] A. Schneider, J. Biernat, M. Von Bergen, E. Mandelkow, and E. M. Mandelkow, “Phosphorylation that Detaches Tau Protein from Microtubules (Ser262, Ser214) Also Protects It against Aggregation into Alzheimer Paired Helical Filaments†,” *Biochemistry*, vol. 38, no. 12, pp. 3549–3558, Mar. 1999.